MEASUREMENT OF THE SPECTRAL DISTRIBUTION OF THE LOW ENERGY ELECTRONS EMITTED AS A RESULT OF M_3VV AUGER TRANSITIONS IN Cu(100)

by

SUMAN SATYAL

Presented to the Faculty of the Graduate School of

The University of Texas at Arlington in Partial Fulfillment

of the Requirements

for the Degree of

MASTER OF SCIENCE IN PHYSICS

THE UNIVERSITY OF TEXAS AT ARLINGTON

December 2011

ACKNOWLEDGEMENTS

I would like to take this moment to acknowledge all the people around me who helped me to put together all the pieces starting from my undergraduate studies to the successful completion of my graduate studies.

My interest in experimental physics grew from the moment my supervising Professor Alexander H. Weiss brought me in the lab and asked me to design some Helmholtz Coil Support System from the Aluminum scrap lying at the corner for the Positron Beam that was under construction. I spent days, may be weeks, to get my first design right. There were times full of frustrations and despair. But, now when I reflect back those moments, I realize it was totally worth it and not to mention that was just the beginning. True knowledge comes from the experience and as a veteran of experimental physics; Dr. Weiss gave me that opportunity which I will be indebted for the rest of my life. On top of that he let me perform this experiment at the Brookhaven National Lab, NY, amidst great scientist and research scholars. He has always been a constant source of my encouragement and motivation. His extensive knowledge on theoretical and experimental physics is so impressive that even my friends from other research group mention him during the seminars. I feel it's a true honor to be around him while working on condensed matter experimental physics. The only way to thank him, as I see, is by following the intuitive path he has shown me.

I am also indebted to our collaborator Dr. Steven Hulbert from the National Synchrotron Light Source, BNL who helped to conduct this research. I was impressed and motivated by his skills of handling things. I would like to thank him for trusting me with the beamlines and letting me play with the photons during the first couple weeks. I only screwed up once with the ERG monochromator, but that was a great lesson in understanding the system. He patiently helped

me fix things around the beamlines and correct my stupid mistakes. Those evenings when we would discuss the physics behind all those photon interactions with Dr. Weiss over the Skype was fun and fruitful. Many thanks to Mr. Dong for his technical assistance while operating the NSLS beamline, U1A.

I would like to thank the professors from the Physics Department for their constant encouragement and support. I sincerely thank Dr. Nail Fazleev and Dr. Koymen Ali for extending their suggestions and accepting to serve on the defense committee. Many thanks to my academic advisor Dr. Qiming Zhang, Professors Dr. Ashok Ray, Dr. Zdzislaw Musielak, Dr. Suresh Sharma and the lord of the underworld, Barry Spurlock for trying to pass wisdom to the new generation. My sincere gratitude to the office staff Margie Jackymack, Stacy Cody, Bethany Harris, Victor Reece, and lab coordinator Doug Coyne; special thanks to Margie for patiently dealing with us and for all the candies.

I cannot forget my friendly, funny, cooperative and helpful lab mates Prasad Joglekar and Karthik Shastry. All those discussions, though few related to physics, during our trip to APS meetings shall be remembered. Thanks for that painstaking time during the poster sessions and practice talks just fly away. I am grateful to Sunil Sahi, Shree Krishna Bhattarai, Kapil Adhikari, Ajani Ross, Narayan Poudel, Tejnath Lamichhane and Billy Quarles for their inspirational discussions on Physics and beyond during the tea times.

I would like to remember my friends Sangam KC, Subin Panta, Suraj Thapa and Nabin Koirala with whom I started my journey in the United States. From high school till now thank you all for your intellectual, emotional and moral support during those days through thick and thin. I can always spend one more semester at Waxahachie and make one more road trip. I would also like to thank my dear friends Ajay Gurung, Dipendra Aryal, Rabi Gautam, Aarati Shrestha and Subash Khadka, my lovely sisters Roshani Rana, Chandani Rana, Silva Shrestha, Ripana Shrestha and Dipti Neupane, and my genius brother Ashesh Rana, for their inspiration and support throughout my career.

Last but not the least I would like to express my deepest feelings towards the Love of my Life – my family. My father, Ram Prasad Satyal, always showed me the intellectual part of the life keeping my spirits higher than the sky and my mother, Goma Satyal, always stood as the symbol of Love and Patience keeping the emotions deeper into her heart. My hearty thanks to my uncle Buddhinath Satyal, aunts Indira Satyal, and Ukha Satyal, sisters Pabitra, Sumitra, Sita, Devaki, Shanti and brothers Santosh, Ujjwal and Susil for their endless love, affection and support. I hope to make you proud one day.

May the force be with us.

November 23, 2011

ABSTRACT

MEASUREMENT OF THE SPECTRAL DISTRIBUTION OF LOW ENERGY ELECTRONS EMITTED AS A RESULT OF M_3VV AUGER TRANSITIONS IN Cu(100)

Suman Satyal, M.S.

The University of Texas at Arlington, 2011

Supervising Professor: Alexander Herman Weiss

Auger Photoelectron Coincidence Spectroscopy (APECS) was used to investigate the physics of the Low Energy Tail (LET) region of the Auger spectrum of a Cu(100) sample. Two Cylindrical Mirror Analyzers (CMAs) were used to select the energy of electrons emitted from the sample as a result of irradiation by 200eV photons. The APECS technique was used to obtain an Auger spectrum taken in coincidence with electrons in the core photoemission peak. The background due to coincidences between pairs of valence electrons emitted as a result of multi-electron photoemission processes was estimated by taking a series of APECS spectra in coincidence with electrons emitted at energies in the range between the photo-emitted core and photo-emitted valence electrons. This background along with an estimate of the contributions to the LET from inelastic processes resulting from scattering before they exit into the vacuum was subtracted from the APECS derived Auger spectra to obtain an estimate of the spectra of electrons emitted solely as a result of intrinsic Auger processes. The Auger spectra so obtained indicate that the number of electrons emitted as a result of intrinsic Auger processes involving multiple electron emission exceeds the number involving single electron emission in

agreement with estimates from previously published positron annihilation induced Auger (PAES) measurements.

TABLE OF CONTENTS

LIST OF ILLUSTRATIONS

LIST OF TABLES

CHAPTER 1

AUGER PHOTOELECTRON COINCIDENCE SPECTROSCOPY (APECS)

1.1 Introduction

This Thesis describes experiments in which Auger Photoelectron Coincidence Spectroscopy (APECS) technique is used to study the physics behind the Low Energy Tail (LET), removal of the LET and finally to obtain the Cu(100) Auger spectrum with the Intrinsic background contribution only. The research was conducted in the facility provided by National Synchrotron Light Source (NSLS), Brookhaven National Lab, Upton, NY.

When a photon of sufficient energy is used to probe an atom, a core electron is emitted. The emitted electron is called photoelectron. The atom, after losing the electron, goes to an excited state which then decays via a transition where a less tightly bound electron from the valence band fills the core hole. The energy released in this decay process is carried away either by a photon (x-ray fluorescence), or by an emission of a second electron (Auger decay process). The emitted electron is called the Auger Electron. For the binding energy of the core electron $\leq$ 1keV the Auger decay process is more likely to occur than the x-ray fluorescence and to a good approximation, every photo excitation generates a Photoelectron and an Auger electron. These mechanisms, Photoelectron Spectroscopy and the Auger electron Spectroscopy, are the two powerful means to probe the electronic structure and chemical composition of the solid surfaces [1-2].

In APECS, a core photoelectron and its associated Auger electron are detected in time coincidence. Since both of these electrons are originated from the same photo excitation event, APECS has the unique capability of probing the local electronic structure.

Auger Photoelectron Coincidence Spectroscopy (APECS) was developed by Haak, Sawatzky and Thomas in 1978 [3] using a conventional x-ray source. Hulbert, Jensen and

Bartynski later adapted APECS to a synchrotron radiation source [4] and performed a number of experiments to reduce core level lifetime broadening in photoemission, isolate individual sites in a solid and probe their local electronic structure, distinguish between “intrinsic” and “extrinsic” secondary electron emission, explore correlated photo-excitation/Auger relaxation events, separate overlapping spectral features, probe electronic structure with improved depth resolution and eliminate uncorrelated secondary background. In each case, APECS has either revealed new materials properties or displayed unexpected physical phenomena, or both [5 and references there in].

1.2 Motivation

Electron, Positron and X-ray induced Auger electron spectroscopy (EAES, PAES and APECS) have been a widely used spectroscopic methods in the field of surface studies. These techniques are surface selective and sensitive to the composition and the chemical environment of the top most layers. However, the Auger spectra obtained from each of these techniques always have a large background which leads to uncertainty in the determination of the Auger line shapes and in the quantitative analysis of Auger spectra. There are various factors contributing to the spectral intensity below the Auger peak. This portion of the spectra has been termed as low energy tail (LET). For example in EAES the LET contribution mostly comes from the secondary electron cascade processes due to the scattering of the incident electron beam. In APECS, it’s due to the inelastic scattering of the valence band photo-electrons and the inelastic scattering of the Auger electrons in the surface and the subsurface region. In PAES, the beam induced secondary electrons can be eliminated by using a low energy positron beam (~1.5eV) which is well below the threshold of the secondary electron emission [6].

To obtain the background free Auger spectra many modern techniques have been developed and applied. The extrinsic background contribution to the Auger spectrum in the low energy region is much bigger than the Auger signal itself. Here we are motivated to remove the extrinsic background from the Auger spectra of Cu(100) obtained by using APECS technique.

The LET region of the Cu Auger spectra entails inelastic scattering of valence band, core and Auger electrons (Extrinsic contributions) and also the electrons from the multiple inelastic scattering events (Intrinsic contribution). The LET extends from the lowest measureable kinetic energy and typically dominates the APECS spectrum as it is related to all primary photoemission features. Since APECS has a unique capability of probing a sample in time coincidence and one of the analyzer can be programmed to select the electrons of particular energy, APECS can eliminate a large fraction of the secondary electrons scattering of the incident photo-electrons. When the fixed analyzer is set at $3p_{3/2}$ core peak, the APECS will selectively probe the decay features associated with the core excitation. However, the Cu $3p_{3/2}$ photoelectron peak typically sits on a plateau of secondary electrons originated from higher kinetic energy photoemission and Auger emission peaks. The APECS spectra can contain contribution from coincidences between parts of photo excited valence band electrons that can be emitted at energies that's total to a value less than or equal to the photon energy. Therefore the Cu(100) M_3VV spectra contain a significant fraction of LET unrelated to the $3p_{3/2}$ excitation event.

The first part of this thesis deals with the removal of this background due to the true coincidences involving pairs of photo excited electrons. The fixed analyzer cannot distinguish the electrons coming from photoemission process or inelastic scattering of the secondary electrons, so APECS technique is not sufficient to get rid of this portion of LET. So here we introduce an extrapolation method to estimate the background of the Cu(100) Auger spectrum taken in coincidence with the $3p_{3/2}$ core peak. For this we take a singles spectra using 200eV photon beam and locate the position of the core and the valence band. It is shown that the contributions due to inelastic scattering of the Valence Band (VB) photoelectrons can be expected to grow as the energy difference between the VB peak and the energy of the fixed analyzer increases. So we fixed one of our Cylindrical Mirror Analyzers (CMA) at the energy 15eV higher than the core and took the coincidence measurement with the background. We

repeated the measurements 4 times with CMA fixed at 4 different energies between the valence band and the core. Then we extrapolated all the five measured APECS LET spectra to estimate the background contribution from the APECS Auger spectra.

A second background due to the Auger electrons that loose energy before being emitted into the vacuum is estimated from published values of the secondary electron yield and inelastic mean free path. Both backgrounds are removed to yield an Auger Spectra, including the LET down to 0eV that stems solely from intrinsic Auger processes. In the final step we compare our data to previous positron annihilation induced auger spectroscopy (PAES) data. We calculate the ratio of the integrated intensities of the LET to that of the Auger. We find that the integrated intensity of the LET is 2 times that of the Auger peak suggesting that intrinsic multi electron Auger process accounts for the major portion of electrons emitted as a result of an Auger transition.

1.3 Electron Emission Processes

1.3.1 CVV Auger Transitions

A beam of photons carrying the energy, hv is used to probe the sample. When one of the core electrons absorbs the sufficient energy it leaves the sample ionizing the atom. The emitted electron is called photoelectron which has the energy equivalent to the incoming photon energy minus its binding energy and the work function of the sample it has to overcome to leave the sample. The ionized atom relaxes via a transition of a less tightly bound electron from the valence band to the core hole. The energy released in this decay process can be carried away either by a photon, the case which is termed as X-ray fluorescence, or by a neighboring valence band electron. This electron is called an Auger electron and the whole mechanism is termed as a Core-Valence-Valence (CVV) Auger transition. For the binding energy, $E_B \leq 1$keV the photoelectron emission is followed by the Auger transition or else X-ray fluorescence takes over.

The CVV Auger emission process is described using an energy level diagram shown in figure 1.1 [6-7]. The Kinetic Energy of the Photoelectron and the Auger electron is given by the equation,

$$KE_{photoelectron} = hv - E_C - \phi \quad (1.1)$$

$$KE_{CVV\ Auger\ electron} = E_C - E_{V1} - E_{V2} - \phi \quad (1.2)$$

Where, E_C is defined as the binding energy of the Core hole, E_{V1} and E_{V2} is the binding energy of the Valence holes created in the process and ϕ is the work function. The figure also shows the final state of the direct Auger process with the two holes in the valence band. All the energies in the equation are in referenced to the Fermi level of the solid. For the Fermi level electrons,

$$E_{V1} = E_{V2} = 0eV \quad (1.3)$$

The CVV Auger electrons emitted from the Fermi level carry the maximum energy,

$$KE_{CVV(max)} = E_C - \phi \quad (1.4)$$

The CVV Auger electrons emitted from the Fermi level carry the minimum energy when both the electrons come from the bottom of the Valence band. The Kinetic Energy of these electrons is given by,

$$KE_{CVV(min)} = E_C - 2W - \phi \quad (1.5)$$

Energy width, W is estimated using the above equations,

$$\Delta KE_{CVV} = KE_{CVV(max)} - KE_{CVV(min)} = 2W \quad (1.6)$$

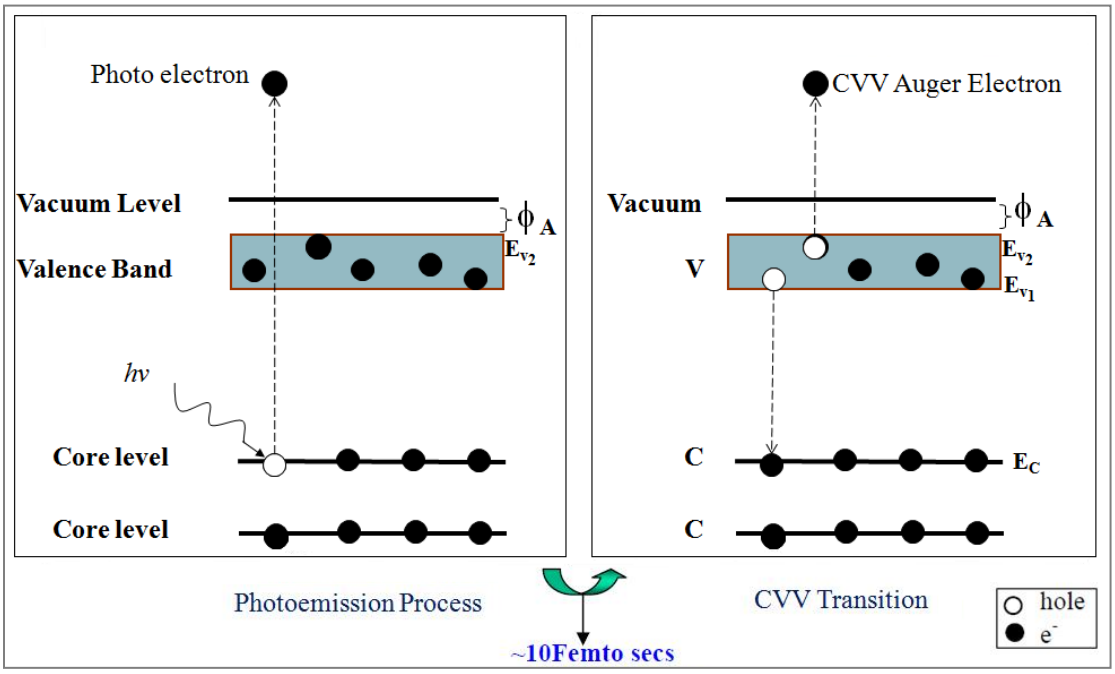

Figure 1.1 Energy level diagrams showing direct CVV Auger Emission process

1.3.2 Inelastic Scattering of the Valence band Photoelectrons

In APECS, a photon beam of energy, hv is used to probe a sample. When an electron in an atom in the top most layers absorbs sufficient energy it may leave the atom and be emitted from the sample, hence ionizing the atom. The electron excitation can happen either in the Valence band or in the Core level. In an event when the Valence band electron is excited its kinetic energy when leaving the sample is given as,

$$KE_{Valence} = hv - E_{V1} - \phi \quad (1.7)$$

When the scattering of the valence band photoelectron is inelastic, let's consider that the photoelectron transfers an energy Δ to a neighboring electron. This electron then has sufficient energy to be emitted from the sample as well. Following equation (7) gives the energy of the emitted inelastic valence band electrons.

$$KE_{InelasticValence1} = hv - E_{V1} - \Delta - \phi \quad (1.8)$$

Figure 1.2 provides a schematic representation of the inelastic scattering of valence band photoelectrons. It follows from the Conservation of Energy that during the inelastic

scattering event the Valence electrons which accept the energy ≤ ΔeV from the photo-emitted valence electron leave the sample with a kinetic energy given as,

$$KE_{InelasticValence2} \leq \Delta - E_{V1} - \phi \quad (1.9)$$

The inequality sign, less than or equal to, reflects the fact that the electrons which absorb the energy ΔeV can undergo additional inelastic processes before being emitted from the sample.

The inelastic scattering of the Valence band Photoelectrons contributes a significant portion of the Low Energy Tail (LET) of the Photoemission Spectra in solids. In figure 1.3 the Singles Spectra taken for Cu(100) shows the contribution from the inelastic scattering of the Valence band Photoelectrons. The inelastic scattering of the Core and the Auger electrons contribute to the LET of the spectra as well. For example, in figure 1.4 of the APECS Cu(100) Auger spectrum, the observed LET from above discussed contributions is indicated by shaded the region.

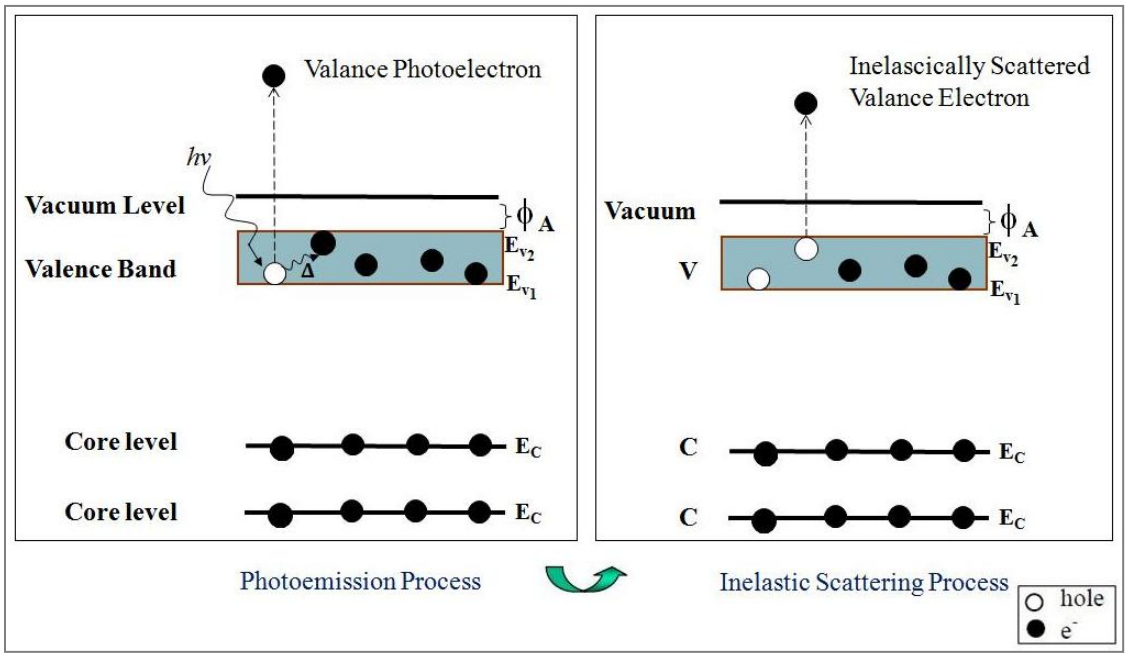

Figure 1.2 The Inelastic scattering of the Valence band Photoelectrons

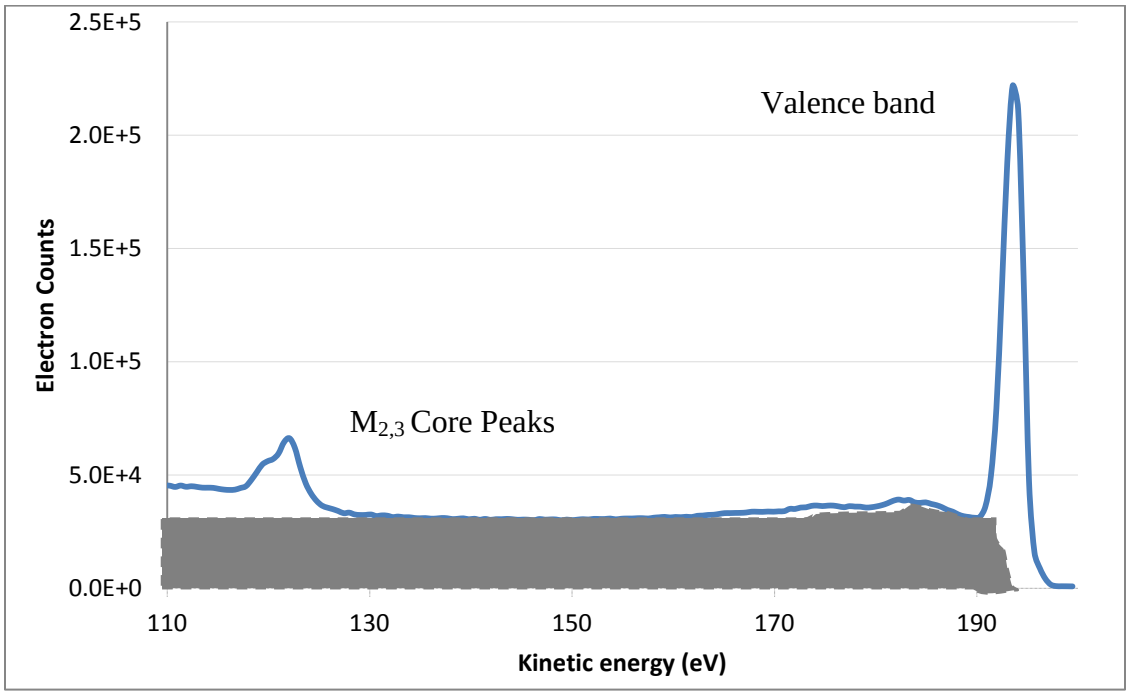

Figure 1.3 The Photoelectron spectra of Cu(100) taken with 200eV photon beam energy. The assumed contribution due to inelastic scattering of the valence band photoelectrons is shown in the shaded region.

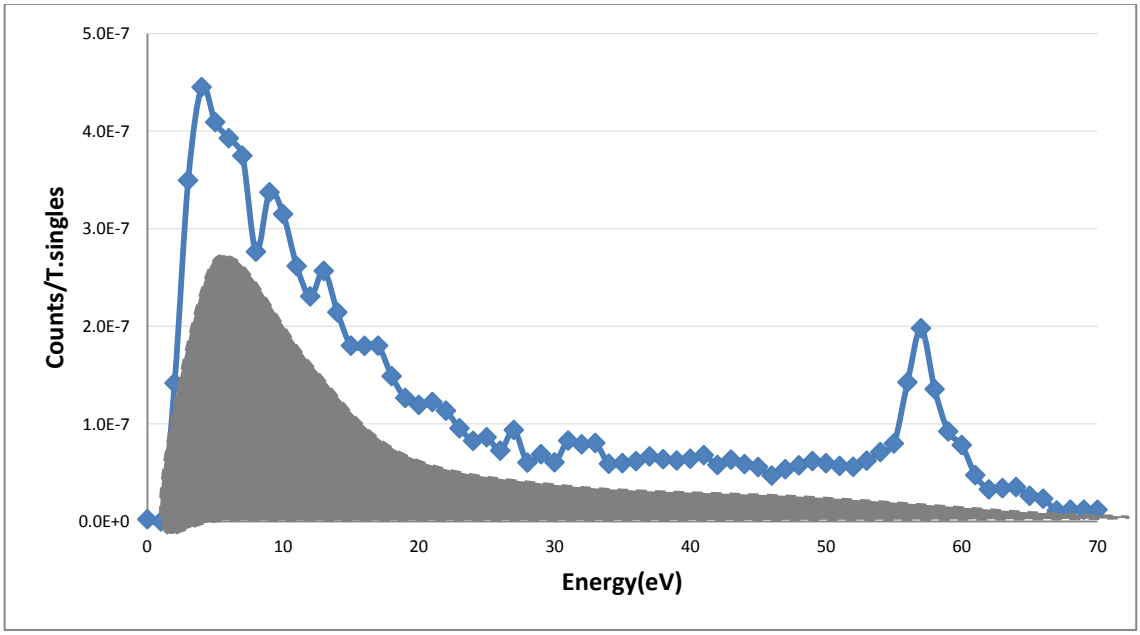

Figure 1.4 The APECS Cu M_3VV Auger Spectrum. The estimated contribution to the LET by the inelastic scattering of the valence band photoelectrons is shown schematically by the shaded region

1.4 Quantification of the APECS Spectrum

The Spectra obtained from the various spectroscopic techniques such as PAES, EAES and APECS can be used to extract the information about the chemical composition of the atoms on the solid surfaces. But before interpreting any Auger line shapes it's critical to remove the contribution of the secondary electrons that are unrelated to the Auger event. Many quantification techniques have been in use since the development of the Auger electron Spectroscopy and have successfully extracted the Auger line shapes.

The Intensity of the signal, I_A, from an element A in a solid is proportional to the molar fraction content, X_A, in the depth to which the sample is being analyzed. [9]

$$X_A = \frac{I_A}{I_A^\infty} \tag{1.10}$$

Where, I_A^∞ is the sensitivity factor and it's the intensity from the pure element. Usually the value of I_A^∞ is not known, but if the value of I_A^∞/I_B^∞ is known then it can be used in the equation below. B here is some constituent of the element.

$$X_A = \frac{I_A/I_A^\infty}{\sum_{i=A,B} I_i/I_i^\infty} \tag{1.11}$$

Here, the sum is over all the constituents in the solid.

The terms contributing to the I_A value can be determined for the APECS technique. As discussed earlier, the APECS Auger spectrum for Cu(100) contains a significant fraction of the Low Energy Tail (LET) emission which is in coincidence with the background emission of the Cu $3p_{3/2}$ (Core) photoelectron kinetic energy. However, this contribution coming from the coincidence is not related to the Cu $3p_{3/2}$ excitation event. This portion of the LET also contains the electrons resulting from the inelastic scattering of the Auger electrons, Valence electrons and the core hole decaying via multi-electron emission processes, a C-VVV process [8] in which two electrons are emitted. The contribution to the LET region is seen as,

$$I_{LET}(E) = I_{LET}Intrinsic(E) + I_{LET}Extrinsic(E) \tag{1.12}$$

The first part of the contribution comes from the intrinsic events (related to the Auger excitation process) and the second one form the extrinsic events. Of the Extrinsic LET, it's partly due to the inelastic scattering of the valence band photoelectrons and partly due to the inelastic scattering of the Auger electrons.

$$I_{LET}Extrinsic(E) = I_{photoelectron}Inelastic(E) + I_{Auger}Inelastic(E) \quad (1.13)$$

After the subtraction of the extrinsic contribution to the LET, only the intrinsic contribution is left in the Auger spectrum. This portion of the LET comes only from the excitation process of Cu $3p_{3/2}$ photoelectrons. Now, this will help us to determine the I_A value which is the characteristic only to the Auger transition and thus results in the better quantification of the acquired data.

1.5 Sample Description

Copper singles crystal was used in the study of the physics behind the Low Energy Tail of the APECS Auger Spectrum. The sample had the crystal orientation of (100)

Atomic number of Copper: 29

Electronic Structure: $1s^2$, $2s^2$, $2p^6$, $3s^2$, $3p^6$, $3d^{10}$, $4s^1$

Table 1.1 Showing the Energy levels of Copper

Shell	Sub-Shells				B. Energy(eV)
	n	l	j (=l+s)		
M	3	1	3/2	M_3 , $3p_{3/2}$	75.1
	3	1	½	M_2, $3p_{1/2}$	77.3
	3	0	½	M_1, $3s_{1/2}$	122.5
L	2	1	3/2	L_3, $2p_{3/2}$	932.7
	2	1	½	L_2, $2p_{1/2}$	952.3
	2	0	½	L_1, $2s_{1/2}$	1096.7
K	1	0	½	K_1, $2s_{1/2}$	8979

CHAPTER 2

APECS EXPERIMENTAL DETAILS

2.1 National Synchrotron Light Source (NSLS)

All of our APECS experiments were conducted in the National Synchrotron Light Source (NSLS), Brookhaven National Lab (BNL). NSLS is one of the best Research facilities to provide the UV and X-Ray light. It is located in Upton, New York and is funded by United States Department of Energy.

The NSLS operates two electron storage rings, the x-ray and the ultraviolet (UV). It uses a simple principle of Synchrotron Radiation to generate photons of varying energy and intensity. Charged particles must accelerate while moving in a circular path. As a result of which the electromagnetic radiation is emitted. Such a process is called synchrotron radiation. Synchrotron radiation has special characteristics such as high intensity, broad spectral range, pulsed time structure, and high polarization which make it a unique spectroscopy tool.

For our experimental purpose the photon beam line from UV section was used. The photon beam energy falls in the range of 10^{8} to 10^{-1}Å wavelength. The lattice constants, the chemical bonds and the atomic and the molecular sizes fall in the range, and hence the photons from the synchrotron radiation can be used in the study of atomic and molecular structures of the topmost layers in solids.

2.2 NSLS Storage Rings and Beam Lines

In the UV storage ring the electron beam is made to travel in the circular trajectory by the use of dipole bending magnets. At each bend the electrons loose energy, synchrotron radiation, so the energy has to be constantly added to the electrons beam. Radio Frequency (RF) Cavity is used somewhere in the ring to add energy to the beam. At the each bend, the

photon shutters are opened so as to let the synchrotron light out to the work stations. The storage rings the beam lines are schematically shown in the figure 2.1.

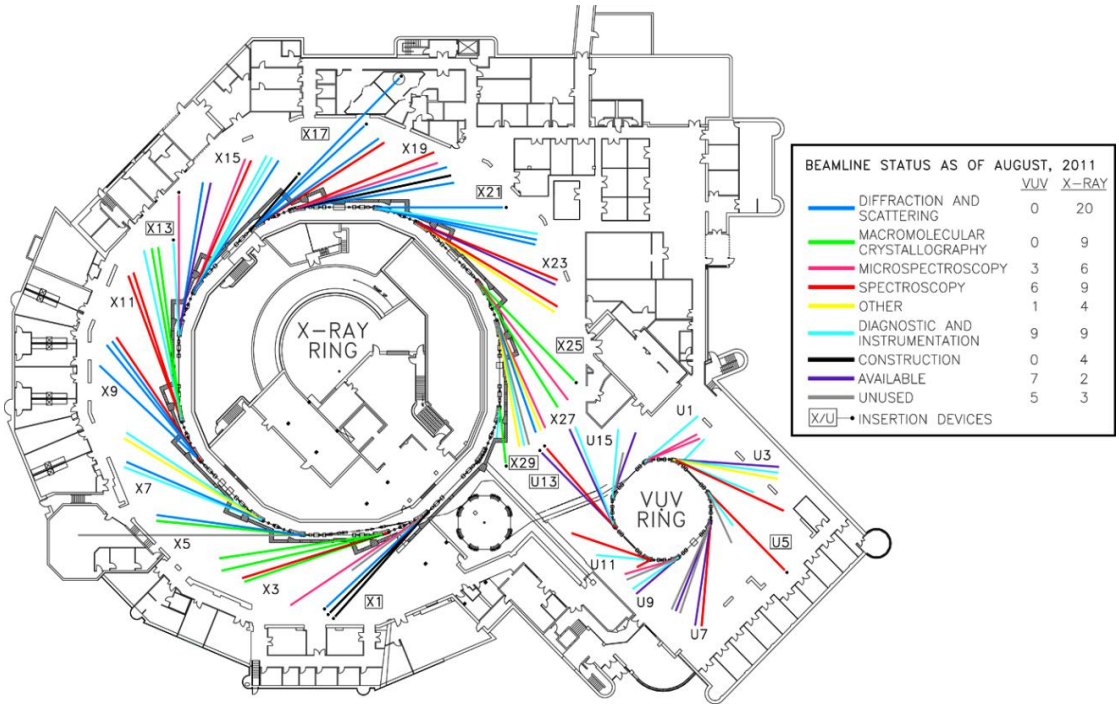

Figure 2.1 The VUV ring and the X-ray ring floor plan of the National Synchrotron Light Source

2.3 Beam Line U1A

2.3.1. U1A Introduction

In the UV ring there are 16 beam lines. Beam line U1A was used for our experimental purpose. The beam that comes out of the UV ring is directed by using the Extended Range Grasshopper (ERG) monochromator designed by F.C. Brown and S. L. Hulbert [10]. The focused beam at the exit slit of the ERG propagates downstream to a 1:1 refocusing mirror that focuses on the sample. This is controlled by computers where we can just type the required photon energy and that would automatically set the beam energy. To preserve the optical quality of the photon focusing mirrors are placed along the beam line The beam, 200eV in our case, is then guided into the sample in the High Vacuum chamber. Figure 2.2 shows the transport of electron from UV ring to the work station.

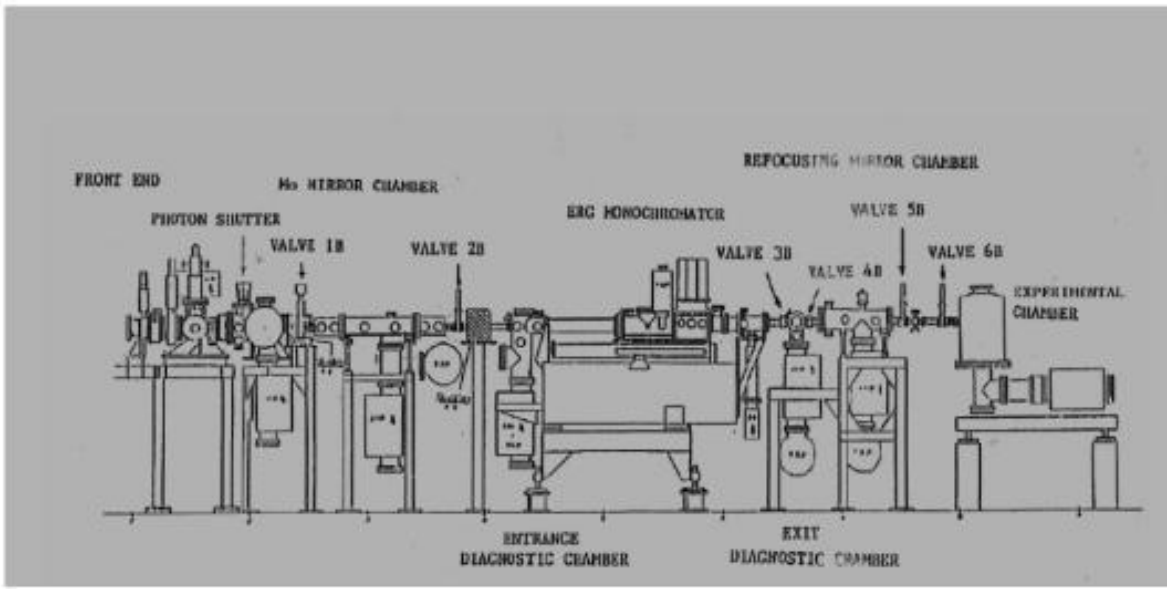

Figure 2.2 The beamline components of U1A, NSLS.

2.3.2 UHV Beam lines and UHV Chamber

From the start when the electrons are generated by the electron gun in the LINAC to the sample chamber where the photons end up, all this happens inside the Ultra High Vacuum, UHV, enclosures. The pressure throughout is ~10^{-10} Torr.

The end station where the experiment is conducted consists of a Vacuum Chamber, Sample manipulator, the electron analyzers and other associated instruments. The UHV chamber is where the sample and the analyzers are housed. The pressure is maintained at ~10-10 Torr. It is mounted on an adjustable table in order to align the analyzers source point to the photon beam. Inside the chamber lies the sample holder directly on the perpendicular path of the photon beam. The sample position can be changed by help of manipulator that lies on the top of the chamber. The manipulator has the 4 degrees of freedom to move (x,y,z,θ). The sample, the light and the analyzer's focal point image has to coincide to get better count rate.

The energy resolution of the analyzers depends on the size of their adjustable aperture. For the small (large) aperture setting the analyzer energy resolution is 0.6% (1.6%) of the pass

energy. Large aperture set up is better for the coincidence spectroscopy, as in our experiments.

The block diagram of the experimental setup is shown in figure 2.2

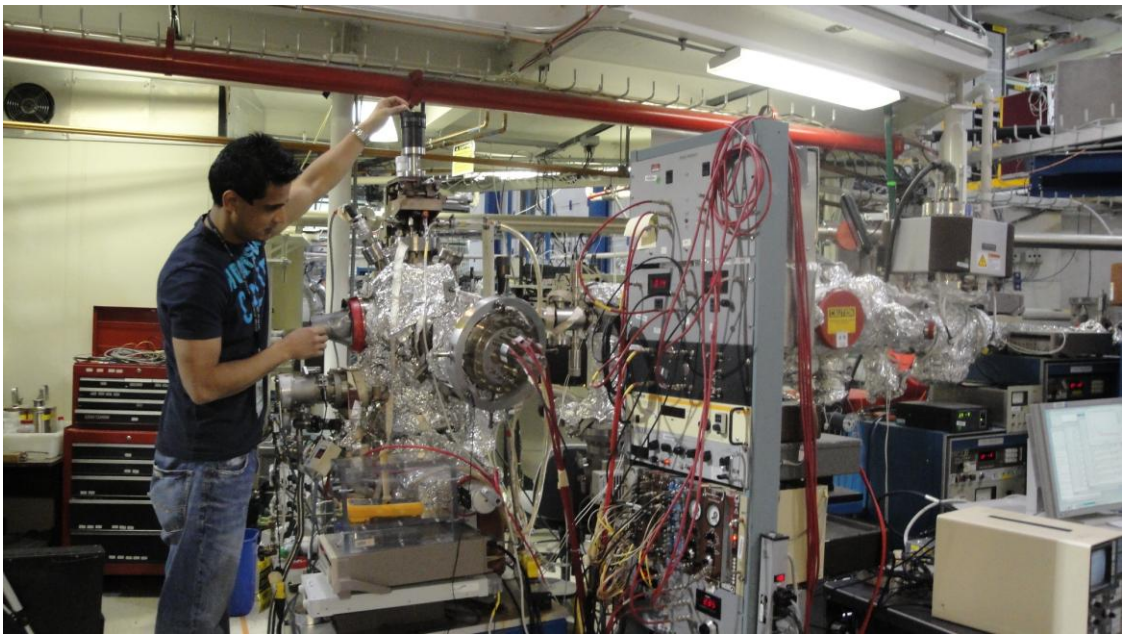

Figure 2.3 Beamline U1A and Chamber

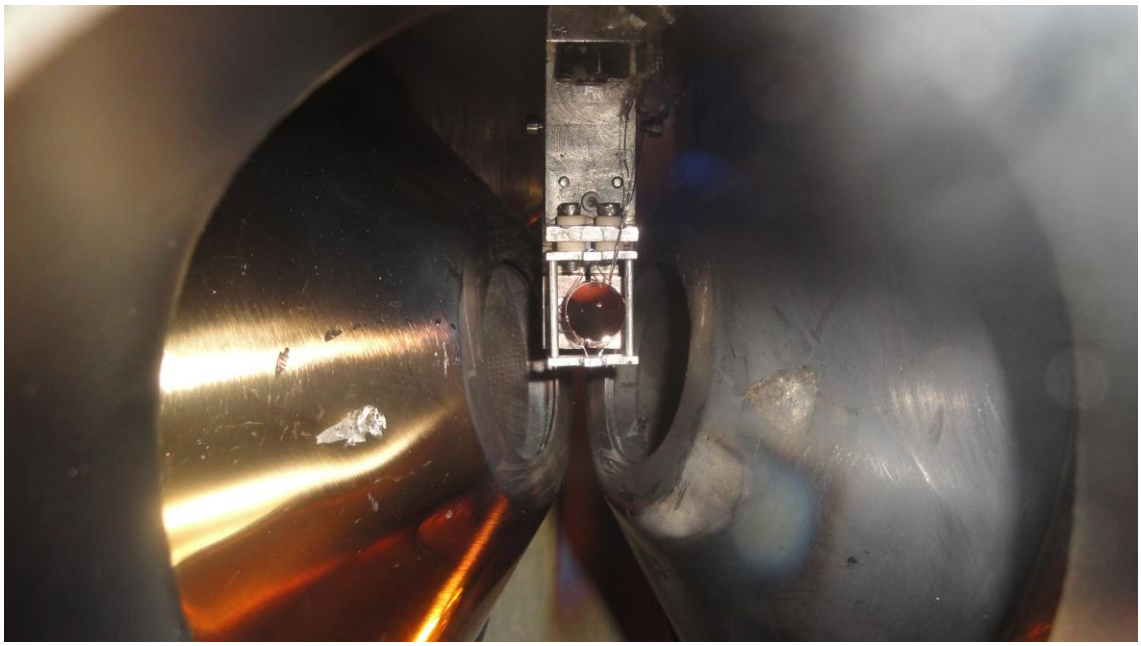

Figure 2.4 Sample in the Sputtering position

2.4 U1A Electronics

2.4.1 CAMAC Crate Components

The central control of the U1A electronics lies in the CAMAC crate (Kinetic System model 1502 CAMAC Crate). It's also the interface between the computer and the other electronics. The computer has the LINUX Operating System and can communicate to the CAMAC and the ERG controller. The CAMAC Crate houses the following modules.

DA Converter: The Digital to Analog (DA) converter converts the 16-bit digital input number to an along ramp signal. The analog ramp voltage is amplified and fed to a visual display unit for easy view. The DA converter receives command from the computer to set the voltage on the panel named "OFFSET SUPPLY" which supplies power to the two analyzers.

Quad V-F converter: It has 4 channels that consist of 4 inputs and 4 outputs. The input receive voltage signals and convert them into pulse train signals with a frequency linearly proportional to the input voltage. The output signals are then fed into TTL-NIM which is then connected to a QUAD SCALER.

QUAD SCALER: The Quad Scaler is a digital signal processing unit. It has 4 inputs and 4 gates coupled together.

Counting Electronics: The CMA signals are discriminated, amplified and converted to NIM signals and fed into the counters which have the gate signals for counting in the real time clock. Similarly the Coincidence counts and the Accidental counts from the PHA are converted to NIM signals and then fed into the Quad Scaler. The wiring schematic of the counting electronics are shown in figure 2.5.

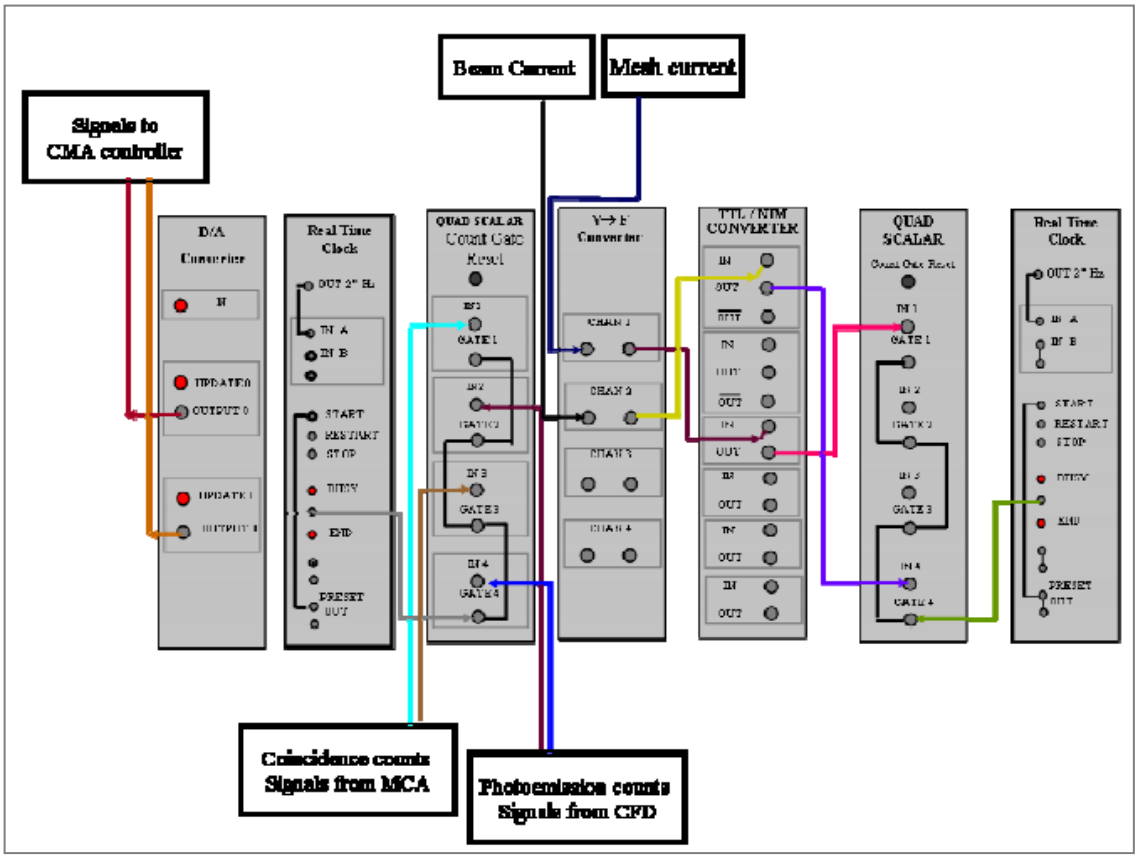

Figure 2.5 Block diagram of the counting electronics

2.5 Cylindrical Mirror Analyzer (CMA)

2.5.1 CMA Introduction

Two double-pass cylindrical mirror electron energy analyzers, PHI Model 15-255G (R) are installed in the two 8 inch ports oriented at 145degrees from one another in a plane 10 degrees below the horizontal. The CMAs consists of two concentric cylinders. The inner cylinder has grid-covered apertures to allow electrons into and out of the region between the cylinders.

2.5.2 CMA Components

Each CMA consists of Channeltrons, Analyzers, Variable apertures, Retardation grid, Internal electron gun and Deflection plates. The aperture control and the flange-mounted terminals on the PHI model 15-255G Precision analyzers are shown below in figure 2.6.

The flange to specimen distance for this model is 27.94 cm, which is important for measuring the kinetic energy of the electrons ejected from the specimen.

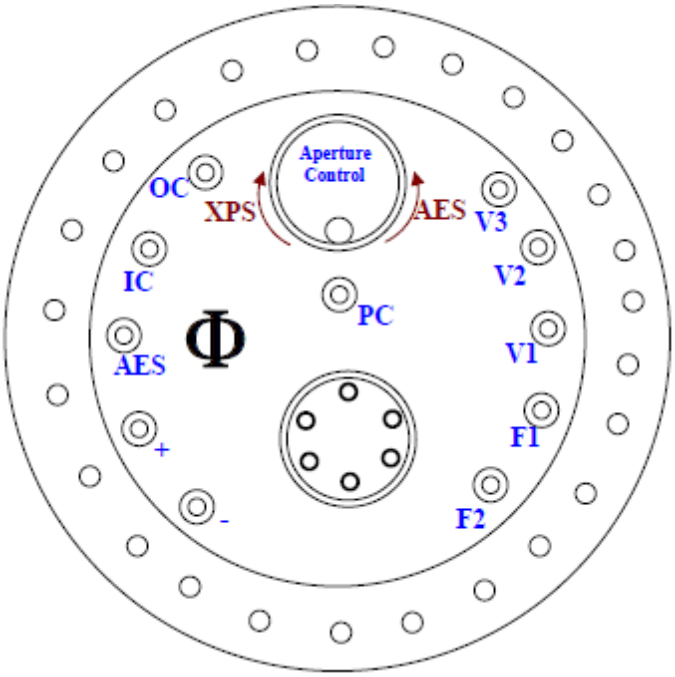

Figure 2.6 The aperture control and the flange mounted terminals on the PHI model 15-255G Precision electron energy analyzer

2.5.3 CMA Power Supplies

The power supply units to set the voltages in the outer and the inner cylinders for the CMA are shown in figure 2.7.

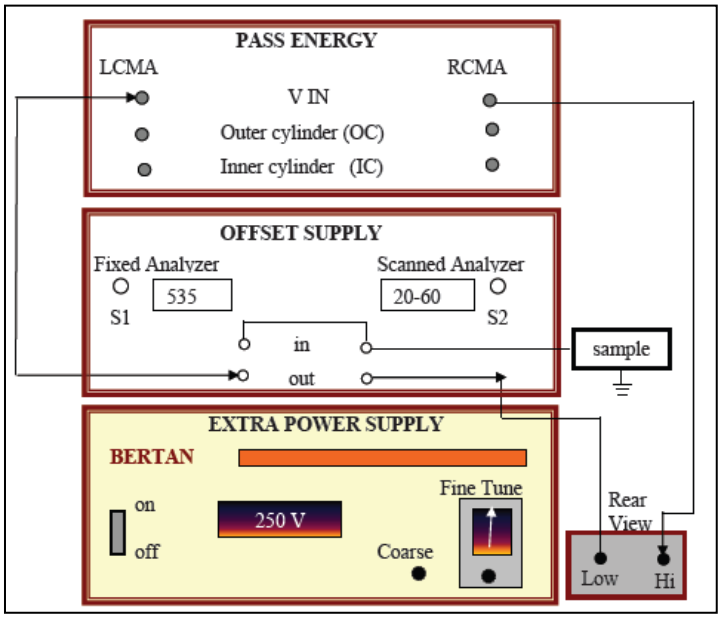

Figure 2.7 Power supply units to set the voltages on the inner and outer cylinders of the CMA

OFFSET Supply: This unit has the power output limit of 0-500V DC which is linearly proportional to the 0-10V DC input from the CAMAC DA module. These power supplies are programmable and thus can be controlled by a computer to set the retarding voltage of the CMA.

Extra Power Supply: This extra power supply is used when the required energy range is > 500 eV. The detailed circuitry of the power supplies that are used to set up the voltages in the CMA and the inner and the outer cylinders are shown in figure (2.5).

Pass Energy: The pass energy is calculated as shown in the formula in the figure 8. The OC and IC are set in a way that the electrons have the KE equivalent to the pass energy alone can reach the channeltron.

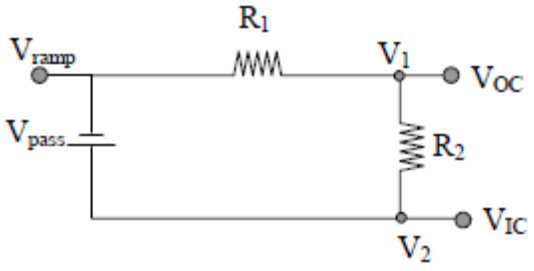

Figure 2.8 Circuit diagram for the pass energy

$V_1 = V_{OC} = V_{ramp} + [R_1/(R_1+R_2)]V_{pass}$ (2.1)

$V_2 = V_{1C} = V_{ramp} + V_{pass}$ (2.2)

The voltages V1 and V2 are calculated using above two equations.

2.5.4 Working of the CMA

When a photon hits the sample, electrons of different kinetic energies are knocked out in all possible angles. Those electrons emitted at an angle of 48° ± 5° pass through the apertures of the CMAs. The outer cylinder is biased negatively with respect to the inner cylinder resulting in a radial electric field between the two cylinders. The incoming electrons from the sample enter the gap between the two cylinders. If the electrons are moving too fast, they will impinge on the outer cylinder while slower electrons will hit the inner cylinder. Hence only the electrons of the specific energy, called the Pass Energy, will make it to the detectors. The pass energy is dictated by the voltage difference between the inner and outer cylinders. The 'double pass' design incorporates a second stage of filtering, intended to reduce the spurious background signal due to secondary electrons generated within the analyzer. Negative voltage is applied to the outer cylinder to repel electrons through openings in the side of the inner cylinder forcing these electrons through the opening in the inner cylinders so that they can enter the electron multiplier. The channeltron electron multiplier amplifies (gain16^6 to 10^7) the electron signal to generate a measureable signal on the collector plate. The inner cylinder is set to attract the electrons; therefore the OC is more negative than the IC. The relationship of the energy of electrons selected to pass through the analyzer and the voltage applied to terminals is $E_{pass} = 1.7(V_{IC}-V_{OC})$.

When a larger aperture is used, a better signal-to-noise ratio can be obtained with a corresponding loss in energy resolution, and when a smaller aperture is used, the energy resolution is improved at the expense of the signal-to-noise ratio. The aperture diameter affects energy resolution and luminosity.

2.5.5 Application of the CMAs in the Coincidence Measurement

Both of the Cylindrical Mirror Analyzers (CMAs) are used in the time coincidence to measure the auger electron and the photoelectron. Suppose the Left hand CMA, call it LCMA, is used to measure the Auger electrons, and the Right hand CMA, call it RCMA, to measure the photoelectron. Figure (2.7) below, shows the configuration of the voltages applied to the Inner Cylinder (IC) and the Outer Cylinder (OC) of the CMA. In both the cases, the electron satisfying the condition of having its kinetic energy equal to the pass energy of the CMA will make it to the detector.

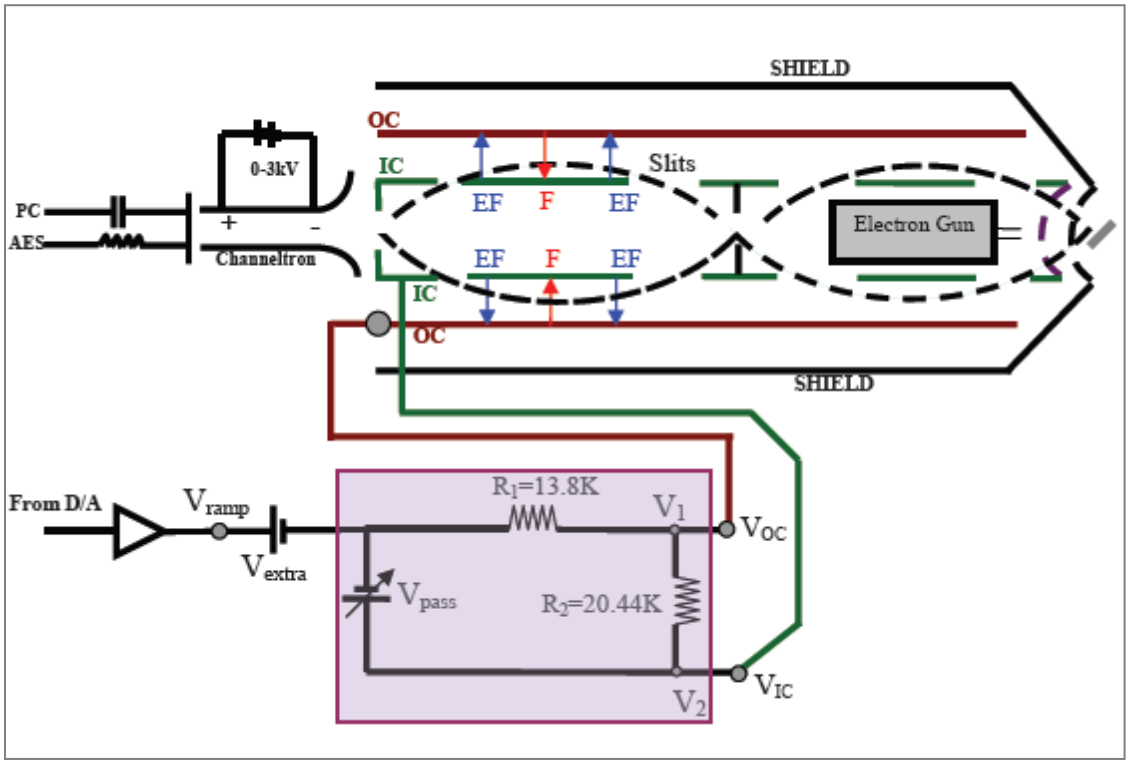

Figure 2.9 Schematics of the voltages supplied to the Inner and the Outer cylinder of a CMA

2.6 Coincidence Electronics

The block diagram in figure 2.8 shows the major components of the coincidence electronics. The output of the CMAs is taken to the Amplifiers and the Constant Fraction Discriminators. The amplified and discriminated signal from one of the CMA is used as the start signal of the time-to-amplitude converter (TAC). The signal from the second CMA is passed

through a delay to bring it to the positive time regime and is used as a stop signal to the TAC. The TAC output is proportional to the start and the stop pulse. Then the pulse height is recorded as histogram in the Micro Channel Analyzer (MCA). The pulses having a particular height are binned in the corresponding timing channel.

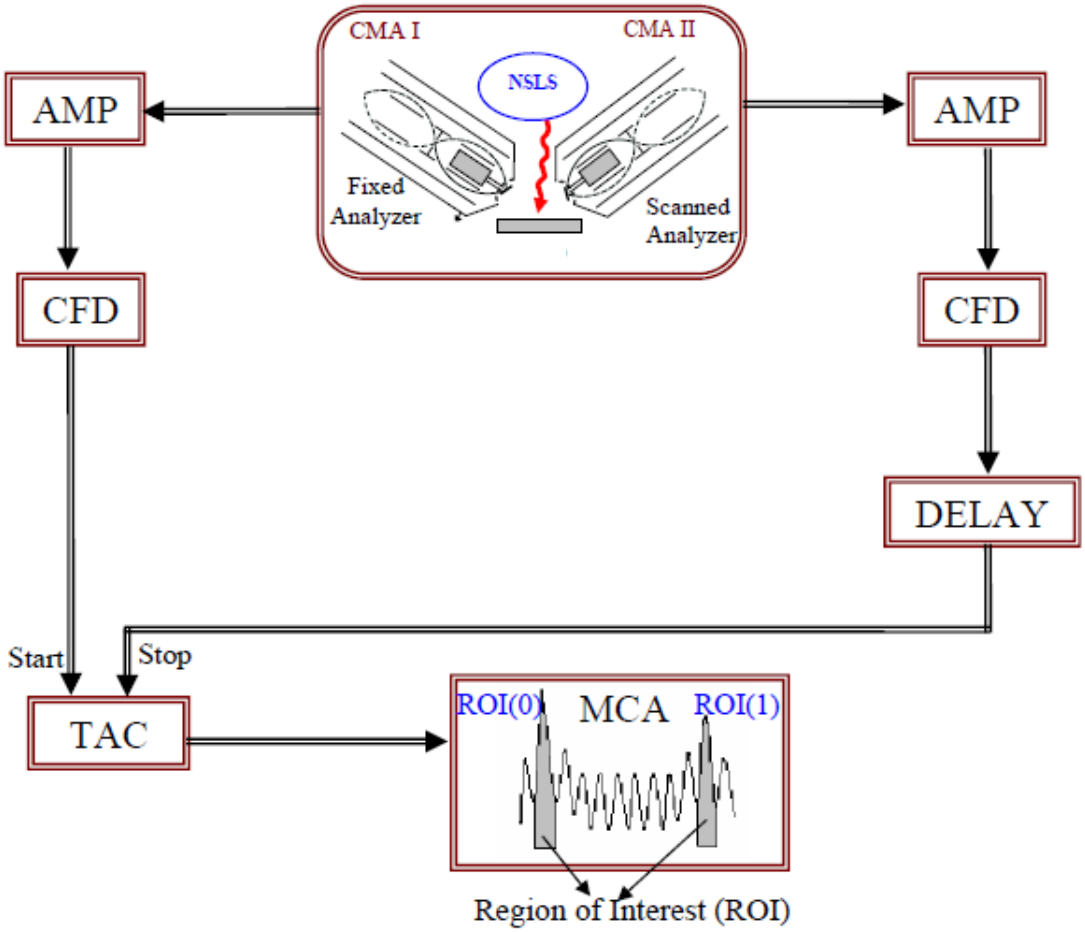

Figure 2.10 Block diagram of Coincidence Electronics

The Nim electronics and each of the individual components are explained below.

Amplifier: The model 612AM is a 6 channel NIM standard module. Each of the 6 channels uses two internal amplifiers to achieve a variable gain up to 40 times.

Constant Fraction Discriminator (CFD): The CFD helps to discriminate against the noise pulses by setting lower level below which the pulses are rejected. The constant fraction provides a way of minimizing timing walk due to pulse height variations.

Delay: The ORTEC Model 425A nanosecond delay unit was used to get a calibrated delay for any type of signal in 1ns in steps of 0 to 63 ns. Longer delays can be obtained by just cascading more of these units and using longer cables. The travel time in the cable is 1ns/ foot.

Time to Amplitude Converter (TAC): The ORTEC model 566 TAC was used to measure the time interval between the start and the stop.

Pulse Height Analyzer (PHA): The PHA was used to display the electron counts in the form of histogram as function of time. The total channels, 1024, were divided in 500ns and the incoming TAC pulse in volts is converted to time ~500ns and the time is converted into counting pulses of a particular height. Based on the voltage of the pulse the counts are put in the particular channel.

Region of Interest: there are two region of interest, ROI (0) and ROI(1). ROI(0) corresponds to the counts coming from both the true and the accidental coincidences. ROI(1) corresponds to the counts coming from the accidental events alone.

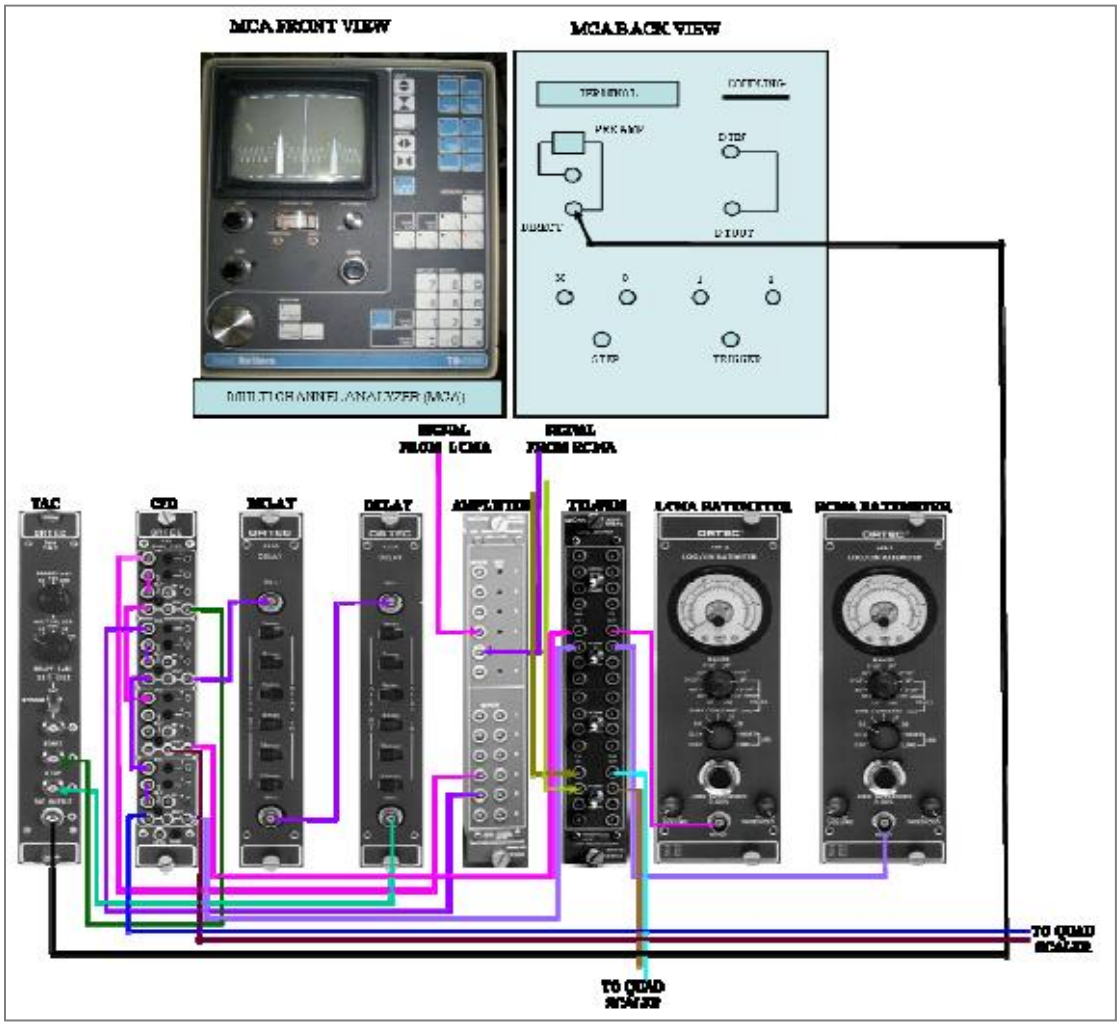

Figure 2.11 Circuit diagrams of the Nim bin constituents

2.7 Timing Electronics

Figure 2.10 shows the timing spectrum recorded by the MCA. The data are reflective of the timing structure of the synchrotron bunches. There are two peaks, which are significantly taller than the rest of the peaks. These peaks correspond to events in which both the pulses are detected by the CMAs at the same time ± 15ns correspond to electrons, resulting from photons from the same synchrotron bunch. This peak is the “coincidence” peak (C). The second large peak corresponds to electrons detected in CMA as the result of the bunch after it travels 170ns once around the ring. This corresponds to the detection of electrons resulting from two different

photon pulses. This peak is the “accidents” peak (A). The resulting spectrum is a result of the timing structure created by the 7 filled buckets out of the 9 buckets in the storage ring. This main peak which is labeled dt=0s is the coincidence peak which contains contribution from both true and accidental coincidences. dt is defined as the time between the emission of electrons into one CMA and the emission of electrons into other CMA. Its width is broadened by three factors:

a. The timing resolution of the CMAs
b. A small contribution (~1ns) from the width of the electron bunches in the storage ring
c. Some timing contributions from the electronic modules.

The other peak, labeled at dt = 170ns highlighted in the fig x is the accidental peak, which occurs 170ns after the coincidence peak. 170 ns correspond to the orbital period of the electrons in the storage ring. This accidental peak does not contain any true coincidence events. There are nine peaks between the coincidence peak at dt = 0ns time and the accidents peak at dt =170ns. These peaks have a different intensity when compared with the coincidence and the accidental peak. A detailed analysis show that the accidental intensity distribution follows a cyclical pattern, starting at the main coincidence peak, of 7/9, 6/9, 5/9, 5/9, 5/9, 5/9, 5/9, 5/9, 6/9, 7/9 and so forth as shown in the figure 2.11 [11].

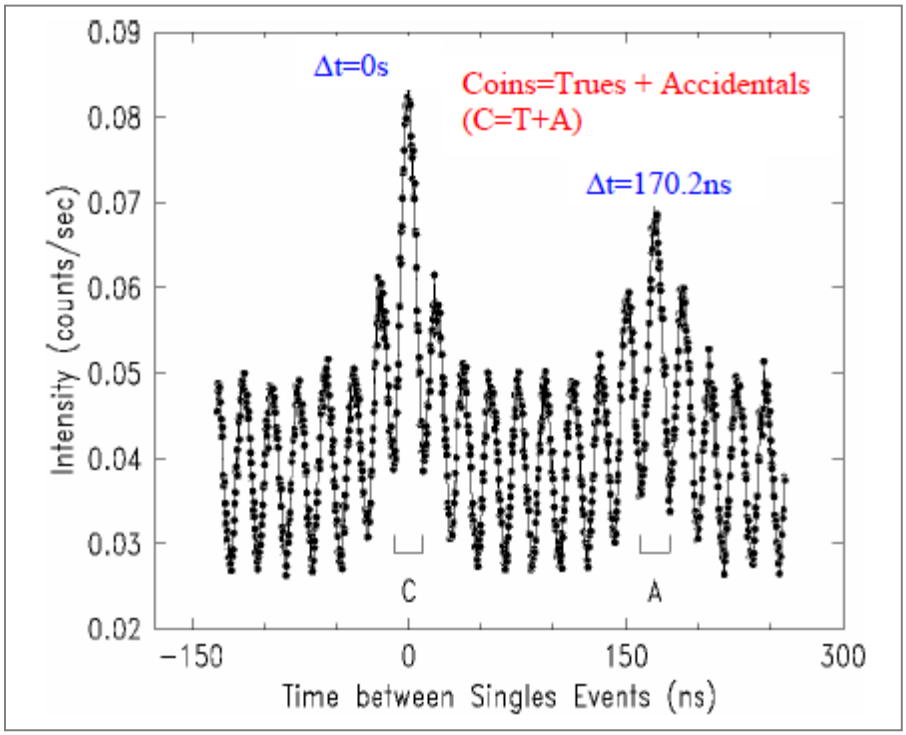

Figure 2.12 MCA timing spectra of the Synchrotron bunch from UV ring.

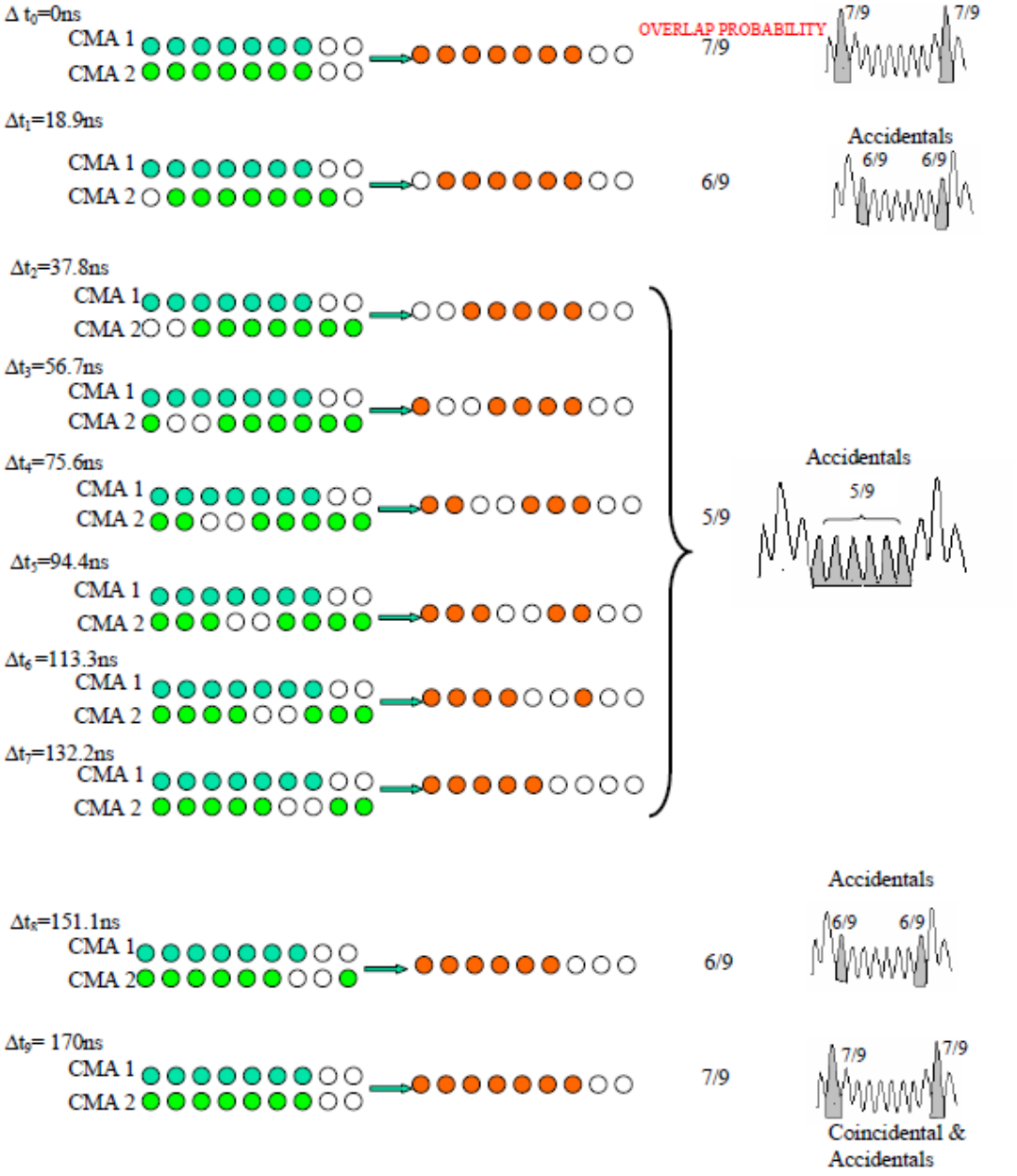

Figure 2.13 Overlap of the empty bunches with the filled bunches.

2.7.1 Coincidence and Accidents events from Synchrotron Radiation

There are nine buckets that revolve around the UV ring. Seven of them are filled with the electrons and the last two are empty. When the first bunch of electrons impinges on the sample it excites multiple atoms. If the photoelectron and the Auger electron come from the

same atom and are simultaneously recorded in the CMAs, it's called the true coincidence. But the CMAs can record the electrons excited from different atoms as they match the pass energy. These electrons are not from the same atom and are considered the accidental coincidence. These events also contribute to the ROI(0) as the true coincidences.

The second possibility of accidental coincidence happens when the second electron bunch from the UV ring comes after 18.9 ns following the first bunch. This sequence is shown in the figure (2.11) above. Here the CMA1 sees the events from 1^{st} electron bunch while the CMA 2 sees no electrons from the empty bunch. In similar fashion there are 6 possibilities of accidental events. There are 7 out of 9 filled bunches, so the probability of having accidental coincidences is 5 times in different combinations.

The other simple way to set ROI(0) and ROI(1) would be by increasing the incident flux to get better MCA spectra and good statistics; however, at the large flux makes the T/A ratio goes to zero. This is not a good way to collect coincidence data. Thus the incidence flux is maintained to keep the T/A ratio between 0.2-0.5.

The time interval between the excitation and the detection in CMA depends upon two factors, electron kinetic energy during the travel time from the sample to the CMA entrance mesh and the pass energy of the analyzers, which is fixed during our experiment. We change the kinetic energy while scanning the auger spectrum from 0 to 80eV. Since this range is large enough to affect the time interval, the timing windows has to be adjusted during each spectral sweep. In order to adjust the ROIs during each sweep, we first took the MCA timing spectra for a fixed kinetic energy corresponding to fixed CMA. Let's say for any fixed energy. We took the MCA timing spectra from 0 to 80eV and noted how the ROIs move as the CMA sweeps from low to high kinetic energy. The details of the MCA timing spectra are given in the next chapter.

CHAPTER 3

EXPERIMENTAL CONSIDERATIONS AND PROCEDURE

The phenomena occurring at the solid-vacuum interface can be studied using various probing methods. Some of the widely used techniques are EAES, XAES, PAES and APECS etc. These are the easy tools that can be used in quantitative surface analysis, such as the specific information about the core electrons, the valence band electron structure, and the chemical composition.

We used Auger Photoelectron Coincidence Spectroscopy (APECS) technique in the study of the correlation between the subsequently emitted electrons from the solid surface. As I mentioned in the introduction part in chapter one, when an atom is excited by sufficient photon energy the core atom is emitted out as a photoelectron, which is followed by the emission of Auger electron. Although these two events have a theoretical time difference, the photoelectron and the Auger electron is considered to be received at the detector simultaneously since the lifetime of the Auger decay is of the order of 10-15 seconds, while timing resolution of our lab equipments is about 10-9 seconds for all the electronic events. Two Cylindrical Mirror Analyzers (CMAs) were used; one to detect the photoelectron and the other was programmed to scan the low energy range which would contain the Auger peak.

The Cu(100) sample was sputtered and annealed and set in the data acquisition position. Before taking the coincidence data, the photon energy was set to 200eV and a wide range photoelectron spectrum, also called singles spectra, was taken. Fig3.1 shows the singles spectra taken at 200eV. The spectrum shows the valence band peak, the core peaks, the auger peaks and the huge secondary electron peak extending in the low energy range of the spectrum. The figure also shows the relative intensity of the peaks. All the peaks are hidden in the gigantic region of secondary electron spectrum. The singles spectra were taken at different

photon energies as well. It shows that the Auger energy for copper is constant and is seen at 55eV. The electrons counts have significantly reduced in the secondary electron peak and the valence band peak. Also the valence band peak shifts to left as we reduce the photon beam energy.

While taking the singles spectra only one of the CMAs was used to scan the whole range.

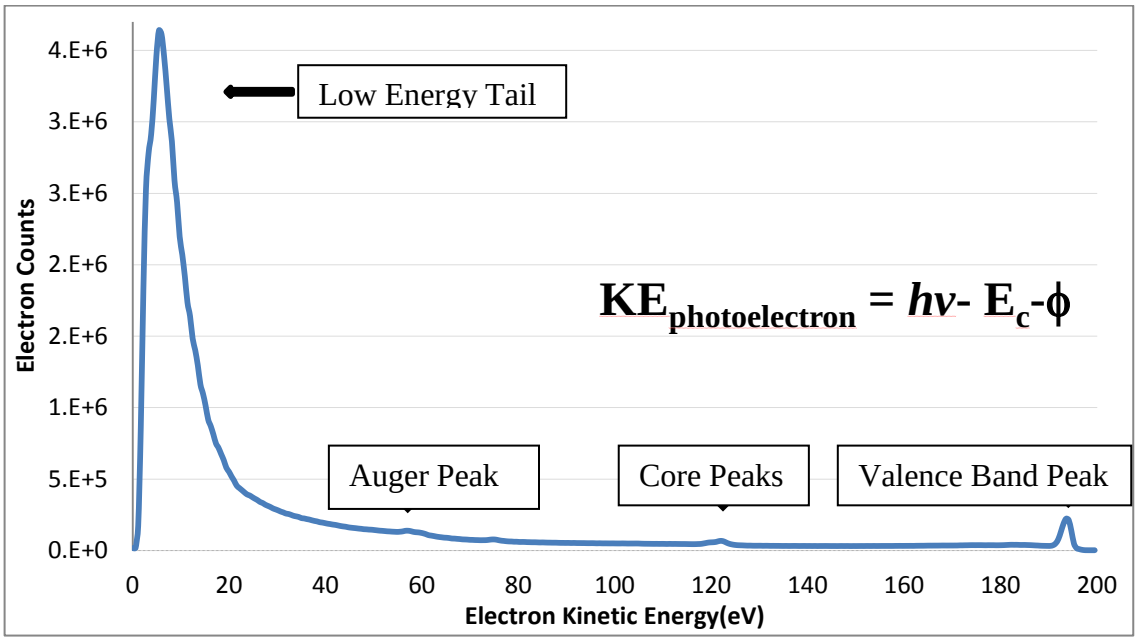

Figure 3.1 Photoelectron singles spectra taken at 200eV photon energy

3.1 Sample Sputtering and Annealing

The Cu(100) single crystal sample used in this APECS experiment was 10 mm in diameter and had 3 mm thickness. The sample was sputtered every other day with Ar+ ion bombardment for 20 minutes. The sputtering was followed by annealing the sample to 600° Centigrade by the radiative heating by a filament fixed right behind the sample. The filament was current was set to 20 A. The potential difference of 1000kV was applied between the sample and the filament to increase the heating rate. The temperature was monitored by connecting the thermocouple to the sample and to a voltmeter. When the voltmeter reading was 25mV the voltage and current supply was turned off. The equivalent of 25mV is 600° C.

3.2 MCA Timing Spectra

As it was mentioned in the previous chapter that the time interval between the photoelectron excitation and its travel time to the CMA entrance mesh is primarily affected by the electron kinetic energy. Since we are doing the coincidence spectroscopy where the true counts were taken from the difference of the Coincidence and the Accidents events, it is of vital importance that we first note how the MCA timing spectra would vary when the electron kinetic energy would change from 0 to 70 eV. While the Scanning CMA would scan this range, the right hand CMA (RCMA) was fixed at one energy value. So, throughout the experiment, every time we changed the fixed energy the MCA timing spectra was taken for each energy point. Figure 3.2 and figure 3.3 show the timing spectra taken before the coincidence data was taken for the Auger spectrum with the fixed analyzer at 121.25eV. The ROI(0) and the ROI(1) had the channel difference of 434 and would shift at the equal rate. Figure 3.4 shows the MCA spectra for 121.25eV fixed electron energy and the scanning CMA at different energy points, from 0 to 70eV.

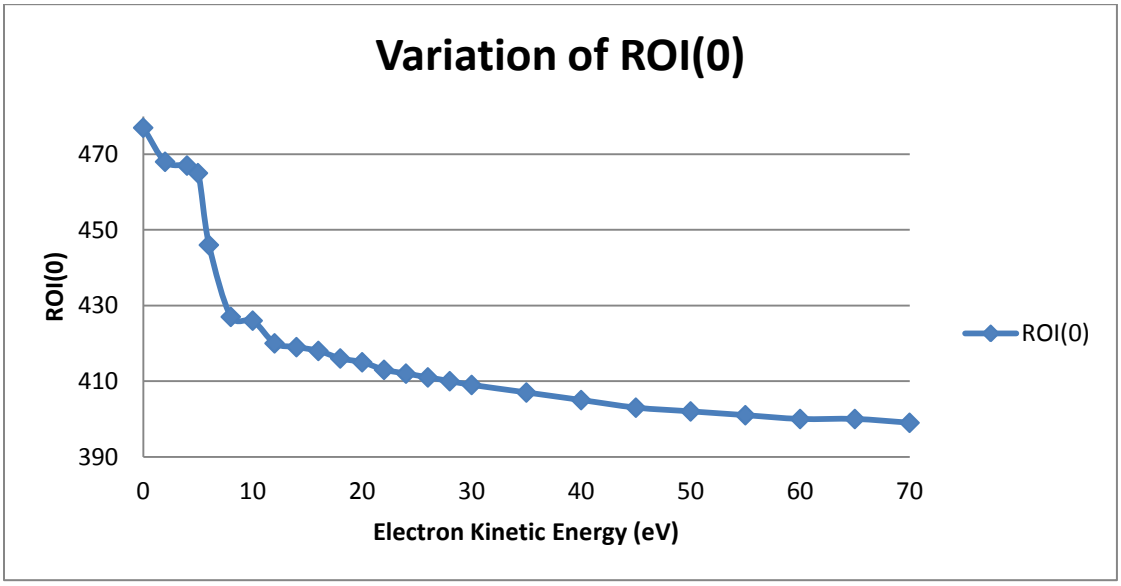

Figure 3.2 The shift of the ROI(0) as the electron kinetic energy changes from 0 to 70eV

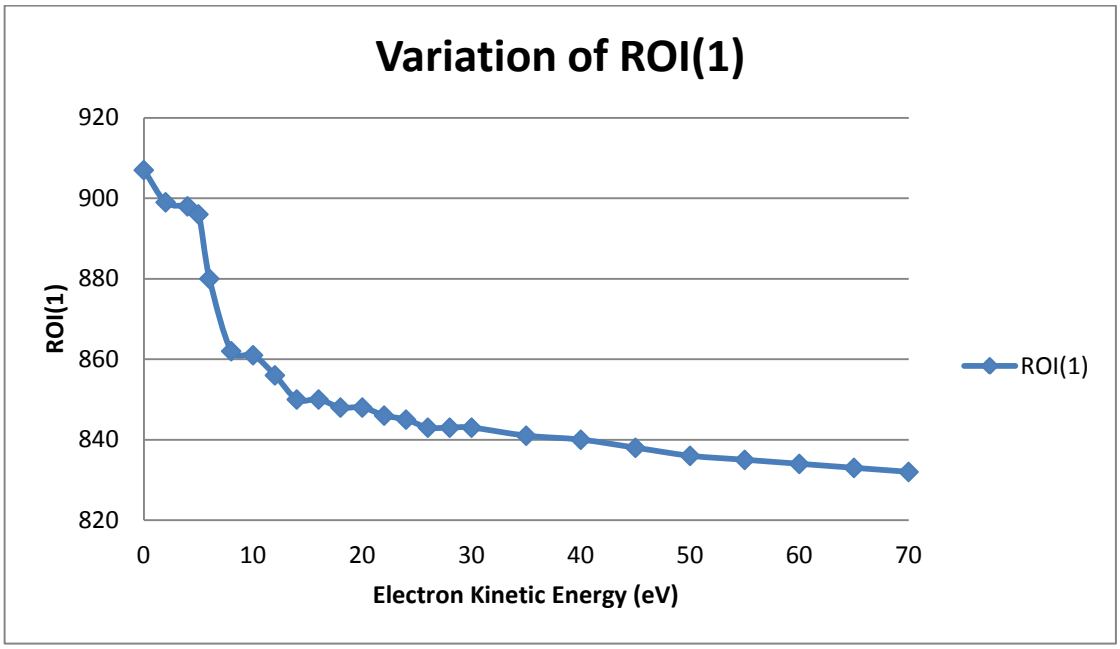

Figure 3.3 The shift of the ROI(1) as the electron kinetic energy changes from 0 to 70eV

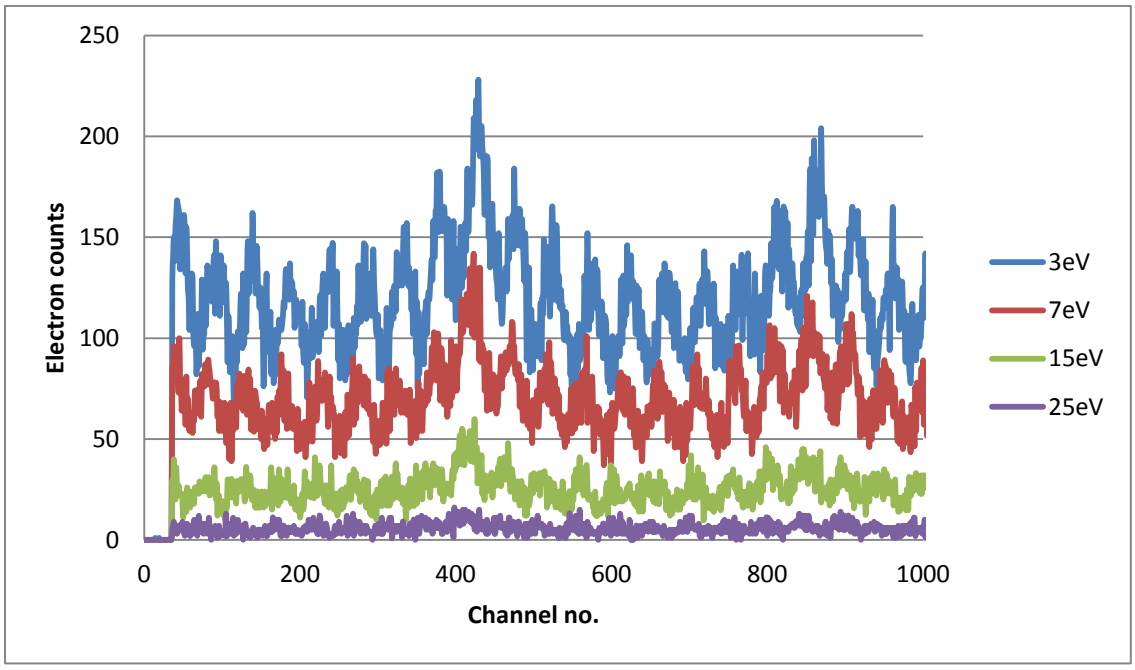

Figure 3.4 MCA spectra for 121.25eV fixed energy and the different electron energy. It shows how the Coincidence and the Accidents peak shift

Most part of our experiment is based on taking the background coincidence data by having one of the CMAs fixed at various energies between the core peaks and the valence

band. For that we needed to find out how the ROIs move for each of the fixed energies. Thus we took the MCA timing spectra for each of those energies to how changing pattern of the ROIs. Figure 3.5 shows the variation of the ROIs with respect to different kinetic energies. The curves were then fitted in the Origin, double exponential form, and the curve fit equations were used to rewrite the program algorithm that controls the MCA-PC communication.

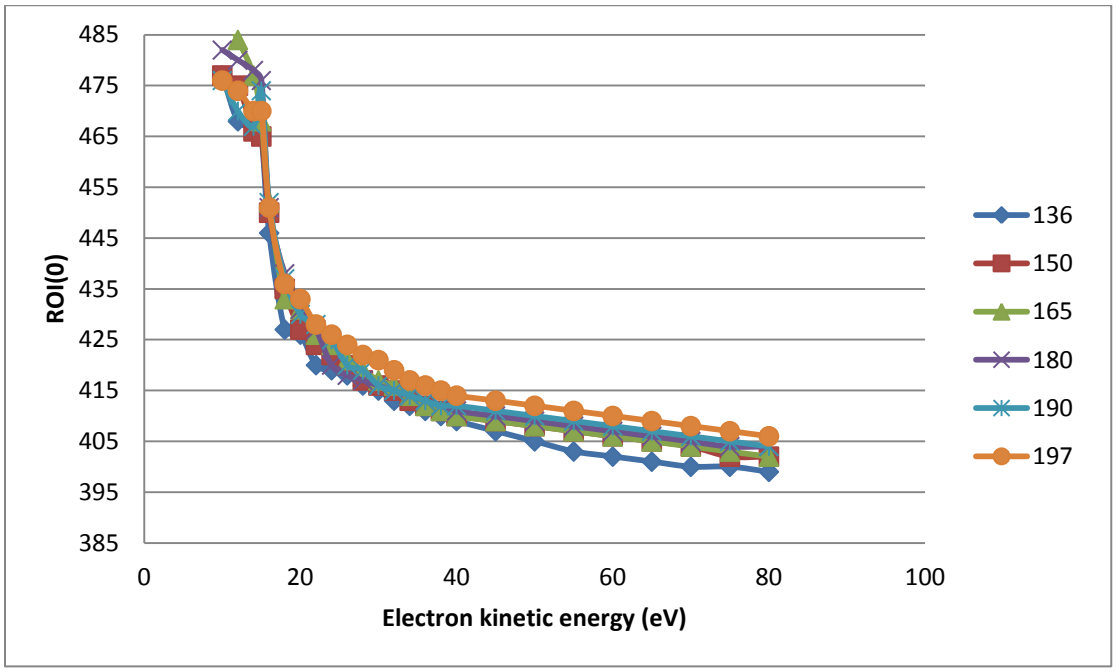

Figure 3.5 Variation of ROI(0) with respect to various Fixed Kinetic Energies. The photon energy was 200eV and 15V sample bias

3.3 ORIGIN Curve Fits

For each of the MCA timing spectra, the ROIs vs. Electron Kinetic energy, was fitted with double exponential curves in the ORGIN and the equation thus obtained was used in the program algorithm while taking data. This would produce the better T/A ratio as the subtraction of the coincidence and accidents events are now more accurate. As shown in figure 3.5 above, the peaks are shifting to the left as we go higher in the electron kinetic energy. One of the examples of the Origin curve fit is shown below in figure 3.6.

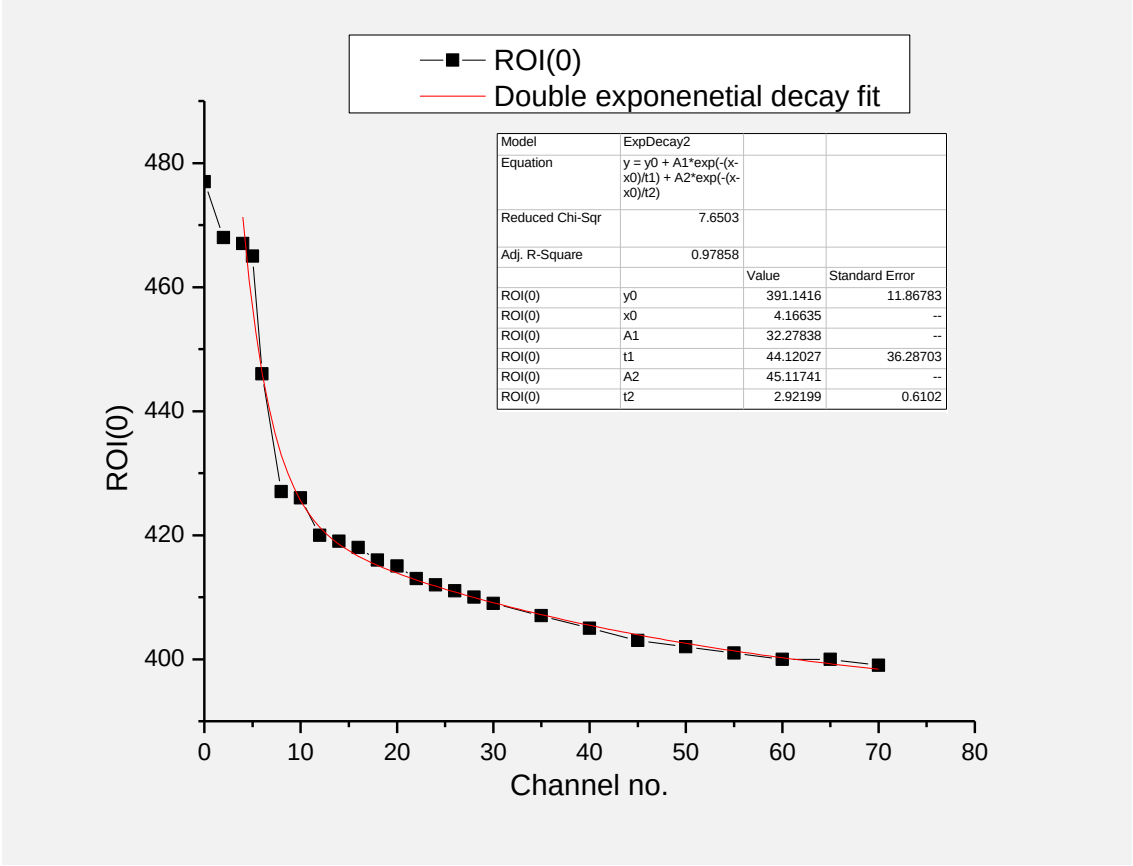

Figure 3.6 Showing the Origin curve fit of the MCA timing spectra for the ROI(0) and the Electron kinetic energy

3.4 APECS Experiments

The high statistics singles spectra of the core peaks was taken to locate the energy of the $3p_{3/2}$ peak while 200eV photon energy was incident on the sample. Figure 3.7 shows the core peaks due to $3p_{1/2}$ and $3p_{3/2}$. The other singles spectra in figure 3.8 shows the Auger peaks due to M_2VV and M_3VV Auger transition. We decided to fix our RCMA to the core energy of 121.25eV while the LCMA would scan the range from 0 to 70eV containing the secondary electron spectrum and the Auger spectrum.

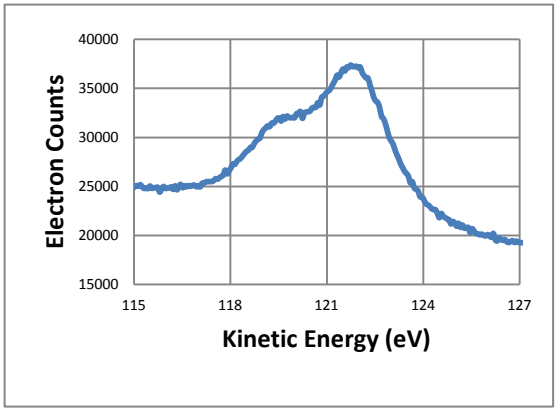

Figure 3.7 Singles spectra of the core peaks

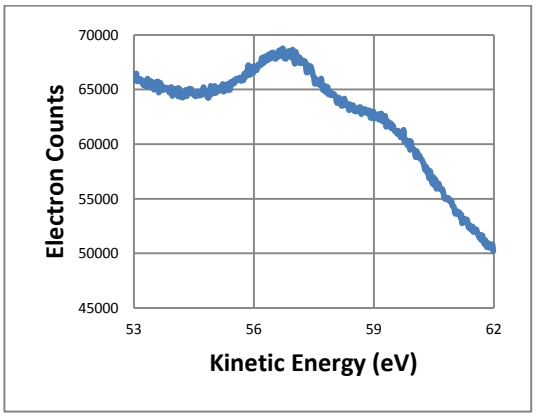

Figure 3.8 Singles spectra of the Auger peaks

3.4.1. Auger Electrons in Coincidence with $3p_{3/2}$ Core Electrons

The photons from the synchrotron radiation with 200eV energy were guided through the high vacuum beam and to the sample. The atom absorbing the sufficient energy emits the core photoelectron of energy 121.25 energy and makes it through the RCMA to the electron analyzer and to the TAC as a start single. The ionized atom now de-excites by the transition of electron from the valence band to the core. The energy released in the decay process is transferred to the neighboring valence band electrons, which come out of the sample as the Auger electrons and/or the Auger induced secondary electrons. The Auger electrons and/or the secondary electrons then make it through the LCMA to the electron analyzer and to the TAC as a stop signal. The 200eV photons were used to create a hole at the 3p sub-shell of M core shell. The electron that emits out of the sample is from the valence band and is called M_3VV Auger electron, the process shown schematically in the figure 1.1.The final state of the CVV Auger transition consists of two holes at the valence band unless it's a CVVV Auger transition, which will be discussed later.

3.4.2. LET in Coincidence with the Inelastic Scattering of the Valence band Photoelectrons

The beauty of the APECS is that it significantly reduces the background contribution due to the beam induced secondary electrons and the Auger spectral line is much prominent compared to the singles spectra taken in non-coincidence. However, the low energy section of

the APECS Spectrum contains the secondary electron contribution due to the true coincidence between photo emitted valence band electrons that undergo inelastic scattering. This happens because of our coincidence technique itself. When photons are incident on the sample they not only excite the core electrons but also excite the valence band electrons. And if any valence band electron leaves the sample with the energy that is equal to the fixed CMA energy it is recorded as a start signal, shown in figure 3.9. Remaining of the energy (Δ eV) is now transferred to the other valence electrons which are detected by the scanning CMA. And hence they end up contribution to the secondary electron spectrum of the Auger spectra. This contribution is due to the events that are unrelated to the Auger excitation process.

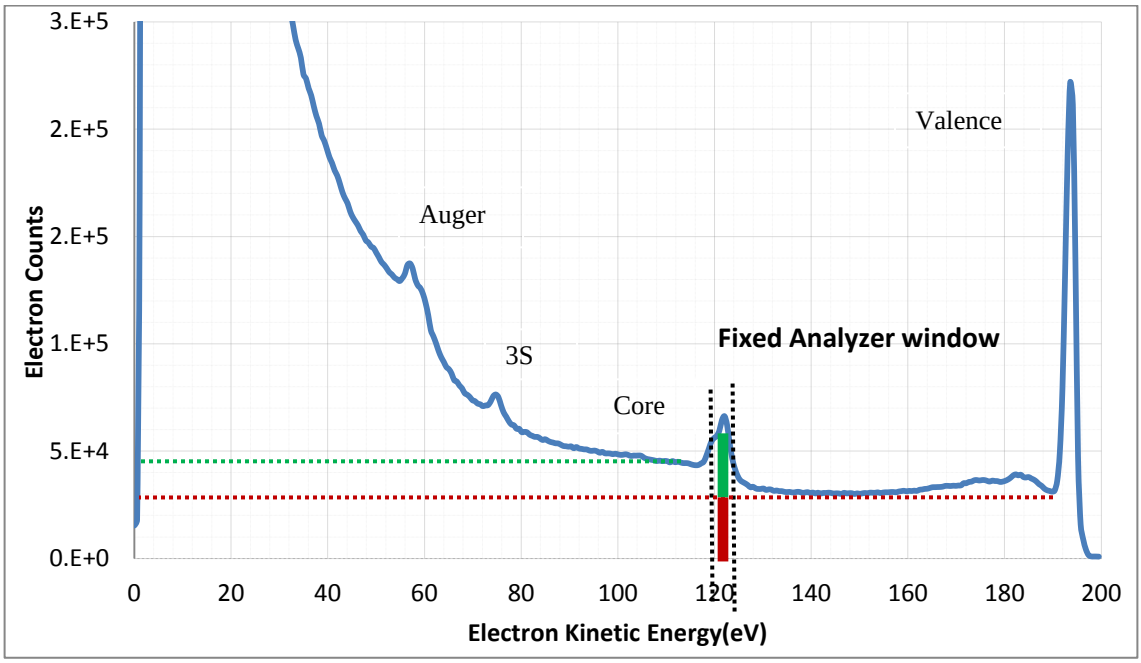

Figure 3.9 Cu(100) photoelectron spectrum. The red window shows the inelastically scattered valence band photoelectrons that are detected in the fixed analyzer.

The background contribution from the inelastic scattering of the photoelectrons is observed exclusively between the 3p Core peak and the valence band peak. The valence band peak sits on the plateau of the secondary electrons that extends further down to 0eV, as shown in figure 3.1. The figure also shows that the Core peak lies on top of this plateau, while the Core itself entails the secondary electrons spectrum further down to 0eV. Therefore, the LET consist

not only the inelastic scattering of the 3p photoelectrons but also the inelastic scattering of the valence band photoelectrons. The LET of the Cu(100) Auger Spectrum contains the significant number of secondary electrons from the events that are unrelated to the hole excitation process. In order to have the better quantitative analysis of the Auger spectra, it is important to remove the APECS LET from the Auger spectra leaving the secondary electrons contribution coming out from the 3p core excitation process only. To remove the contribution from the inelastic scattering of the valence band photoelectron, same coincidence technique is applied but in a different way, as explained below.

The contribution to the LET portion seems to increase as we increase the difference between the core and valence band energy. So, a series of background coincidence measurements were made between the valence band and the core peak. The fixed analyzer energy was randomly chosen to be at 150eV, 165eV, 180eV, 190eV and 197eV for photon energy of 200eV and after considering the sample bias of 15V. To test our assumption first took the background coincidence measurement by setting the fixed analyzer at the Fermi level. The background contribution from this level was expected to be ~0.

When the photons of 200eV energy is incident on the sample, for the first background measurement at 150eV, we can think of it as the first analyzer sucking up this energy and leaving 50eV minus the work function of the sample to redistribute among the other valence electrons. So the one or multiple valence electrons with total energy of 45eV will be sucked up by the scanning CMA and end up contributing to the LET.

Referring to equation (1.8) from the chapter 1, we can calculate this Δ energy that is distributed among the valence electrons,

$$KE_{InelasticValence1} = hv - E_{V1} - \Delta - \phi$$

$$\Delta = hv - KE_{InelasticValence1} - E_{V1} - \phi \quad (3.1)$$

Where, $KE_{InelasticValence1}$ represents the energies at which the fixed analyzer is set, starting with 150eV as mentioned above.

hv = photon energy

E_{V1} = Binding energy of the outgoing valence electro

= 0eV for the case of Fermi level electrons

ϕ = Work function of the sample

= 4.59 for Cu(100) single crystal

All the background coincidence experiments were carried by applying 15V bias to the sample. Using equation (3.1) the Δ values for the chosen fixed energy analyzer values were calculated, as shown in table 3.1 below.

An electron in the valence band absorbs this Δ energy and emits out towards the vacuum with an energy given by equation (1.9),

$KE_{InelasticValence2} \leq \Delta - E_{V1} - \phi$

This is the threshold value below which the contribution from the inelastic scattering of the valence band electrons would be observed in the LET region. The $KE_{InelasticValence2}$ values for different fixed analyzer energy values are calculate using equation (1.9) and tabulated in table 3.2.

Table 3.1 Fixed analyzer energies with their corresponding Δ values

Fixed Analyzer Energies	Δ(eV)
150eV	53.5eV
165eV	38.5eV
180eV	23.5eV
190eV	13.5eV
197eV	6.5eV
208eV	~0eV

Table 3.2 Energy of the Inelastic Scattering of the Valence band Photoelectron

Fixed Analyzer Energies	$KE_{InelasticValence2}$
150eV	≤ 54eV
165eV	≤39eV
180eV	≤24eV
190eV	≤14eV
197eV	≤7eV
208eV	~0eV

Using the singles spectra taken by photon energy of 200eV plus the 15V sample bias fixed energy values were marked, as shown in figure 3.10.

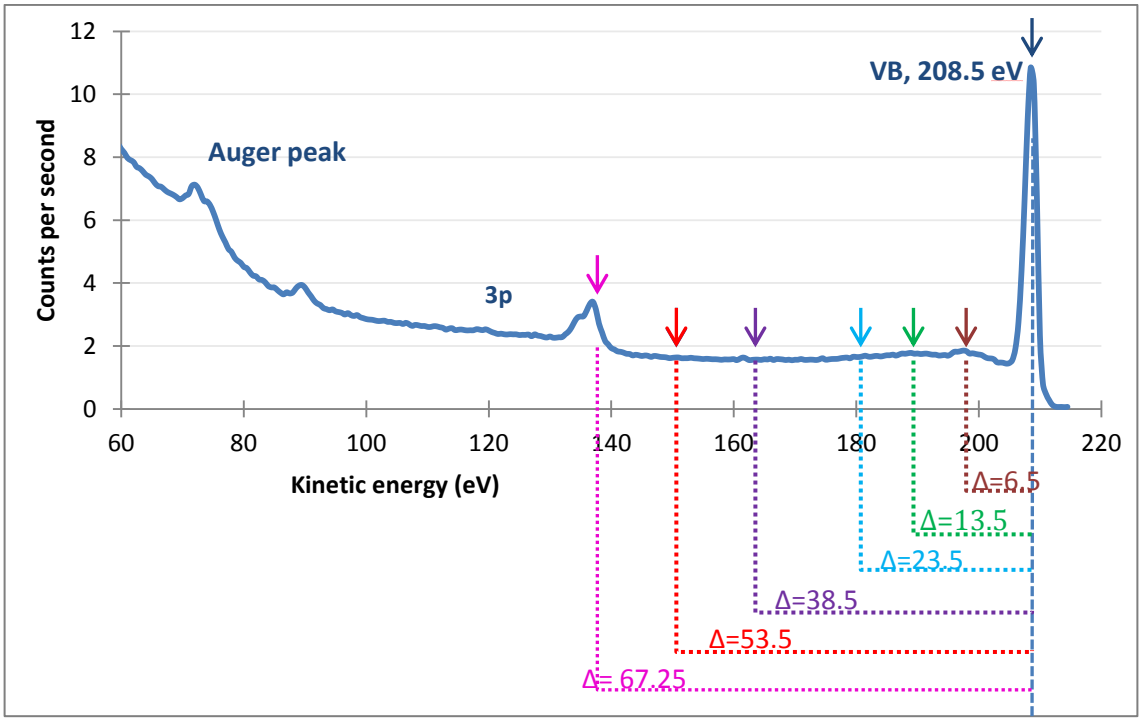

Figure 3.10 Cu(100) photoelectron spectrum at hv = 200eV, and 15V sample bias. The fixed analyzer positions are shown and the respective Δ values are indicated.

3.4.3 Correction of the TRUE Coincidence Data

So far in the APECS experiments conducted using the photons form the synchrotron radiation the True counts were considered as the difference of Coincidence and Accident events. Considering the TAC start and the stop failures we make slight changes to the traditional method of obtaining True counts by developing a new formula to calculate Corrected TRUES.

$$\text{Define, } \varepsilon = \frac{\#\ of\ times\ TAC\ is\ Started\ and\ NOT\ stopped\ by\ t{=}t1}{\#\ of\ times\ TAC\ is\ Started} \tag{3.2}$$

But TAC is either Stopped or NOT stopped, so we can now write,

$$1 = \frac{\#\ of\ times\ TAC\ is\ Started\ and\ NOT\ stopped\ by\ t1}{\#\ of\ times\ TAC\ is\ Started} + \frac{\#\ of\ times\ TAC\ is\ Started\ and\ is\ Stopped\ by\ t1}{\#\ of\ times\ TAC\ is\ Started}$$

The first term in the above equation is what we have defined as the efficiency, ε in equation 3.2. Therefore,

$$\varepsilon(t_1) = 1 - \frac{\#\ of\ times\ TAC\ is\ Started\ and\ is\ Stopped\ by\ t1}{\#\ of\ times\ TAC\ is\ Started}$$

$$= 1 - \frac{\#\ of\ Counts\ (0<t<t1)}{(\#\ of\ starts/sec)(live\ time)}$$

$$= 1 - \frac{\#\ of\ Counts\ (0<t<t1)}{(\#\ of\ Fixed\ Counts)(\frac{livetime}{Realtime})} \tag{3.3}$$

Now, since the True counts is the difference of Coincidence and Accident events,

$$T = ROI(0) - ROI(1) \tag{3.4}$$

But instead the corrected formula is given by,

$$T = ROI(0)/\varepsilon(t_0) - ROI(1)/\varepsilon(t_1) \tag{3.5}$$

Where t_0 is stopping time of the ROI(0) and t_1 is the stopping time of the ROI(1). $\varepsilon(t_0)$ and $\varepsilon(t_1)$ were calculated using equation 3.3. To get the number of counts for $(0<t<t_1)$, the number of fixed counts, and the live time, the MCA timing spectra was taken for each energy point from 0 to 70eV.

CHAPTER 4

EXPERIMENTAL DATA AND ANALYSIS

4.1 Cu(100) Photoelectron Spectra

With one of the CMAs scanning the wide range, large aperture, the photoelectron spectra, also known as singles spectra was taken, shown in figure 4.1. If both the analyzers are used it's called doubles spectra, or popularly known as coincidence spectra. Since only one analyzer is used to collect the photoelectron spectra, it's called singles spectra.

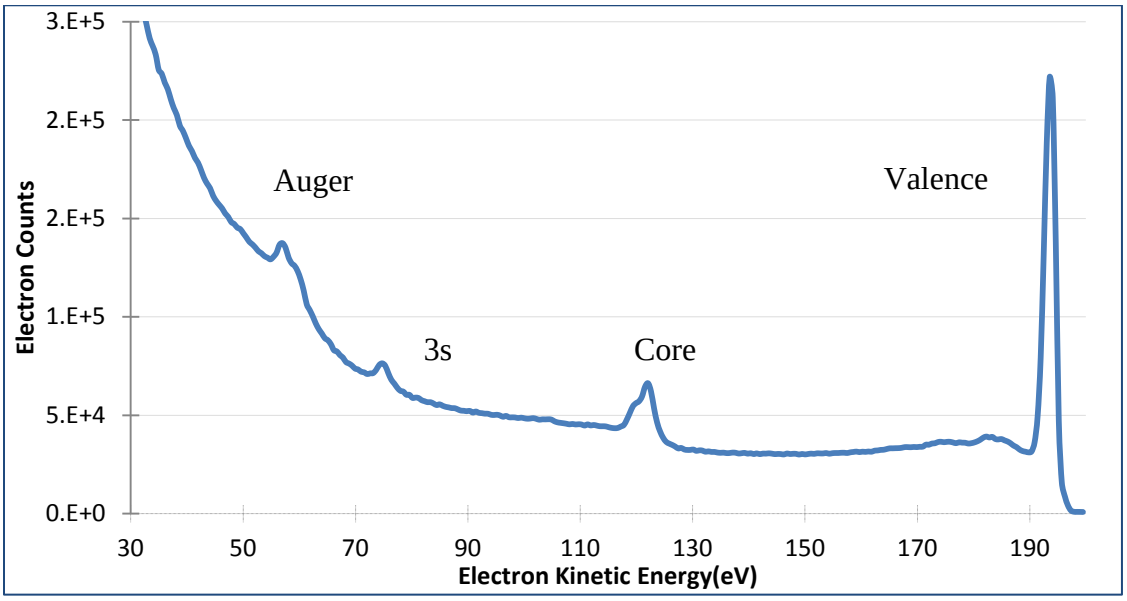

Figure 4.1 Cu(100) Photoelectron spectra taken at with 200eV photons and 15V sample bias

4.1.1 Singles Spectra for Different Photon Energy

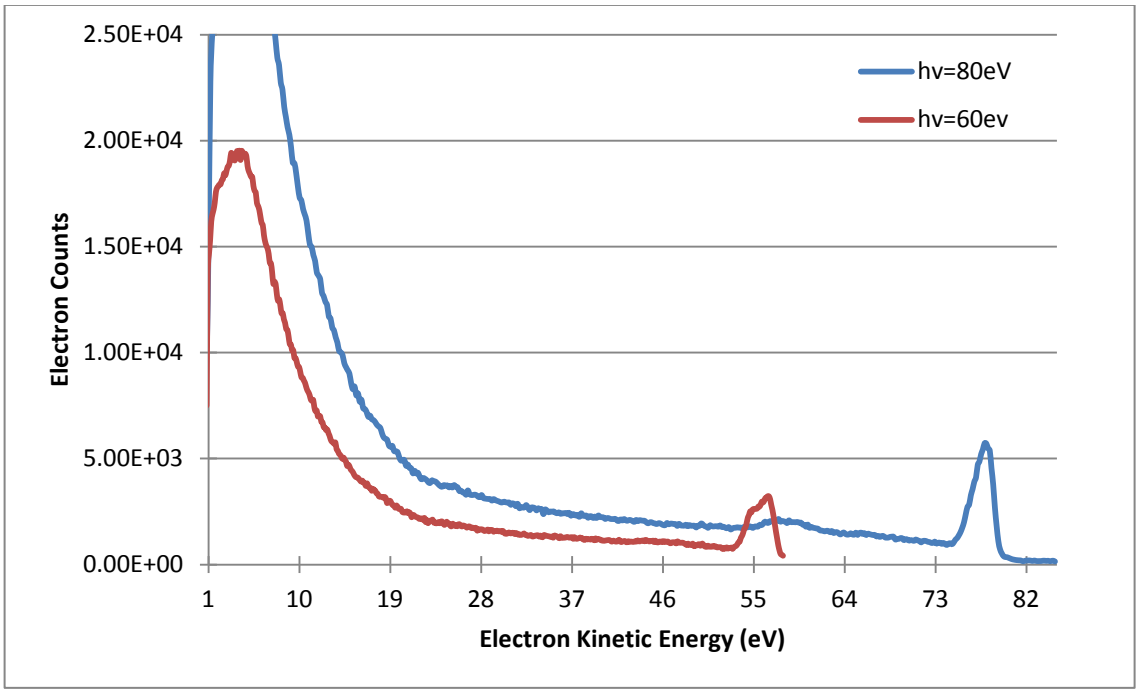

Figure 4.2 Singles spectra taken with two different photon energies

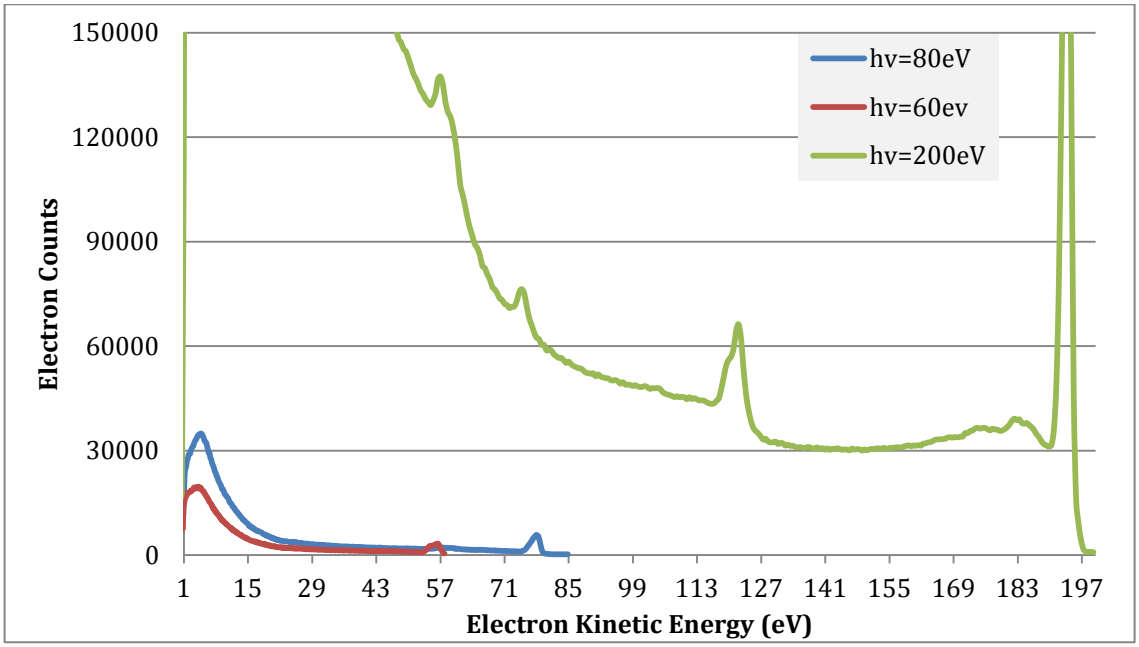

Figure 4.3 Singles spectra taken with two different photon energies. For lower photon energy, the contribution to the secondary electron spectrum is reduced significantly and the valence band peak shifts to the left as the photon energy is reduced

4.2 Cu(100) M_3VV A PECS Auger Spectrum

From the singles spectra taken about the core region of the Cu(100) with the photon energy of 200eV , we identified the $3p_{3/2}$ peak whose energy is 121.25eV. The fixed RCMA analyzer was set at 3p3/2 energy while the second LCMA was used to scan the LET range along with the Auger peak, from 0 to 70eV. The graph in figure 4.5 shows the spectrum for True counts and the Corrected True counts. As discussed in section 3.5.3 the True counts are not just the difference of the Coincidence and the accident events but each events divided by the efficiency $\varepsilon(t_0)$ and $\varepsilon(t_1)$ given by equation (3.5).

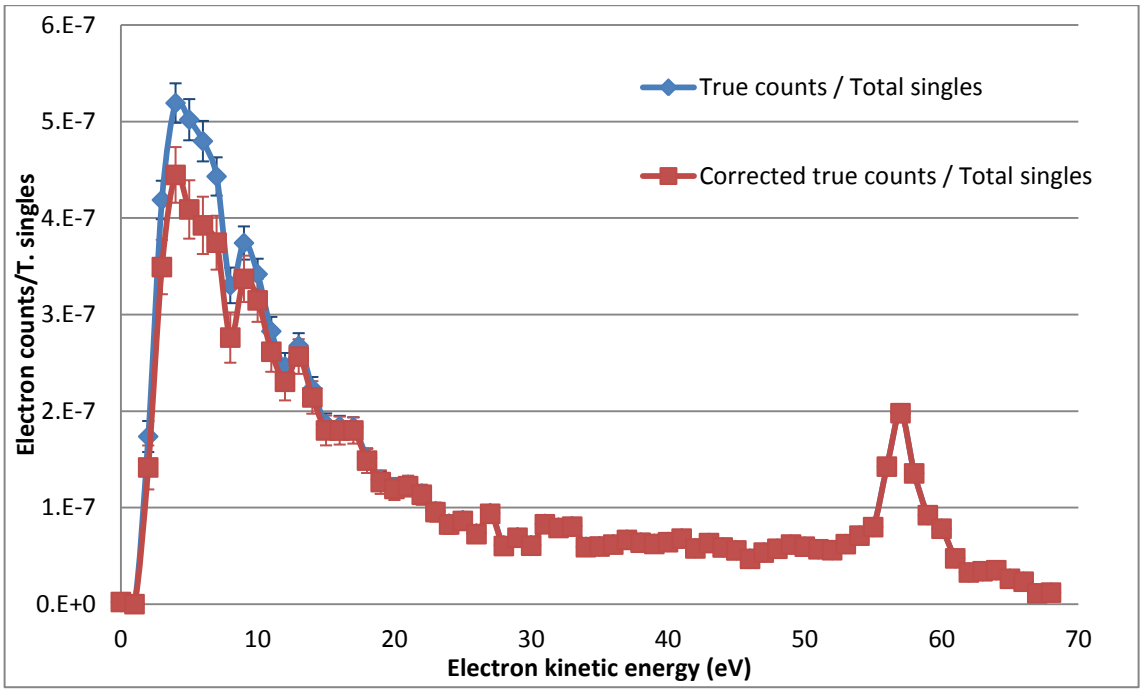

Figure 4.4 APECS Auger spectra showing the True counts taken from the MCA vs. the corrected True counts based on the calculations we made in section (3.5.3)

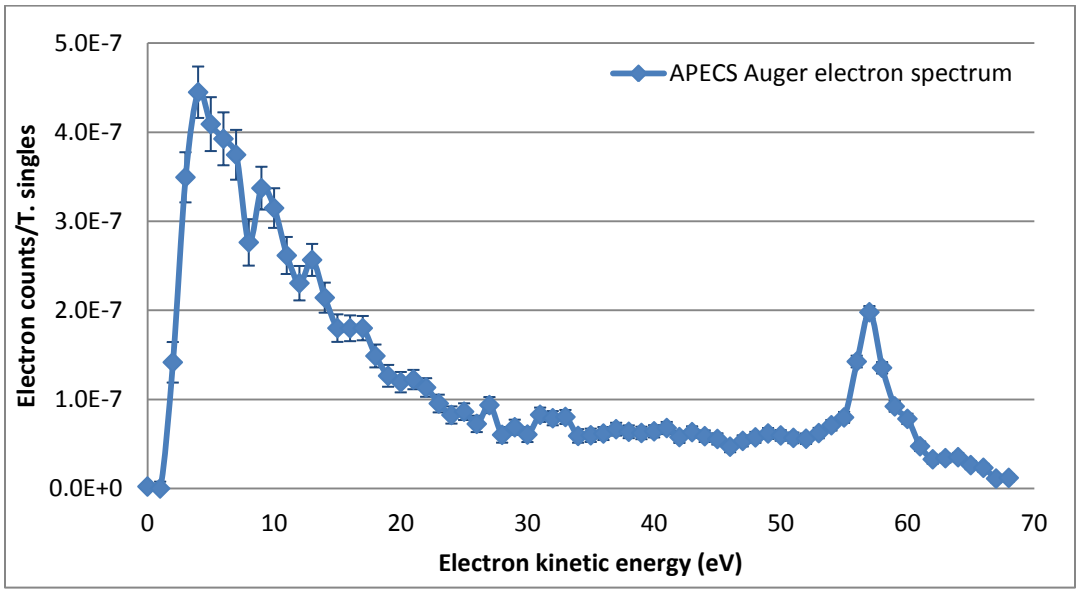

Figure 4.5 Cu(100) M_3VV APECS Auger Spectrum

4.2.1 Comparison of APECS spectrum with Photoelectron spectrum

One of the beauties of the APECS technique is that it significantly reduces the background contribution due to the secondary electrons. Figures 4.7 and 4.8 compares the two spectra. The APECS spectrum is 10^{10} times what it was obtained from the coincidence measurements.

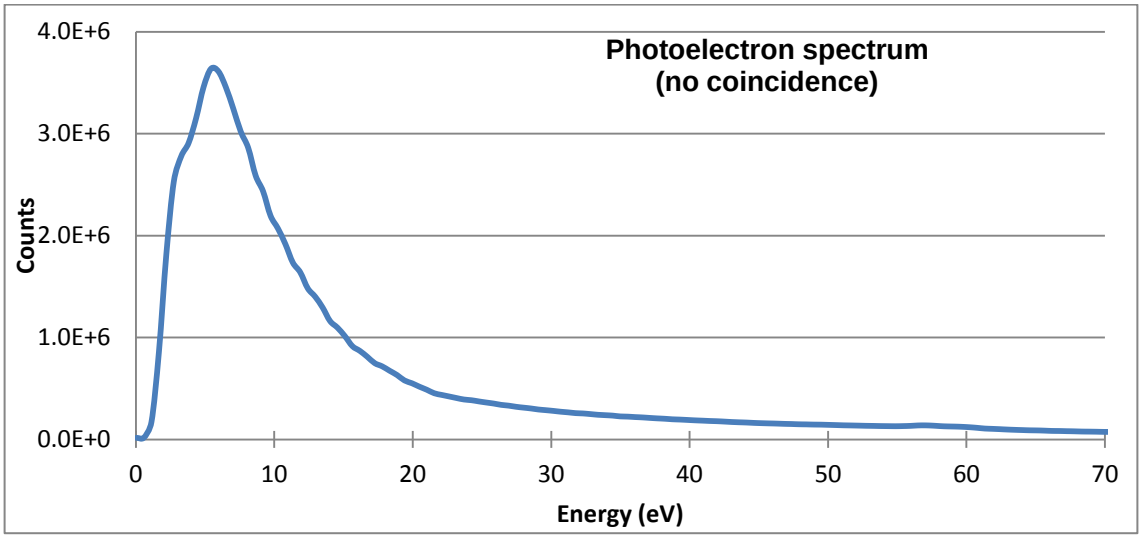

Figure 4.6 The photoelectron spectrum taken with the same photon energy of 200eV

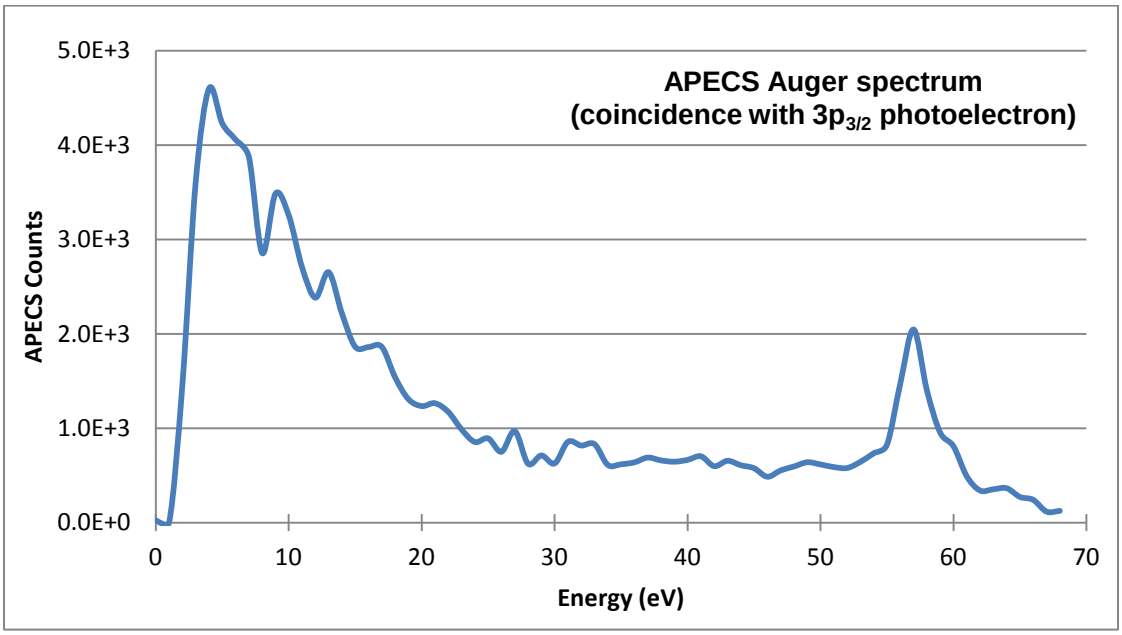

Figure 4.7 The APECS Auger Spectrum taken in coincidence with $3p_{3/2}$ core peak.

4.3 Extrinsic Contribution to the LET of the APECS Auger Spectrum

The LET intensity associated with the Auger spectrum can be separated into two types, Extrinsic and Intrinsic contributions [13-14]. The contribution to the extrinsic part is caused by the primary beam and the inelastic scattering of the Auger electrons. Since we used the Coincidence technique in our experiment there is no contribution to the LET from the beam induced secondary electrons. However, as we discussed earlier, the LET of the APECS consists of the accidental coincidence events from the valence band. Schematic description is shown in figure (1.2). This inelastic scattering of the valence band electrons are the primary cause of the APECS LET. First part of this experiment is focused to estimate and eliminate this contribution from inelastic scattering of the valence band electrons.

In the scenario of the inelastic scattering of the valence band electrons when a photon of energy hv is incident on the sample, a photoelectron is emitted with the energy equal to the fixed analyzer pass energy (136.25eV). The remainder of the photon energy, ΔeV is transferred to the neighboring valence band electrons. The Δ value is given by equation (1.8) and the

electrons absorbing this energy are emitted out into the vacuum with the energy ≤ ΔeV, hence satisfying the principle of Conservation of Energy.

4.3.1 Coincidence Measurement of Inelastic Scattering of the Valence band electrons at 150eV

With the fixed analyzer set at 150eV, the scanning CMA was used to sweep the energy range of 0 to 70eV. The figure 4.6 below shows the contribution to the secondary electron spectrum from 200eV photons when the coincidence measurement was made with the valence band photoelectron of 150eV. As discussed in section 3.5.3 the True counts are not just the difference of the Coincidence and the accident events but each events divided by the efficiency $\varepsilon(t_0)$ and $\varepsilon(t_1)$ given by equation 3.5, $\Delta - \phi = 208.5 - 150 - \phi = 53.5$ eV**.**

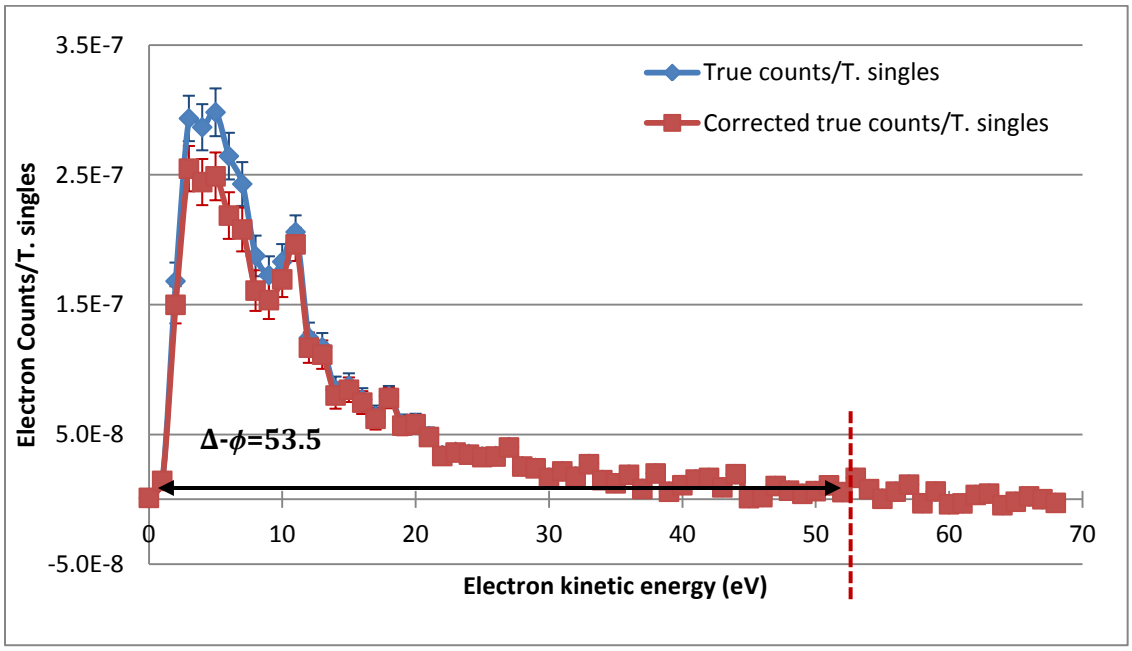

Figure 4.8 EECS Spectrum with the fixed analyzer set at 150eV valence band photoelectron energy

The spectra have been shifted by 15eV to account for the sample bias. The Δ value, the redistributed energy among the valence band electrons is seen to have contributed to the low energy side from 0 to 60.5eV, calculated from equation (3.1).

4.3.2 Coincidence Measurement of Inelastic Scattering of the Valence band electrons at 165eV

With the fixed analyzer set at 165eV, the scanning CMA was used to sweep the energy range of 0 to 70eV. The figure 4.7 below shows the contribution to the secondary electron spectrum from 200eV photons when the coincidence measurement was made with the valence band photoelectron of 165eV. As discussed in section 3.5.3 the True counts are not just the difference of the Coincidence and the accident events but each events divided by the efficiency $\varepsilon(t_0)$ and $\varepsilon(t_1)$ given by equation (3.5), $\Delta\text{-}\phi = 208.5 - 165 - \phi = 38.5$ eV

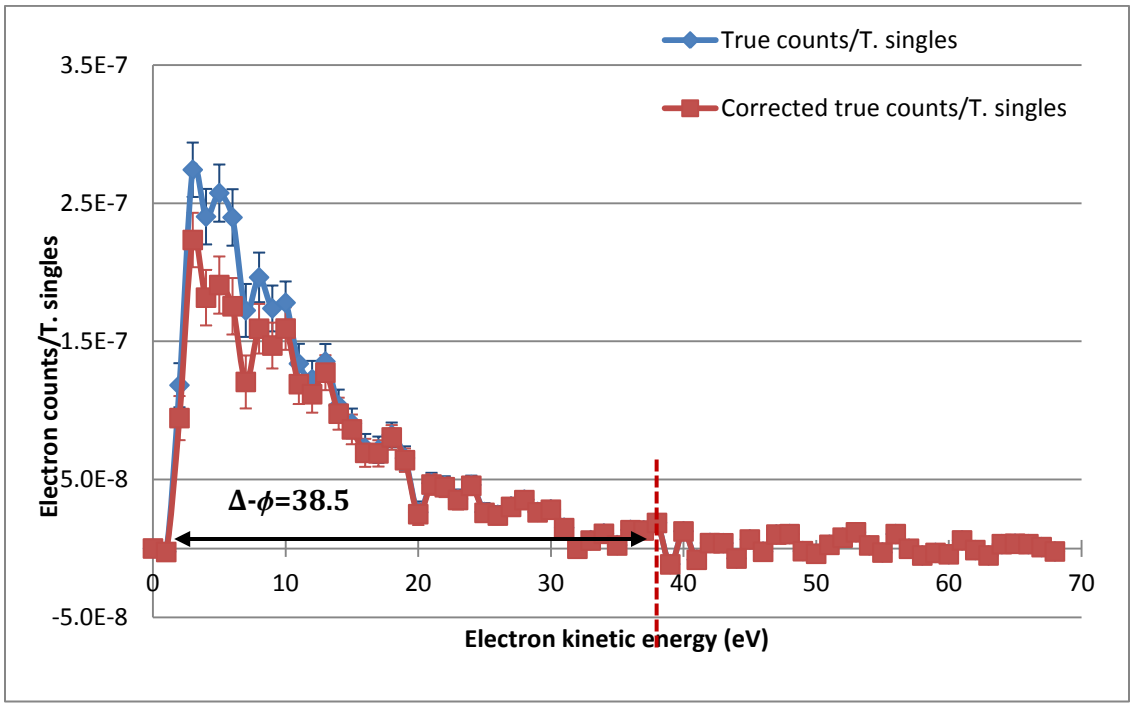

Figure 4.9 EECS Spectrum with the fixed analyzer set at 165eV valence band photoelectron energy

The spectra have been shifted by 15eV to account for the sample bias. The Δ value, the redistributed energy among the valence band electrons is seen to have contributed to the low energy side from 0 to 45.5eV, calculated from equation (3.1).

4.3.3 Coincidence Measurement of Inelastic Scattering of the Valence band electrons at 180eV

With the fixed analyzer set at 180eV, the scanning CMA was used to sweep the energy range of 0 to 70eV. The figure 4.8 below shows the contribution to the secondary electron spectrum from 200eV photons when the coincidence measurement was made with the valence band photoelectron of 180eV. As discussed in section 3.5.3 the True counts are not just the difference of the Coincidence and the accident events but each events divided by the efficiency $\varepsilon(t_0)$ and $\varepsilon(t_1)$ given by equation 3.5, $\Delta\text{-}\phi = 208.5 - 180 - \phi = 23.5$ eV.

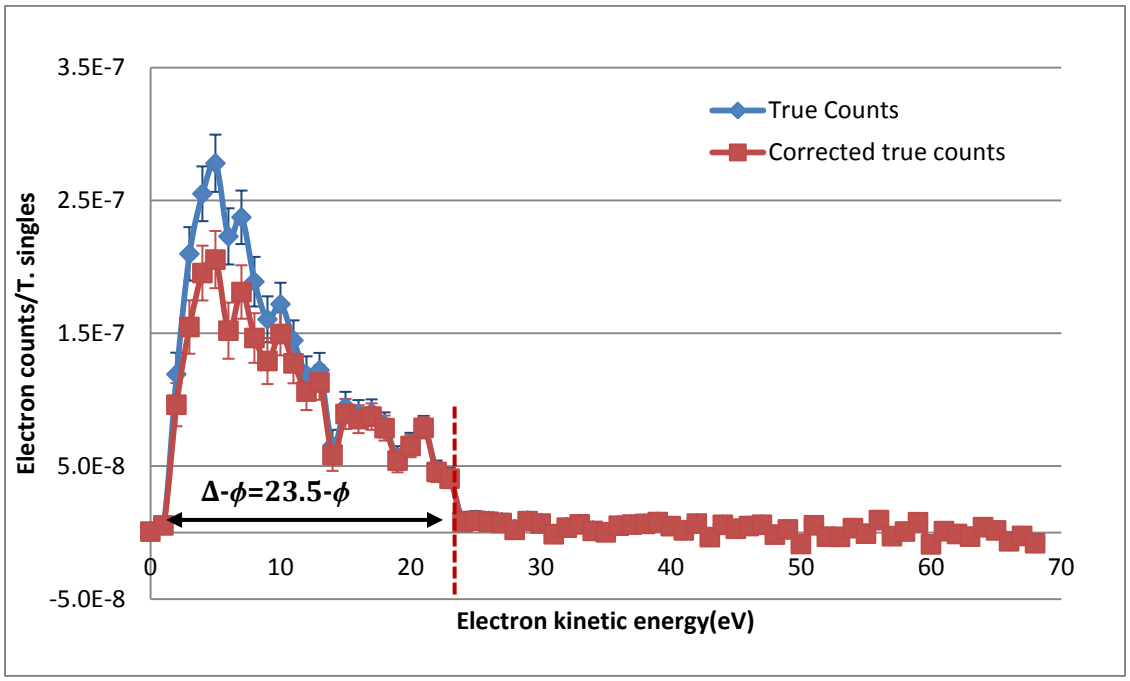

Figure 4.10 EECS Spectrum with the fixed analyzer set at 180eV valence band photoelectron energy

The spectra have been shifted by 15eV to account for the sample bias. The Δ value, the redistributed energy among the valence band electrons is seen to have contributed to the low energy side from 0 to 30.5eV, calculated from equation 3.1.

4.3.4 Coincidence Measurement of Inelastic Scattering of the Valence band electrons at 190eV

With the fixed analyzer set at 190eV, the scanning CMA was used to sweep the energy range of 0 to 70eV. The figure (4.9) below shows the contribution to the secondary electron spectrum from 200eV photons when the coincidence measurement was made with the valence band photoelectron of 190eV. As discussed in section 3.5.3 the True counts are not just the difference of the Coincidence and the accident events but each events divided by the efficiency $\varepsilon(t_0)$ and $\varepsilon(t_1)$ given by equation 3.5, $\Delta\text{-}\phi = 208.5 - 190 - \phi = 13.5$ eV.

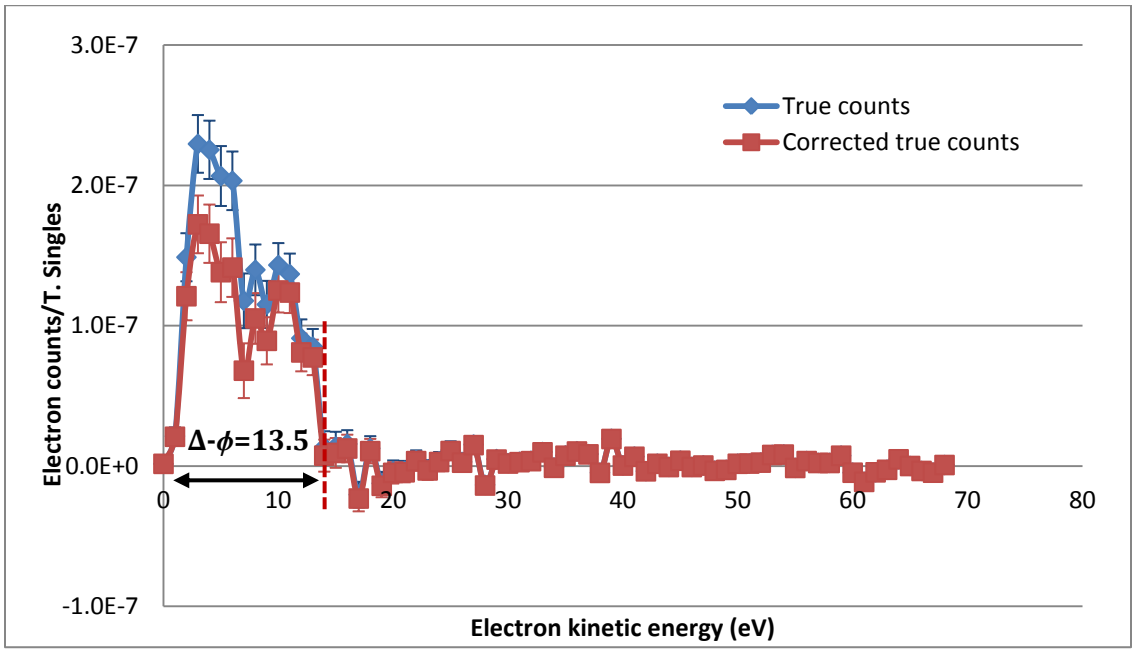

Figure 4.11 EECS Spectrum with the fixed analyzer set at 190eV valence band photoelectron energy

The spectra have been shifted by 15eV to account for the sample bias. The Δ value, the redistributed energy among the valence band electrons is seen to have contributed to the low energy side from 0 to 20.5eV, calculated from equation 3.1.

4.3.5 Coincidence Measurement of Inelastic Scattering of the Valence band electrons at 197eV

With the fixed analyzer set at 197eV, the scanning CMA was used to sweep the energy range of 0 to 70eV. The figure 4.10 below shows the contribution to the secondary electron spectrum from 200eV photons when the coincidence measurement was made with the valence band photoelectron of 197eV. As discussed in section 3.5.3 the True counts are not just the difference of the Coincidence and the accident events but each events divided by the efficiency $\varepsilon(t_0)$ and $\varepsilon(t_1)$ given by equation 3.5, $\Delta - \phi = 208.5 - 190 - \phi = 6.5$ eV

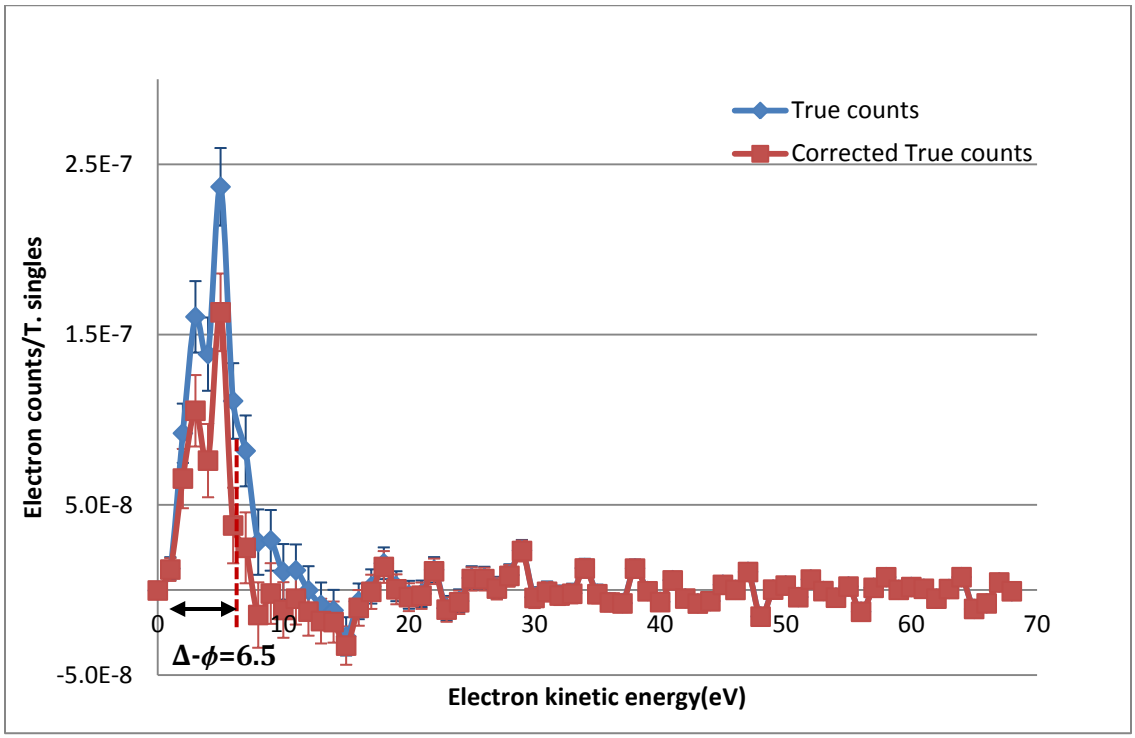

Figure 4.12 EECS Spectrum with the fixed analyzer set at 197eV valence band photoelectron energy

The spectra have been shifted by 15eV to account for the sample bias. The Δ value, the redistributed energy among the valence band electrons is seen to have contributed to the low energy side from 0 to 13.5eV, calculated from equation 3.1.

4.3.6 Coincidence Measurement of Inelastic Scattering of the Fermi level electrons at 209.2eV

With the fixed analyzer set at 209.2eV, the scanning CMA was used to sweep the energy range of 0 to 70eV. The figure (4.11) below shows the contribution to the secondary electron spectrum from 200eV photons when the coincidence measurement was made with the Fermi level photoelectron of 209.2eV. As discussed in section 3.5.3 the True counts are not just the difference of the Coincidence and the accident events but each events divided by the efficiency $\varepsilon(t_0)$ and $\varepsilon(t_1)$ given by equation 3.5.

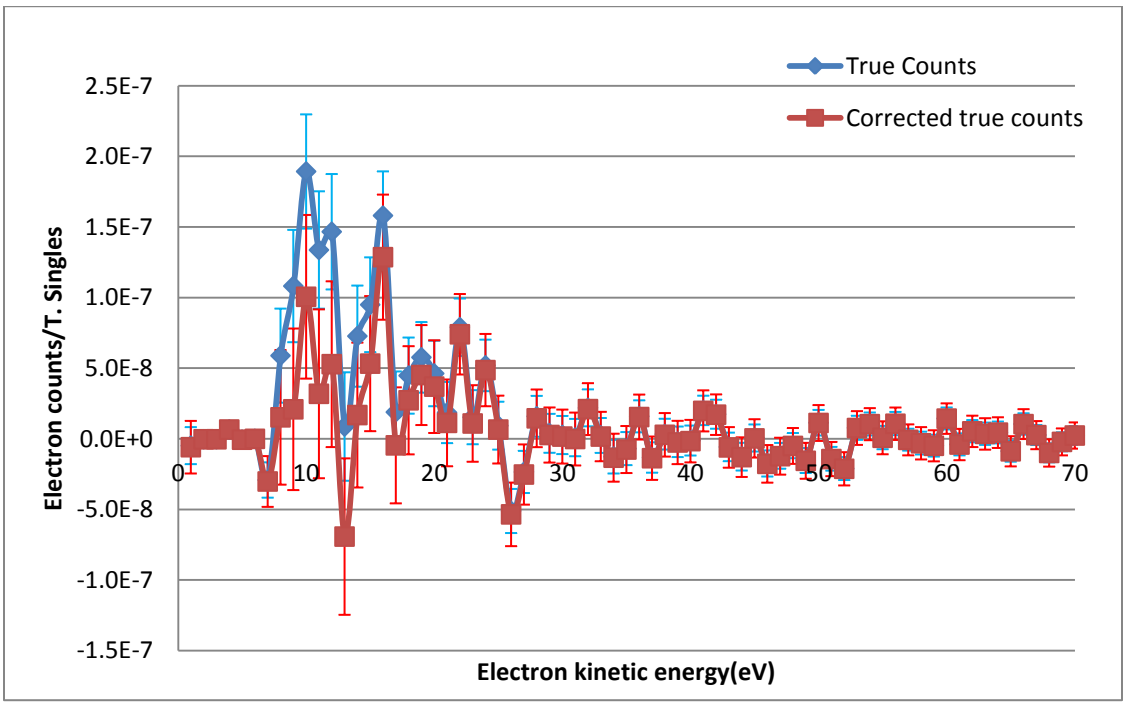

Figure 4.13 EECS Spectrum with the fixed analyzer set at 209.2eV Fermi level photoelectron energy

The spectra have been shifted by 15eV to account for the sample bias. As discussed earlier, the total average electron counts is ~0, since the Δ value is almost 0eV, there would be no electrons coming out of the Fermi level and to the scanning CMA.

4.3.7 Overlap of the Background coincidence Spectra

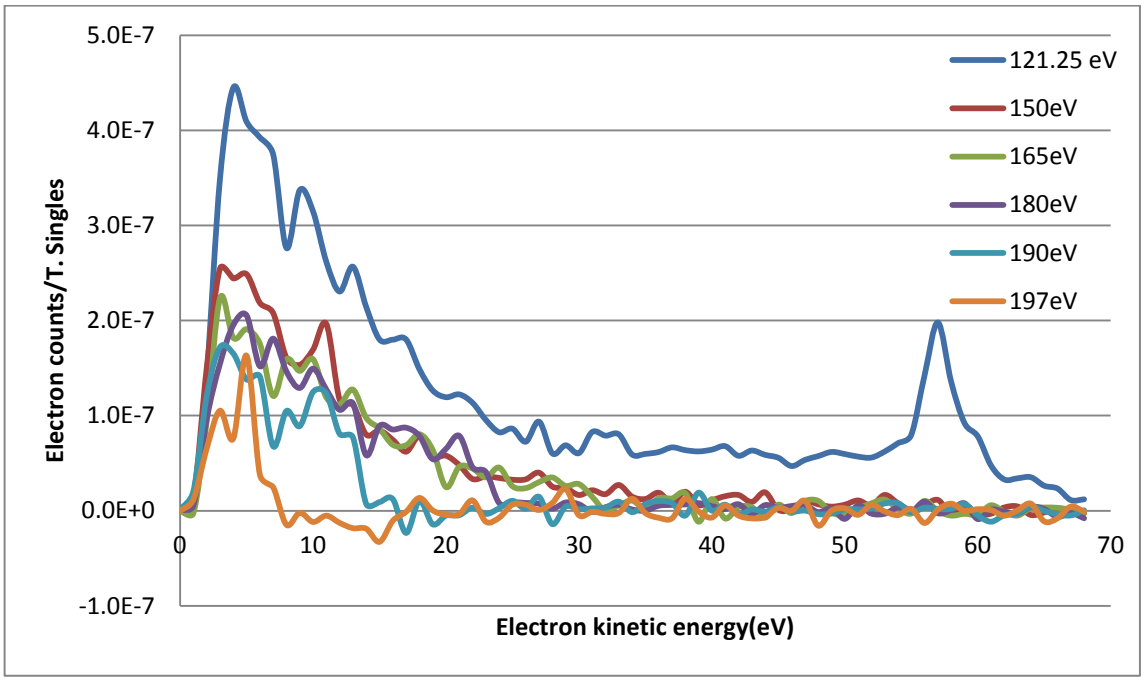

Figure 4.14 Background coincidence spectra at various fixed energies

All the spectra have been shifted by 15eV to account for the sample bias and they are all normalized to the total singles. The blue curve taken at 121.25eV is the APECS Auger Spectrum. Rest of the five other background coincidence spectra are the estimated measurements of the contribution from the inelastic scattering of the valence band electrons.

Here, we've noticed that the background spectra have shown a trend as we raise the fixed analyzer energy; which is same is lowering the Δ value. We predicted in previous chapter that lower the Δ value, smaller is the contribution to the LET, which is what we exactly see here. The count rate reduces for each spectrum along the x-axis till its Δ value is reached, and after that the count rate goes to zero.

4.4 Analysis of the LET from Photo-emitted Valence band Electrons

With the distinct trend seen with the background coincidence spectra taken at 5 different energies between the valence band and the core, we can now approximate the background contribution to the APECS Auger spectrum due to inelastic scattering of the valence band photoelectrons.

4.4.1 A Functional Description of the Secondary and Redistributed Primary Electrons

The Auger lineshapes can be extracted from an experimental Auger electron spectrum by removing the background after numerically integrating the derivative spectrum [15]. Ramaker et. al. developed a method to remove the background by least square fitting of an appropriate function to the desired range in the Auger spectrum by using the S and P LVV Auger lineshapes for the third row oxyanions, SO_4^{2-} and PO_4^{3-}. The function is also based on the descriptions for the true secondary electrons [16] by Seah, and redistributed primary electrons [17] by Inokuti. The background function B(E) developed by Ramaker is given below.

$$B(E) = \frac{A(E)}{(E+\mathrm{E}_0)(E+\phi)^m} + \frac{B\ln[(E_p-E)/E_b]}{[(E_p-E)/E_b]^n} + C \qquad (4.1)$$

Where A, B, C, m and n are determined by a non-linear least-squares fit of the observed coincidence background due to inelastic scattering of the valence electrons. m (=1.6)and n(=2) are constant values for Cu(100) calculated by Seah and Ramaker [12]. The other variables in the equation are given as follows:

E = Energy of the secondary electron with respect to vacuum level

E_p = Primary beam energy (**Δ** eV)

E_b = Binding energy of the primary electron

E_0 = Energy constant determined based on an optimal least square fit to the observed data

The **Δ** value is given by the equation,

$$\Delta\text{-}\phi = \mathrm{hv}\text{-}E_{fixed}\text{-}E_B\text{-}\phi_{A.} \qquad (4.2)$$

During the valence band photoelectron emission process in Cu(100), the electron can transfer energy Δ eV to the neighboring electrons. This energy stimulates the inelastic emission process and hence the APECS LET consists of electrons, one coming from the primary beam energy and the other from the sample as a true secondary electron. The valence electrons that absorb the entire Δ eV energy and emit out of the sample are the primary electrons. The secondary electrons are those which are emitted by mutually sharing the primary beam energy. The secondary electrons have the energy $\leq \Delta$ eV.

The plots in figure 4.6 to 4.10 and the combined background spectra in figure 4.12 help us to determine a trend of these EECS spectra. The Δ eV energy transferred by the valence photoelectron to the neighboring electrons is treated as the primary beam energy, E_p, as mentioned by Ramaker in the functional form of his equation. To best fit the data, we set E_0 as a constant D and rewrote the equation as,

$$B(E) = \frac{A(E)}{(E+\mathrm{D})(E+\phi)^m} + \frac{B \ln[(E_p-E)/E_b]}{[(E_p-E)/E_b]^n} + C \qquad (4.3)$$

The above equation was used to fit the observed LET taken at various fixed energies using ORIGIN Pro Version 8.1 Software. Using all the fits the A, B, C and D parameters are estimated for the 121.25eV core energy.

4.5 The Background Function Fit

4.5.1 Curve fit for 150eV RCMA Energy

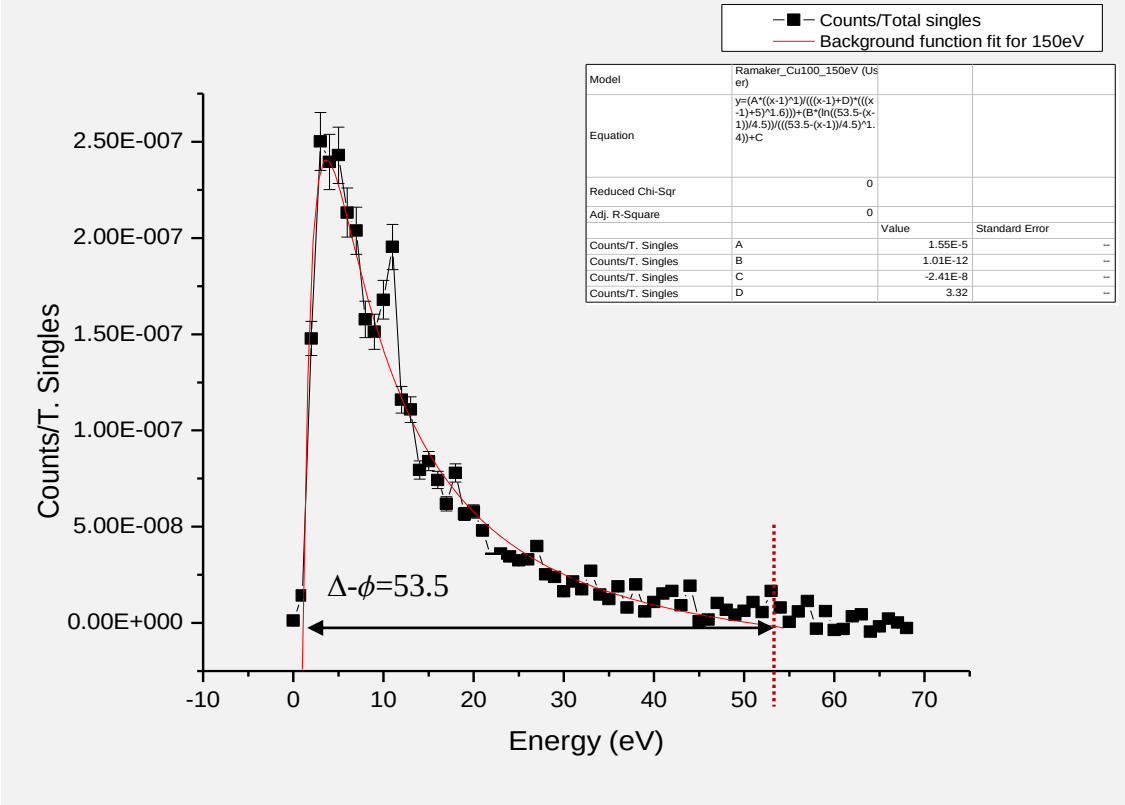

Figure 4.15 EECS spectrum showing the LET contribution when the fixed analyzer is set at 150eV. The red curve is the Background function fit

The spectra have been shifted by 15eV to account for the sample bias. The Δ value, the redistributed energy among the valence band electrons is seen to have contributed to the low energy side from 0 to 53.5eV. The Background Function B(E) is estimated based on the function determined by Ramaker et. al.

4.5.2 Curve fit for 165eV RCMA Energy

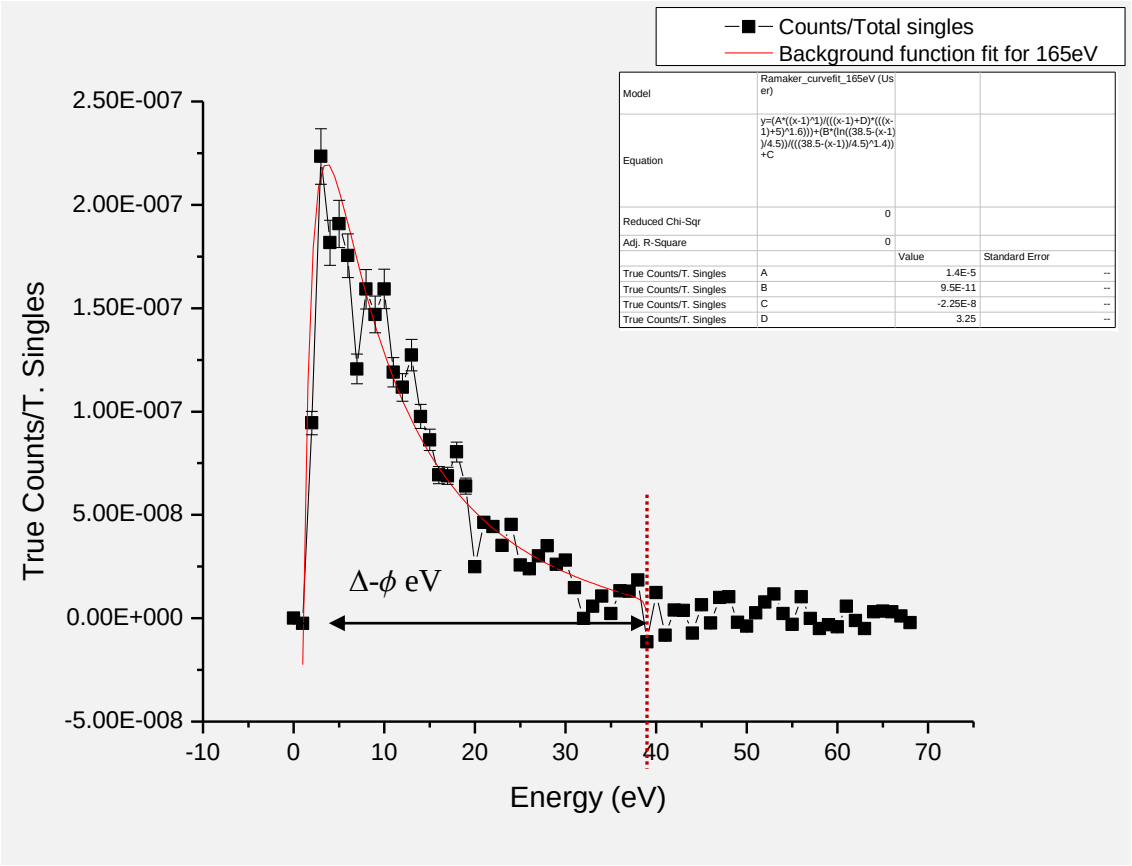

Figure 4.16 EECS spectrum showing the LET contribution when the fixed analyzer is set at 165eV. The red curve is the Background function fit

The spectra have been shifted by 15eV to account for the sample bias. The Δ value, the redistributed energy among the valence band electrons is seen to have contributed to the low energy side from 0 to 38.5eV. The Background Function B(E) is estimated based on the function determined by Ramaker et. al.

4.5.3 Curve fit for 180eV RCMA Energy

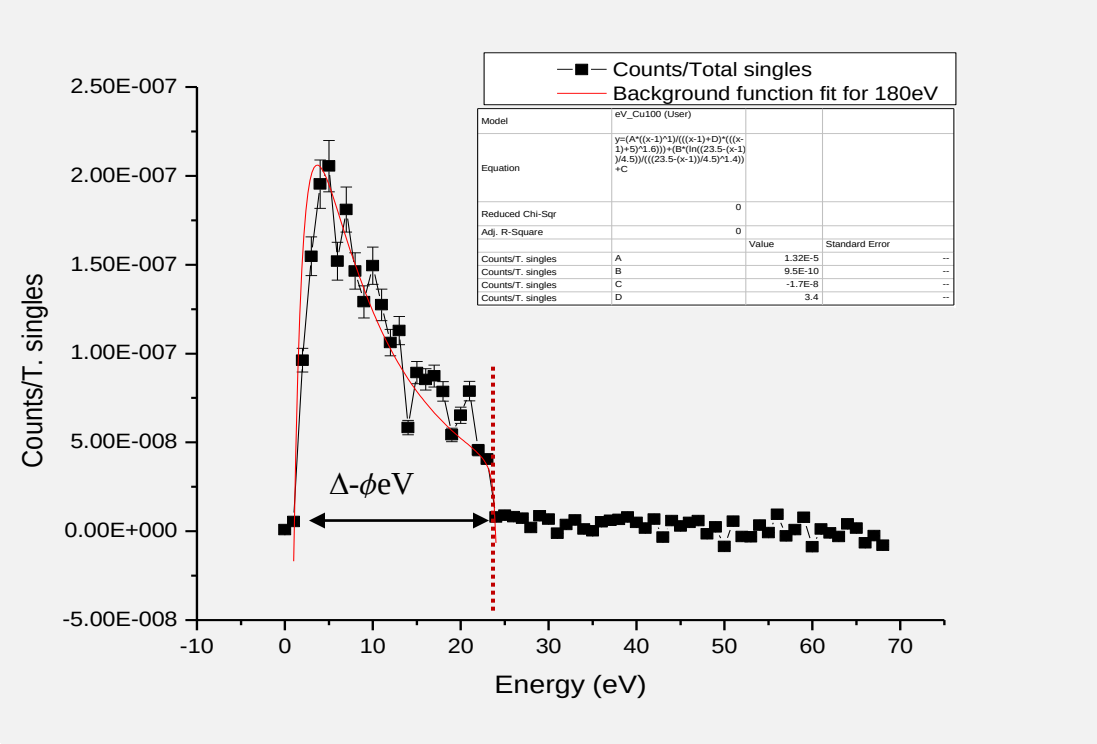

Figure 4.17 EECS spectrum showing the LET contribution when the fixed analyzer is set at 180eV. The red curve is the Background function fit

The spectra have been shifted by 15eV to account for the sample bias. The Δ value, the redistributed energy among the valence band electrons is seen to have contributed to the low energy side from 0 to 23.5eV. The Background Function B(E) is estimated based on the function determined by Ramaker et. al.

4.5.4 Curve fit for 190eV RCMA Energy

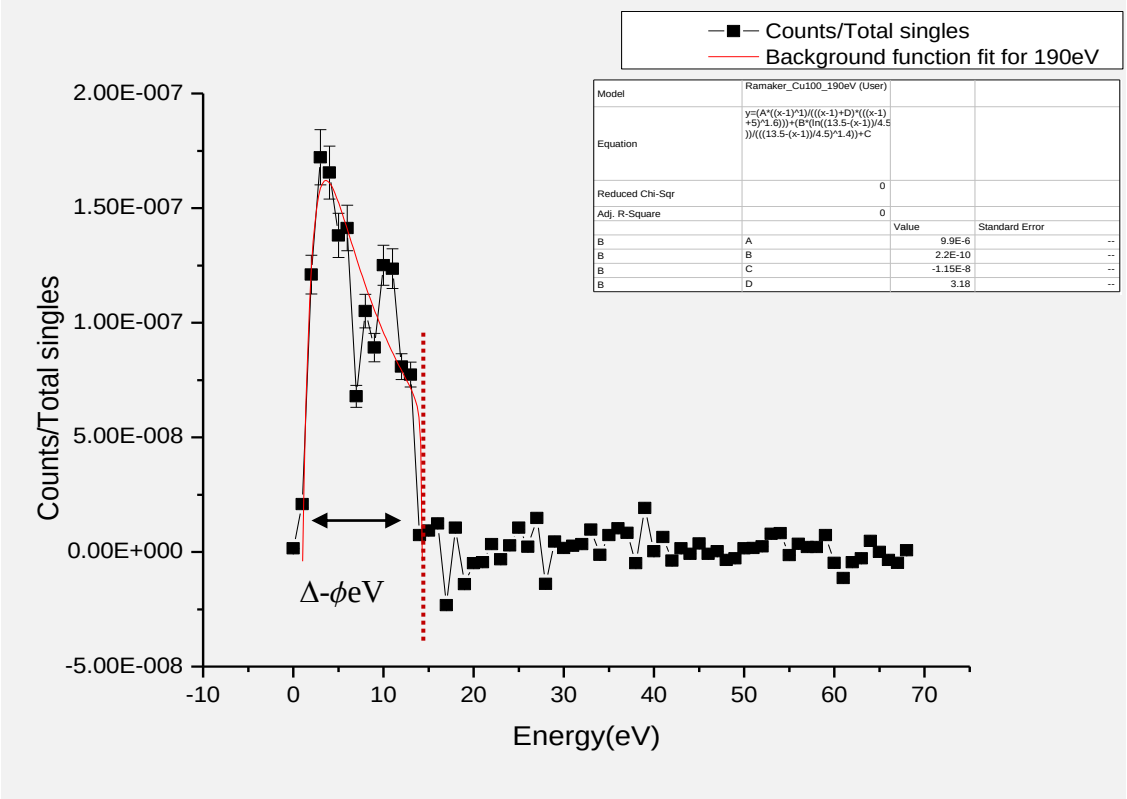

Figure 4.18 EECS spectrum showing the LET contribution when the fixed analyzer is set at 190eV. The red curve is the Background function fit

The spectra have been shifted by 15eV to account for the sample bias. The Δ value, the redistributed energy among the valence band electrons is seen to have contributed to the low energy side from 0 to 13.5eV. The Background Function B(E) is estimated based on the function determined by Ramaker et. al.

4.5.5 Curve fit for 197eV RCMA Energy

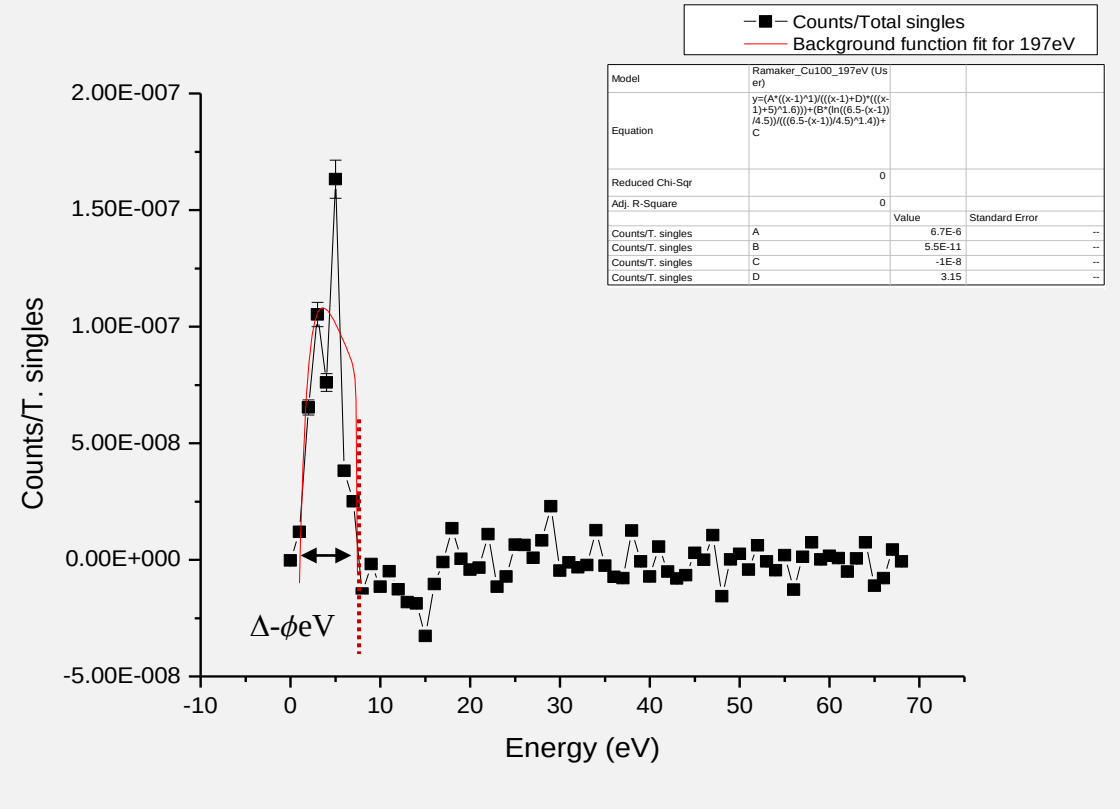

Figure 4.19 EECS spectrum showing the LET contribution when the fixed analyzer is set at 197eV. The red curve is the Background function fit

The spectra have been shifted by 15eV to account for the sample bias. The Δ value, the redistributed energy among the valence band electrons is seen to have contributed to the low energy side from 0 to 6.5eV. The Background Function B(E) is estimated based on the function determined by Ramaker et. al.

4.6 Background Estimation of the APECS Auger Spectrum

The parameters from the background function fit were extracted and used to estimate the background contribution from the fixed analyzer at 136.25eV.

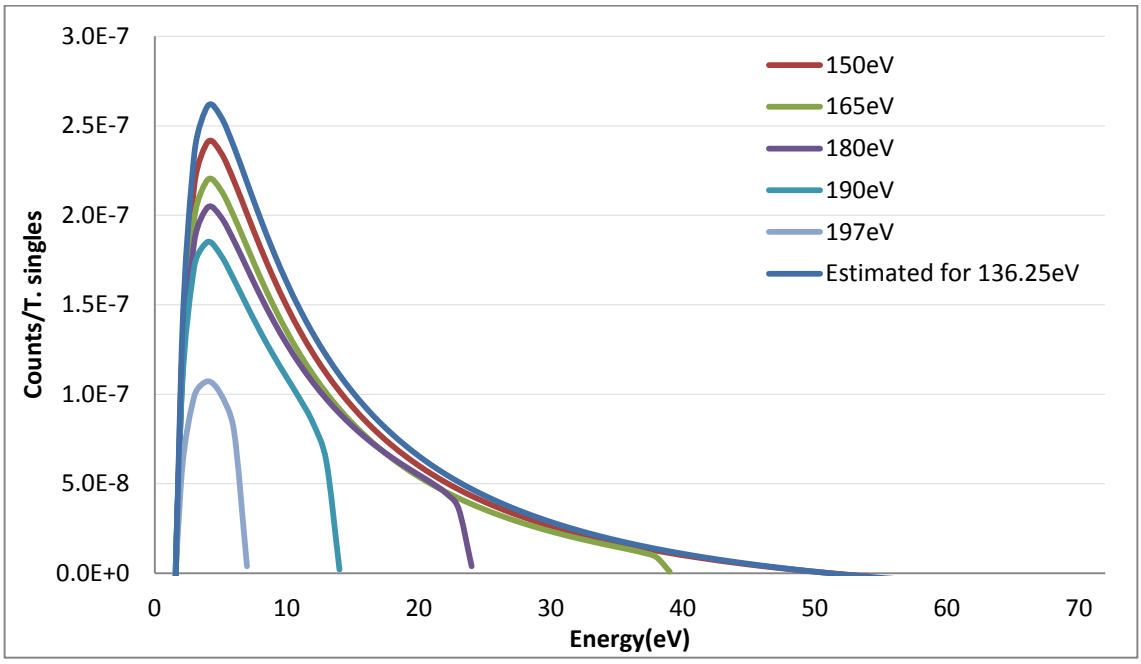

Figure 4.20 The extrapolation of the background based on different fixed energy. The blue curve shows the estimated background contribution.

All the spectra have been shifted by 15eV to account for the sample bias. The curves are the representation of the secondary electron spectrum at the low energy region. It's seen that higher the Δ values more the contribution to the secondary electron spectrum. The spectrum for 197eV has the Δ value of only 6.5eV, and hence the estimated contribution is significantly smaller than that's seen for 150eV, which has Δ value of 53.5eV. As we move closer the fixed analyzer energy at 136.25eV, more electrons are emitted at the low energy side, as expected. We subtract this estimated secondary electron spectrum from the Auger Spectrum. When we integrate the area under each curve within the limit of Δ value, the sum should reduce as we go higher in the fixed analyzer energy. The graph of the integrated LET sum at different energy is shown in the figure 4.20.

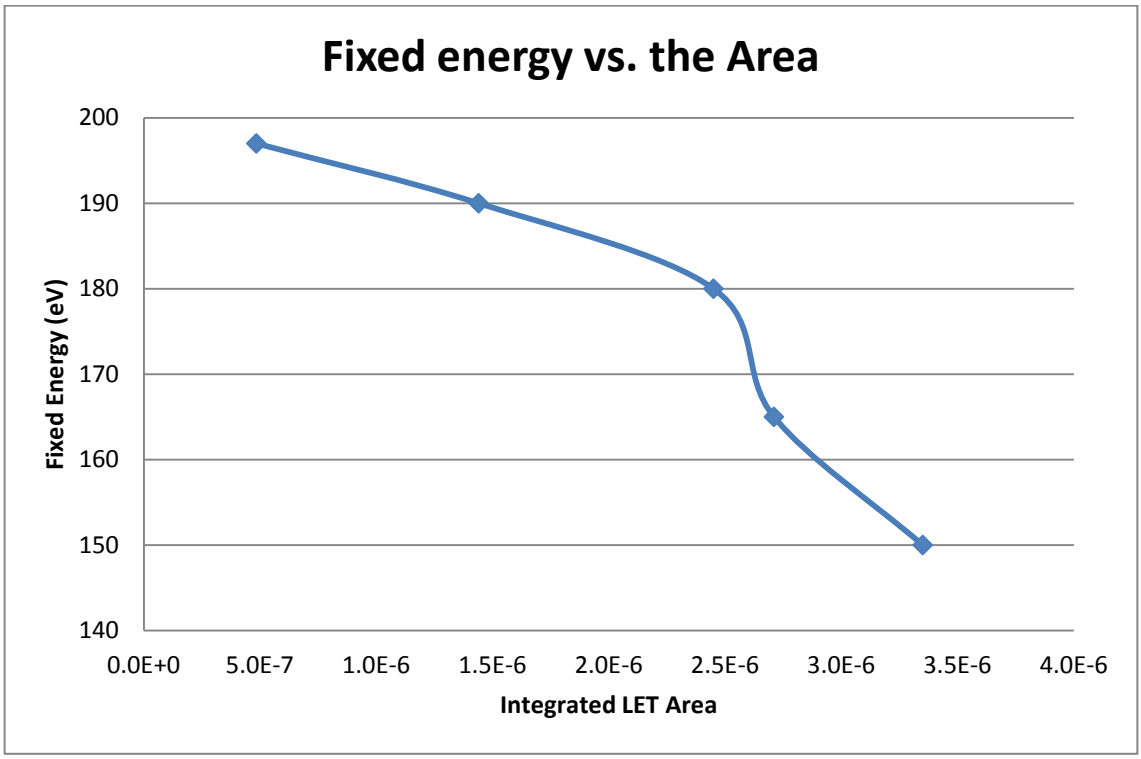

Figure 4.21 The integrated LET area vs. the fixed energy.

The contribution to the area varies as we go from 150eV to 197eV. The ratio of the integrated area at 150eV and 165eV is 1.24. Going from 165eV to 180eV the area doesn't change much, with the ratio of only 1.1. As we go higher in the fixed energy from 180eV to 190eV the ratio of the integrated area is 1.72 and finally from 190eV to 197eV has the ratio of 2.98.

4.7 Extrapolation of the Background Spectra

The background contribution from all the spectra was used to extrapolate the estimated background for the APECS Auger Spectrum.

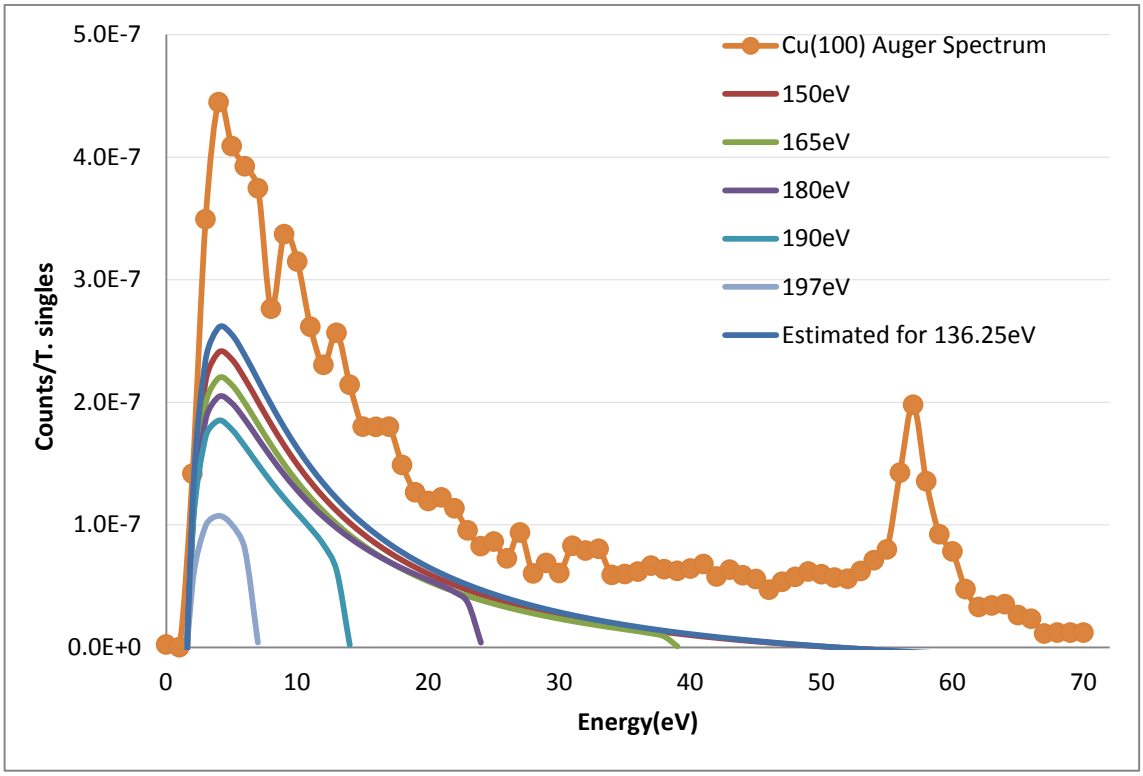

Figure 4.22 The extrapolation of the background showing the background contribution from the inelastic scattering of the valence band photoelectrons emitted at 136.25eV

The spectra have been shifted by 15eV to account for the sample bias. The intensity of the Low energy tail (LET) is expected to rise below 50eV down to 0eV.

4.8 Background Subtracted APECS Auger Spectrum

The extrinsic contribution from the inelastic scattering of the valence band photoelectrons is subtracted from the APECS Auger Spectrum. The resulting spectrum is shown in figure 4.21.

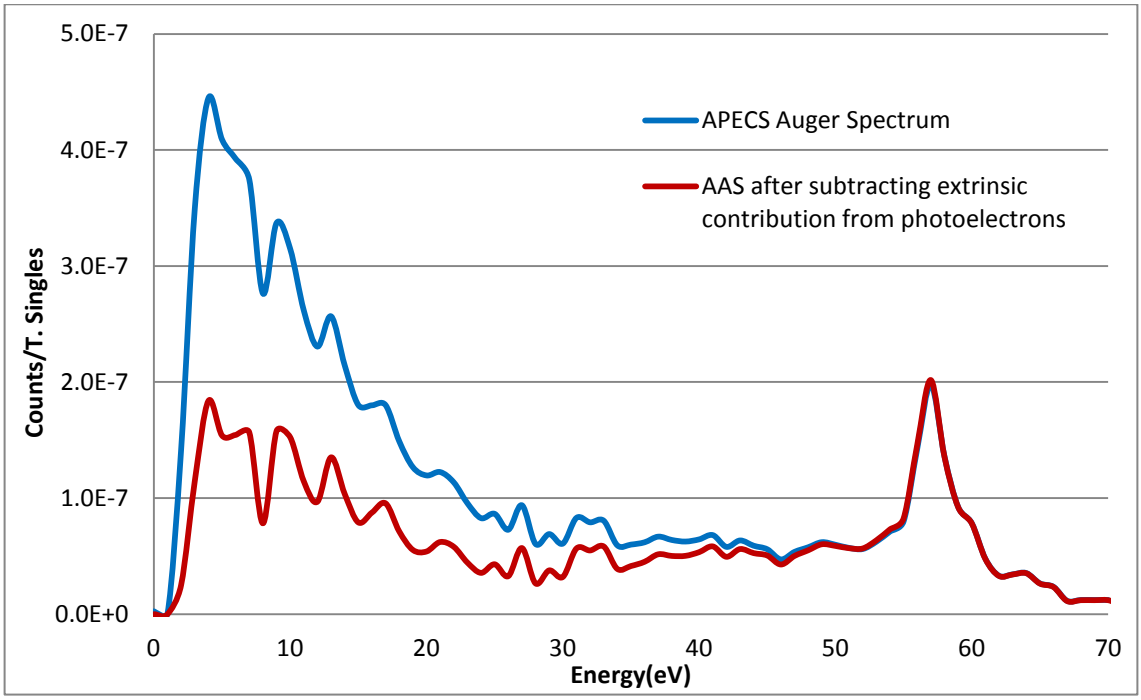

Figure 4.23 Background subtracted APECS Auger Spectrum. The extrinsic contribution from the inelastic scattering of the photoelectrons is subtracted from the LET.

The spectra have been shifted by 15eV to account for the sample bias. The LET intensity comes from two different contributions, the extrinsic and the intrinsic. The extrinsic intensity is again due to two events, the inelastic scattering of the photoelectrons and the Auger electrons. The spectrum after removal of contribution from first event is given figure 4.21. The estimation and removal of contribution to the LET intensity from the Auger electrons are presented in the following section.

4.9 Analysis of the LET Contribution from the Auger Electrons

The contribution to the LET of the Auger spectrum comes from the extrinsic and the intrinsic phenomenon. The contribution to the extrinsic part comes from the two events. One we discussed in section 4.8 and the other is due to the inelastic scattering of the Auger electrons in the surface and sub-surface region. This contribution is estimated by accounting the proper electron escape probability at low energies [16]. Equation 4.1 below describes the secondary electron emission for Cu when m is 1.6.

$$I(E) = E(E+E_{PB})^{-1}(E+\phi)^{-m} \quad 4.1$$

Where, I(E) is the intensity of the secondary electron spectrum, E is the electron energy, E_{PB} is the primary beam energy, ϕ is the work function of the metal and m is the constant. The Auger electron induced extrinsic spectrum (Figure 4.22) has been normalized such that [18]

$$\int_0^{E0} I_{LET}ExtrinsicdE = I_{peak}[\delta_{surface}[(1-T)/(T+R) + \delta_{bulk}[(1-R)/(T+R)]] \quad 4.2$$

Where, I_{LET}(I_{peak}) is the intensity of the LET(peak) region. For the isotropic emission half of the emitted Auger electrons are assumed to be emitted towards the sub surface regions and other half towards the vacuum. Some of the Auger electrons emitted into the bulk will elastically backscatter and will contribute to the Auger peak, given by ratio R [19]. Some of the Auger electrons emitted towards the vacuum leave the sample without suffering any inelastic collision. The ratio of these Auger electrons to all the electrons emitted in the forward direction is given by the transmission factor T [20]. The ratio of R and T is calculated to be 0.04 and 0.6.

The number of inelastically scattered Auger electrons is then given by $I_{peak}[(1-T)/(T+R)]$ and the secondary electron yield due to these electrons is termed as $\delta_{surface}$ and its value is 1. Similarly, the number of Auger electrons emitted into the bulk is given by $I_{peak}[(1-R)/(T+R)]$ and their secondary electron yield is referred to as δ_{bulk} and its value for copper is 0.2.

4.9.1 Estimation of the LET

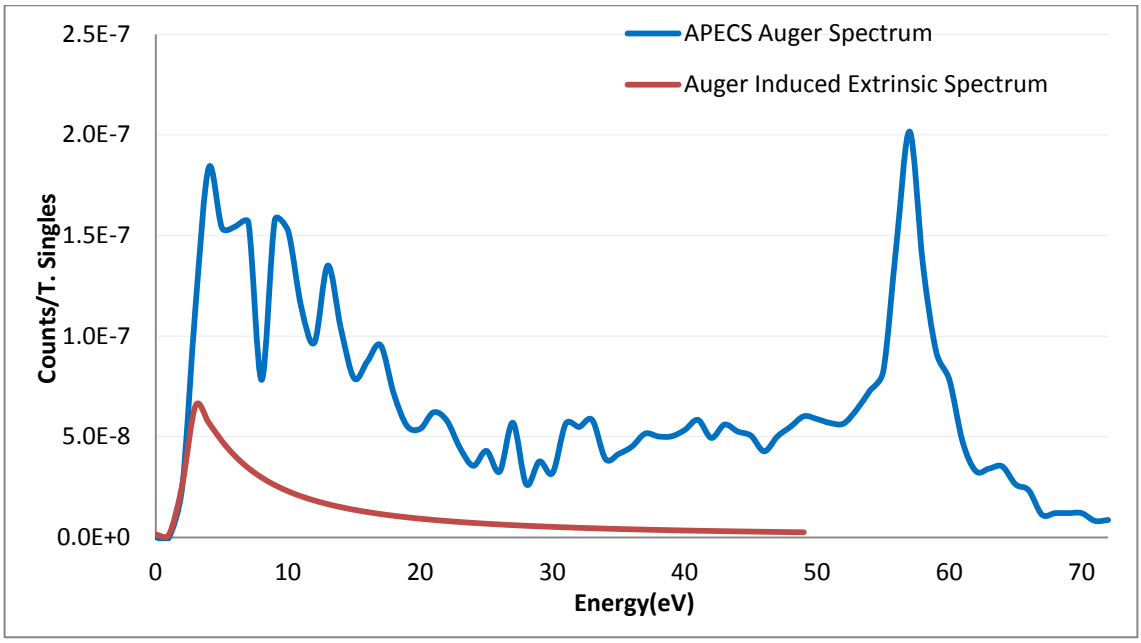

Figure 4.24 Estimate of the extrinsic background due to inelastic scattering of the Auger electrons in the surface and sub-surface region.

4.9.2 APECS Auger Spectrum with LET from Intrinsic Contribution

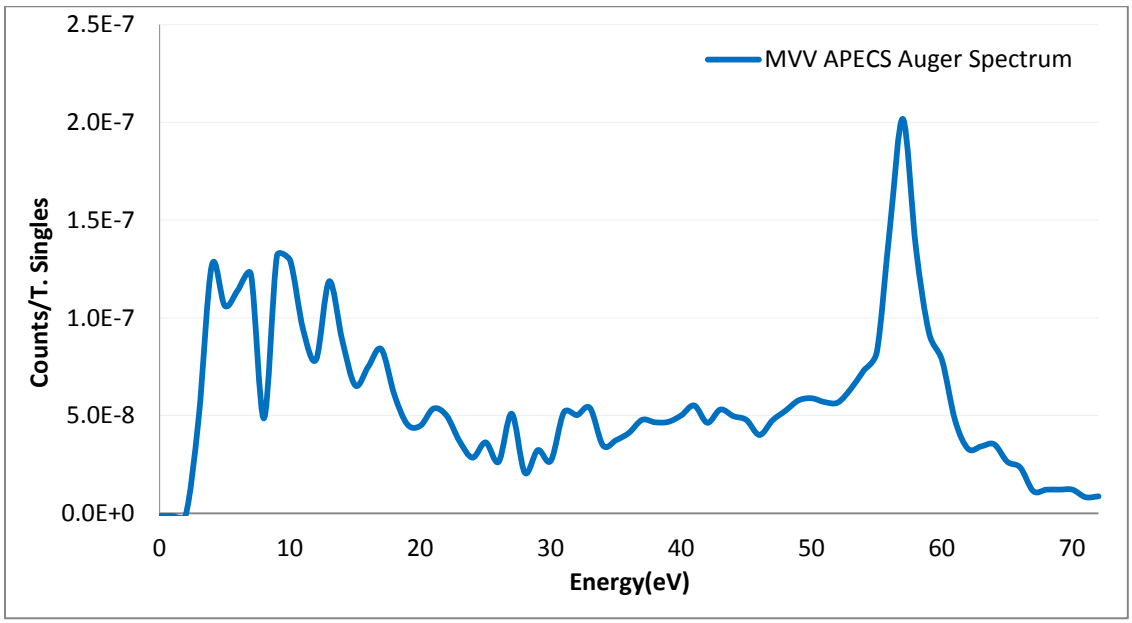

Figure 4.25 The Cu(100) APECS Auger Spectrum after the subtraction of both of the Extrinsic Contribution.

The final spectrum of the Cu(100) M_3VV APECS Auger Spectrum after the subtraction of the background due to the Extrinsic contributions. The remainder of the LET spectrum is the pure intrinsic contribution created by the excitation of the Cu $3p_{3/2}$ photoelectrons only. A relative comparison of Auger spectrum before and after subtraction of extrinsic contribution from secondary electrons is shown in figure 4.24.

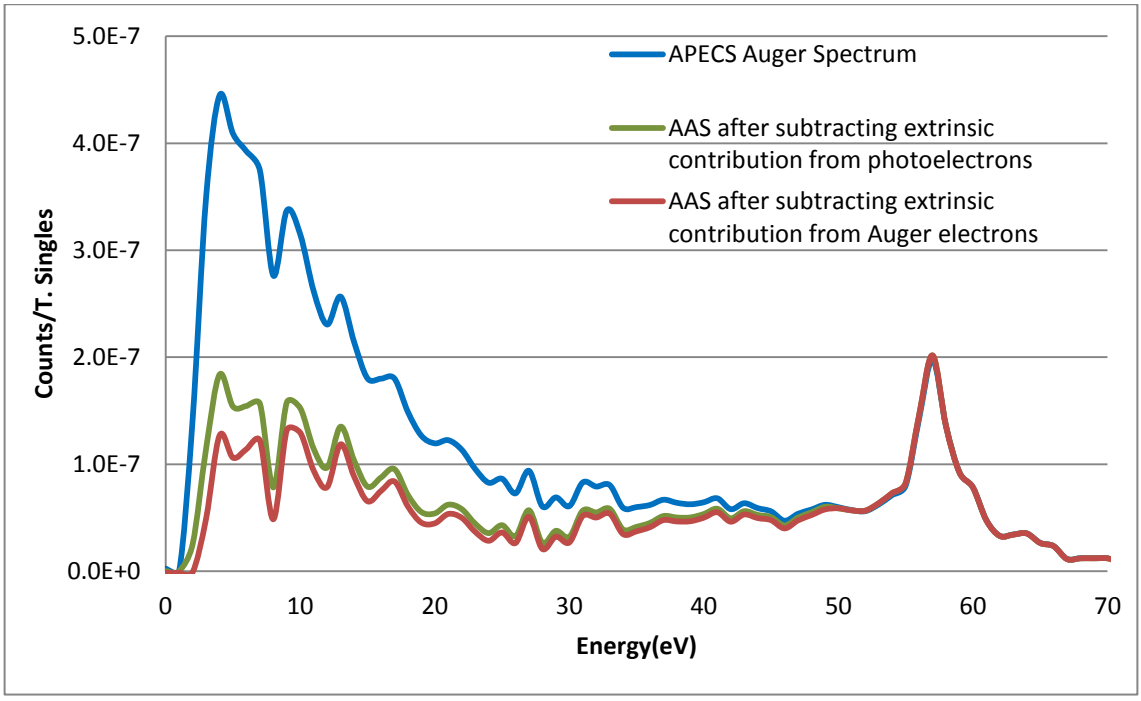

Figure 4.26 Showing the relative comparison between the Cu(100) M_3VV Auger spectrum and the subtraction of the background due to extrinsic contribution from the inelastic scattering of the valence band photoelectrons and the Auger electrons.

4.9.3 Comparison of APECS spectrum with PAES spectrum

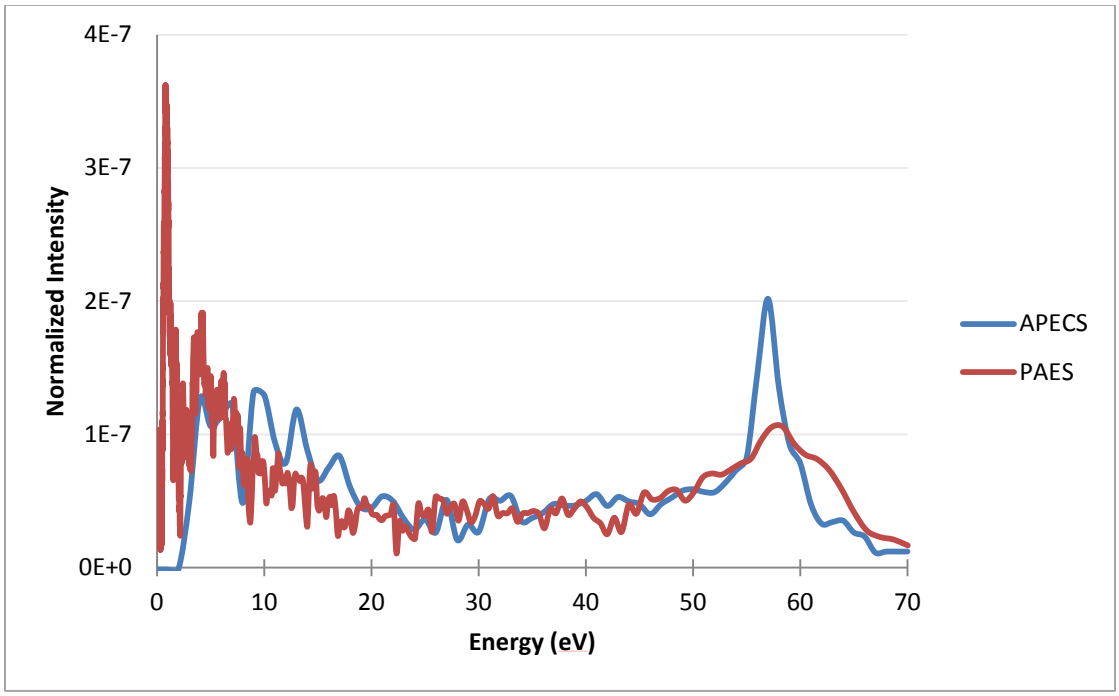

Figure 4.27 Showing the two Cu(100) spectra taken by using two different techniques, APECS and PAES. They are normalized to the Auger Intensity

CHAPTER 5

CONCLUSION AND FUTURE WORK

We have measured the contribution to the Low Energy Tail (LET) from the secondary electrons due to the inelastic scattering of the valence band photoelectrons and the Auger electrons in the surface and subsurface region of Cu(100) single crystal. Two different background functions are used to estimate the secondary electron spectrum arising from the two different events. The function to estimate extrinsic contribution from the inelastic scattering of the valence band photoelectrons was derived from a series of auxiliary coincidence measurements. Another function to estimate the contribution from the inelastic scattering of the Auger electrons was modeled from equation 4.1, which was normalized to the total intensity of the LET due to extrinsic contribution. After subtracting the extrinsic contribution to the LET, a final Auger spectrum is presented that consist only of the secondary electrons LET that are intrinsic to the Auger transition.

We had assumed that both intrinsic and extrinsic processes play a role in LET generation, however, the intrinsic part plays the dominant role. In figure 4.23 the red curve is the estimation of the LET from the inelastic scattering of the Auger electrons. Before subtracting this estimation the ratio of the I_{LET}/I_{Auger} is 2.7 and after subtraction it's 2.2. This is consistent with what was hypothesized by Jensen [13]. The Major portion of the Auger LET is intrinsic to the CVV decay process.

The ratio of the intensity of the LET and Auger of the APECS Auger Spectrum, I_{LET}/I_{Auger} is 5.6. After the subtraction of the extrinsic contribution from the secondary electrons, the same ratio is found to be 2.20. The similar experiment done with the PAES technique on Cu(100) has the I_{LET}/I_{Auger} ratio of 1.81 [18].

The remaining intrinsic LET in the Auger Spectrum can be interpreted as a result of core hole decaying via multi electron emission processes, C-VVV process in which 2 Auger electrons are emitted from the valence band [12]. Which is similar as saying that more than two electrons participate in the decay process; the Auger final state is not a two-valence hole, one electron state, but an n-valence hole, n–1 electron state with n > 2 [13]. The multi-electron process can also be triggered by the Plasmon generation and decay [21]. The probability of Shake up and Shake off upon ionization is ~0.01 for Cu(100) and hence the secondary electrons generated from this event can be safely ignored [22].

Jensen had estimated that Two-Hole part of the intrinsic spectrum carries about 35% of the spectral weight based coincidence measurements made on Al(100). Similar APECS data that we took on Cu(100) shows that it is 31%; and the PAES data on Cu(100) shows it is 36%.

The possibility of LET generation by inelastic scattering within the analyzer, or within the sample surface and the probability of escape of the two electrons being not independent have been ruled out [13].

Future work can be done on the Ag and Au sample to calculate the intrinsic contributions and to quantify what fraction of the decay events are of this n-hole type.

APPENDIX A

ABBREVIATIONS

UTA	University of Texas at Arlington
BNL	Brookhaven National Libratory
NSLS	National Synchrotron Light Source
IR	Infrared
VUV	Vacuum Ultra Violet
UV	Ultra Violet
AES	Auger Electron Spectroscopy
PES	Photo Electron Spectroscopy
APECS	Auger Photo Electron Coincidence Spectroscopy
SR	Synchrotron Radiation
MCA	Multi Channel Analyzer
PHA	Pulse Height Analyzer
CFD	Constant Fraction Discriminator
CMA	Cylindrical Mirror Analyzer
TAC	Time to Amplitude Converter
ROI	Region Of Interest
LINAC	Linear Accelerator
AMP	Amplifier
ERG	Extended Range Grasshopper
LEBT	Low Energy Beam Transport
XPS	X-Ray Photoelectron Spectroscopy
AAS	APECS Auger Spectrum
IC	Inner Cylinder of the CMA
OC	Outer Cylinder of the CMA
KE	Kinetic Energy
VB	Valance Band

D/A	Digital to Analogue
EF	Electric Field

APPENDIX B

EXAMPLE OF APECS M_3VV AUGER SPECTRA AND APECS BACKGROUND SPECTRA

Tue Jun 28 22:56 2011

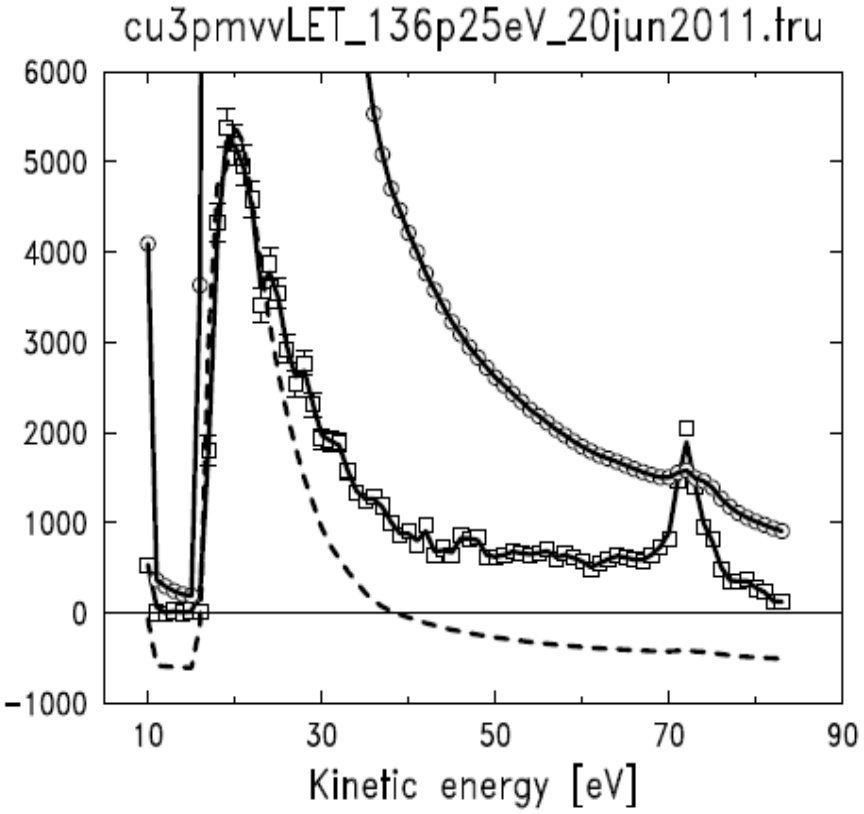

◊ True (raw)
—— True (smooth:1.0eV)
○ s1*K = s1*(Σs2/Σs1)
----- s1 rescaled

χ^2 = 4.267762

K = 5.3257e−05

Iguana sums:

S1 : 1.034e+10
K * S1 : 550863.0
S2 = A : 550863.0
Coi = T+A : 643392.0

T = : 92529.0
T/A = : 0.167971

Sun Jul 10 15:07 2011

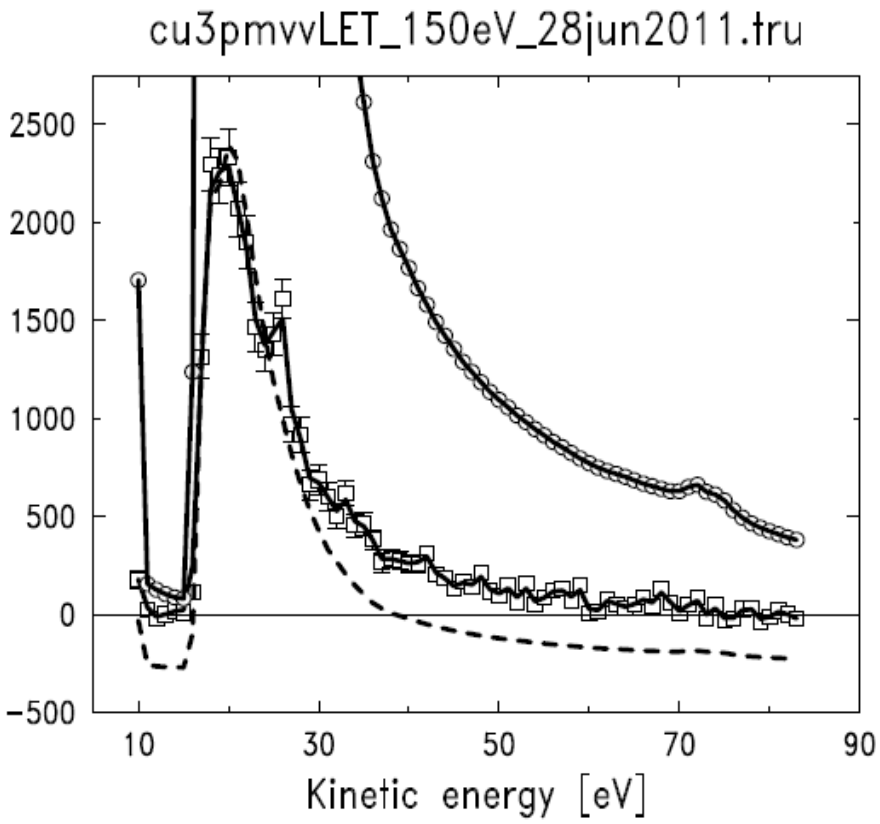

◊ True (raw)
—— True (smooth:1.0eV)
○ s1*K = s1*(Σs2/Σs1)
----- s1 rescaled

χ^2 = 1.392999

K = 2.9385e−05

Iguana sums:

S1 : 7.817e+09
K * S1 : 229703.0
S2 = A : 229703.0
Coi = T+A : 258856.0

T = : 29153.0
T/A = : 0.126916

Mon Jul 18 11:32 2011

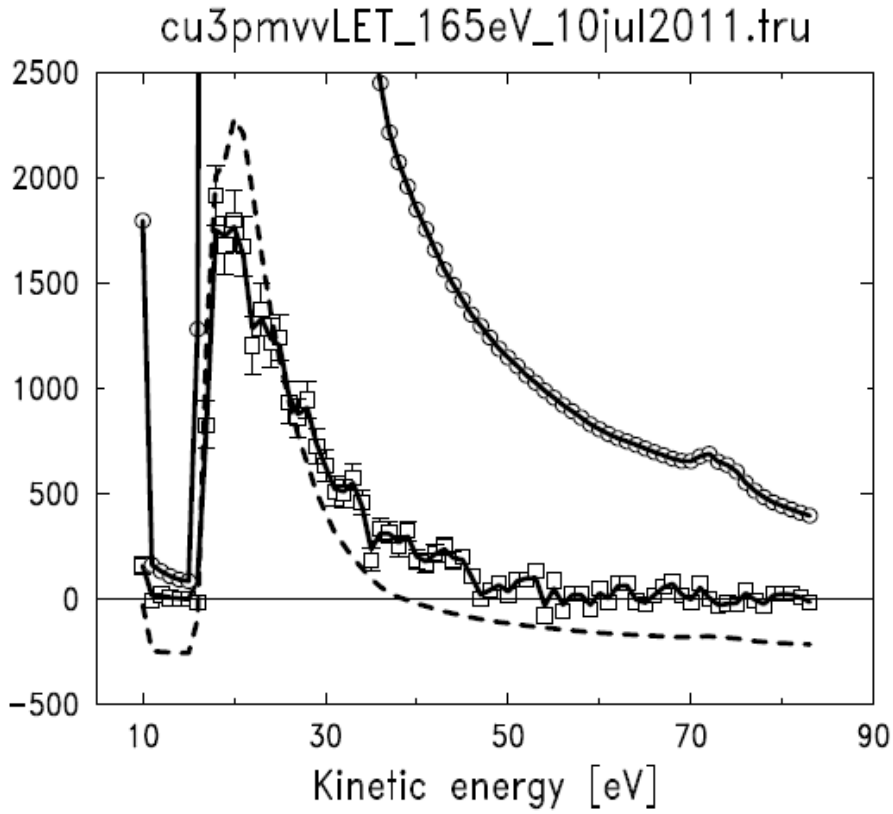

◊ True (raw)
—— True (smooth:1.0eV)
○ s1*K = s1*(Σs2/Σs1)
----- s1 rescaled

χ^2 = 1.514299

K = 3.4565e−05

Iguana sums:

S1 : 6.978e+09
K * S1 : 241196.0
S2 = A : 241196.0
Coi = T+A : 263836.0

T = : 22640.0
T/A = : 0.093866

Mon Jul 18 11:28 2011

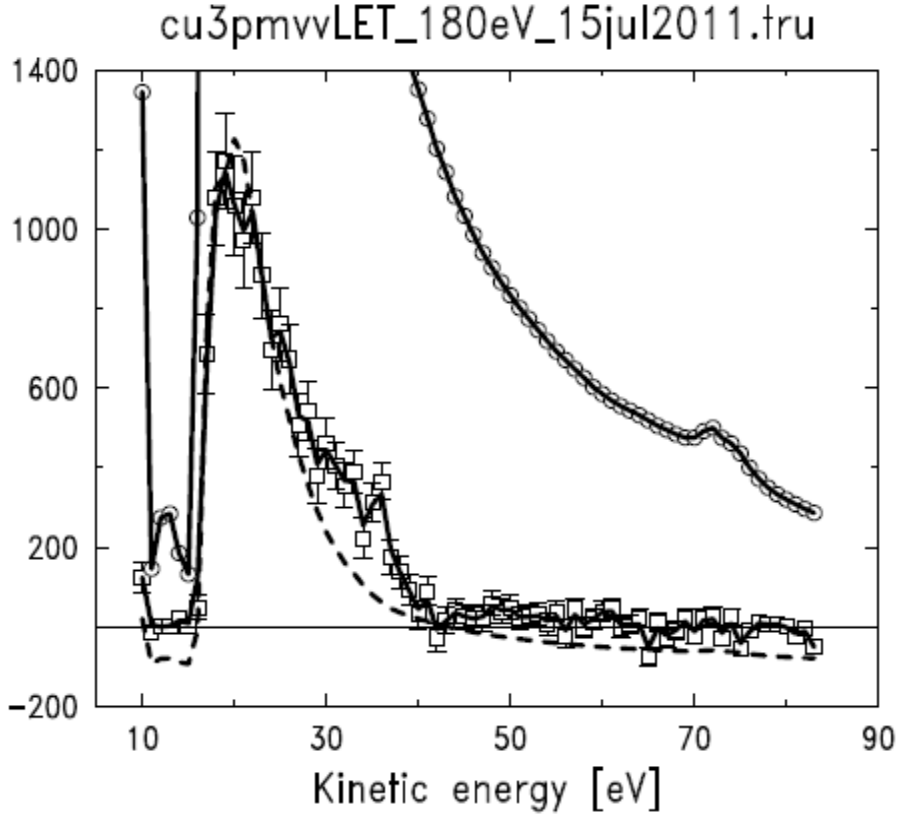

◊ True (raw)
—— True (smooth:1.0eV)
○ s1*K = s1*(Σs2/Σs1)
----- s1 rescaled

χ^2 = 1.473449

K = 4.0108e−05

Iguana sums:

S1 : 4.456e+09
K * S1 : 178714.0
S2 = A : 178714.0
Coi = T+A : 192762.0

T = : 14048.0
T/A = : 0.078606

Thu Jul 28 18:07 2011

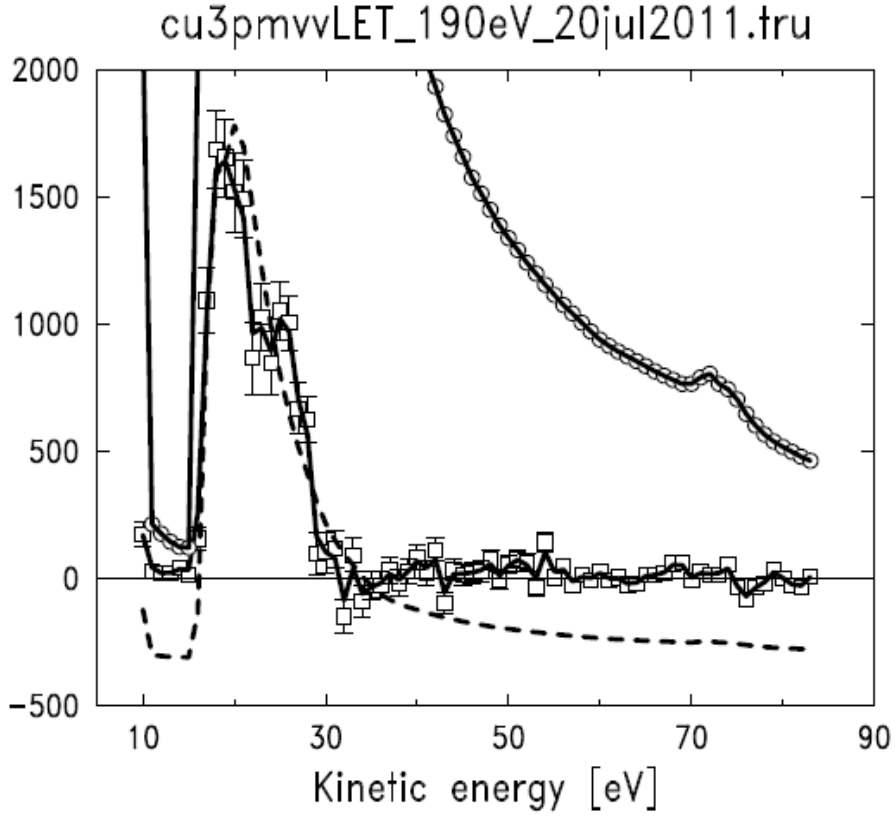

◊ True (raw)
—— True (smooth:1.0eV)
○ s1*K = s1*(Σs2/Σs1)
----- s1 rescaled

χ^2 = 1.319219

K = 3.9095e−05

Iguana sums:

S1 : 7.343e+09
K * S1 : 287057.0
S2 = A : 287057.0
Coi = T+A : 301838.0

T = : 14781.0
T/A = : 0.051492

APPENDIX C

ALGORITHM FOR ADDING SPECTRA

ALGORITHM FOR ADDING ALL SPECTRA [11]

The data acquired in APECS experiments consists of data from singles, coincidence and accidents events. The data obtained is collected in blocks of 30 sweeps each. Thus the block with unforeseen malfunction in some specific part of the experiment can be eliminated later by analyzing the individual files obtained. Elimination of these specific files can avoid loss of a large amount of data. The final spectra are calculated by adding all the individual 30 sweep blocks one by one.

The coincidence data contains the summed coincidence counts, and the corresponding error bars as a function of the kinetic energy of electrons.

The Error Bar = $\sqrt{N}$

Here, N is the number of all coincidence counts at a given energy.

Similarly, the Singles and Accidents data consists of the summed singles and accidents counts as a function of energy respectively.

DETERMINATION OF THE TRUE COINCIDENCE SPECTRUM

The definition of the Trues, T is given as T = C - A

Notations:

T : Trues

A : Accidental Counts

S : Singles Counts

C : Coincidence Counts

Here, we replace A with K.S where K = ∑A / ∑S . This helps in improving the statistics.

Error Bar (T) = Error Bar (C) + Error Bar (A)

Error Bar (A) being negligible, Error Bar (T) = Error Bar (C)

CALCULATION OF CHI-SQUARED

The chi-squared difference between A and K.S. is

$$\chi^2 = \frac{\sum_{i=1}^{N} \frac{(K.S_i - A_i)^2}{K.S_i}}{N-1}$$

Where, i is the number of points of the N-point spectrum. χ^2 is normalized to unity., with a 1-σ error bar of $2/\sqrt{N}$. If χ^2deviates from 1 by significantly more than $2/\sqrt{N}$, it indicates something non-statistically wrong with the measurement apparatus which needs to be corrected before proceeding.

APPENDIX D

EXTRAPOLATION OF RAMAKER FUNCTION PARAMETERS

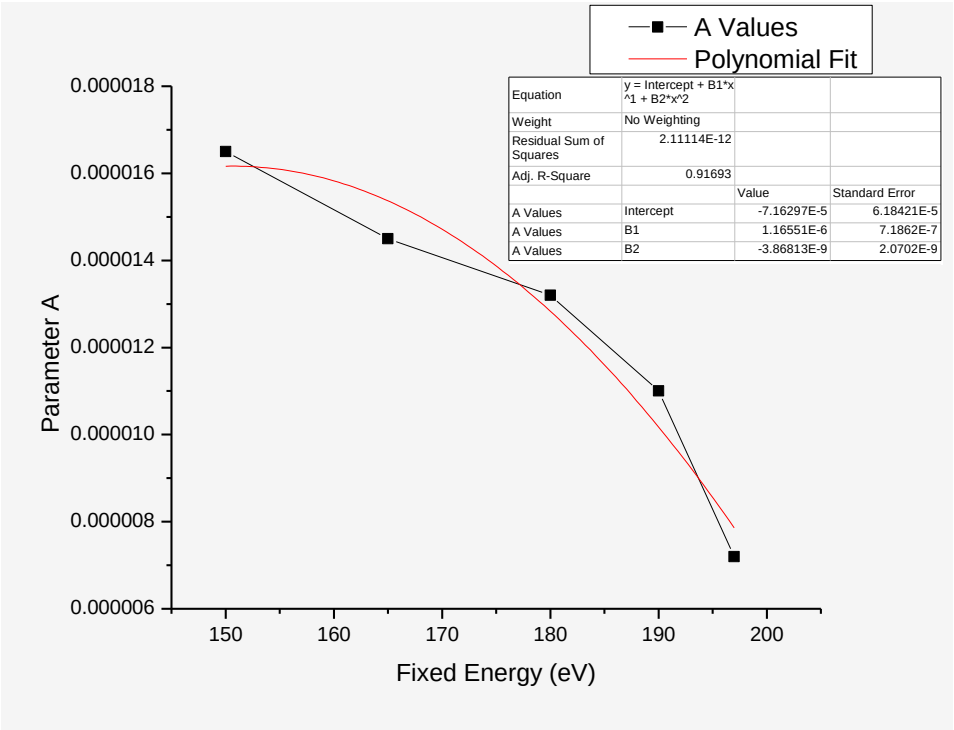

Figure D1. Extrapolation of Background Function Parameter A

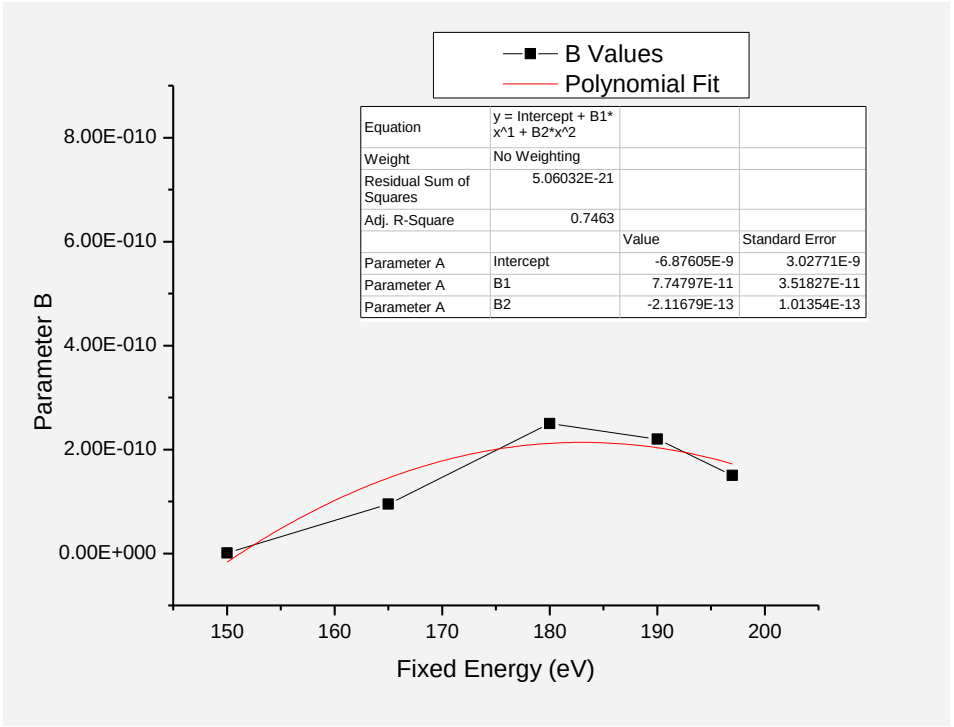

Figure D2. Extrapolation of Background Function Parameter B

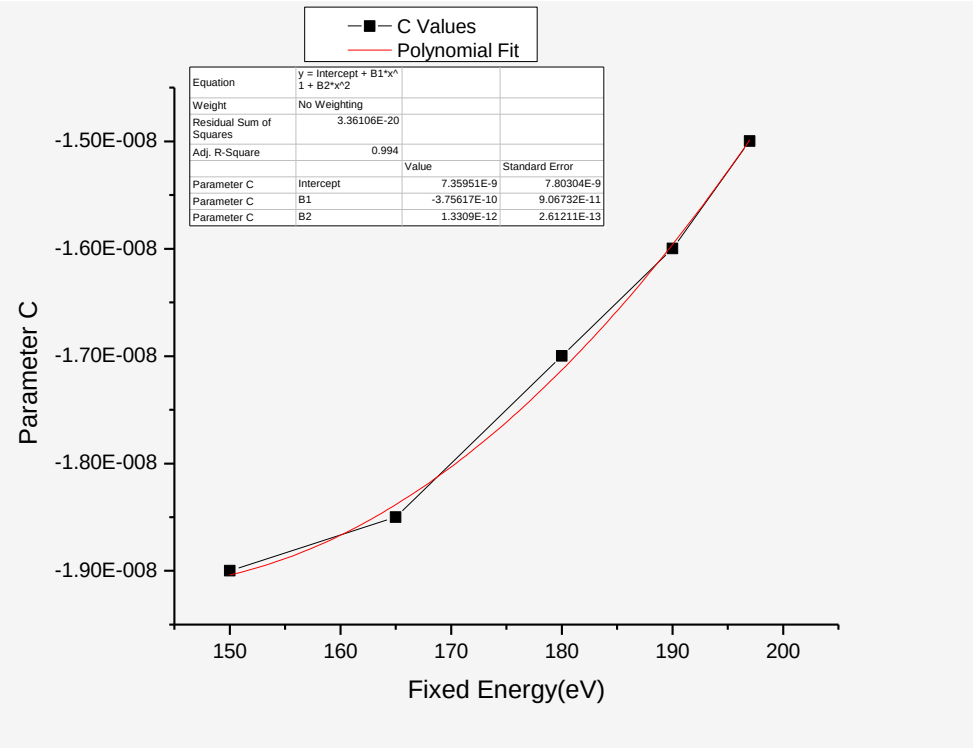

Figure D3. Extrapolation of Background Function Parameter C

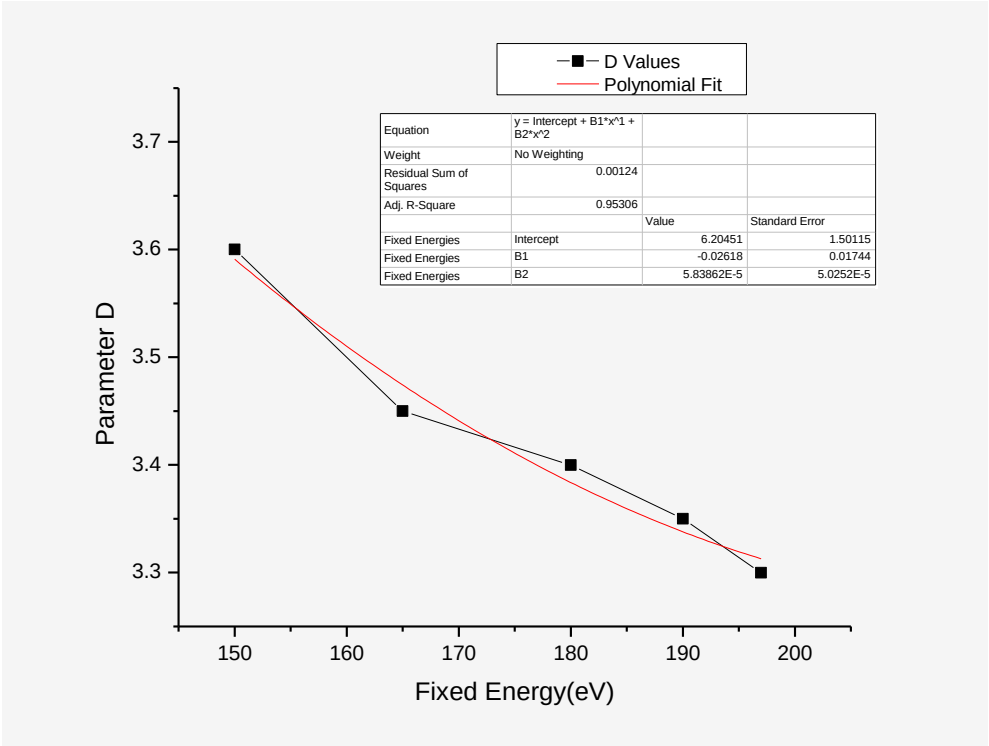

Figure D4. Extrapolation of Background Function Parameter D

REFERENCES

[1] Plummer, E.W. and Eberhardt, W.E., Adv. Chem. Phys. **49**, 533 (1982).

[2] Houston, J.E. and Rye, R. R., in : “Auger Electron Spectroscopy”.

[3] Haak, H.W., Sawatzky, G.A. and Thomas, T.D., Phys. Rev. Lett. **41**, 1825(1978).

[4] R. A. Bartynski, Eric Jensen, S. L. Hulbert, C.-C. Kao, Progress in Surface Science, Vol. 53, Nos 2-4, pp. 155-162, (1996).

[5] R. A. Bartynski, Eric Jensen, S. L. Hulbert, Physica Scripta. Vol. T41, 168-174, (1992).

[6] S. Mukherjee, M. P. Nadesalingam, P. Guagliardo, A. D.Sergeant, B. Barbiellini, J. F. Williams, N. G. Fazleev, and A. H. Weiss, Phys. Rev. Lett. **104**, 247403 (2010).

[7] E.H.S. Burhop, The Auger Effect and other Radiationless Transitions, (Cambridge Univ. Press, (1952).

[8] W.Mehlhorn, “The Auger Effect” Report from the Behlen lab of Phys., Univ of Nebraska (1970).

[9] Practical Surface analysis, M. P. Seah and D. Briggs.

[10] S. L. Hulbert, J, P. Stott, F. C. Brown, and N, C. Lien, Nucl. Instrum. 1 208, 43(1983).

[11] R. Sundaramoorthy, First direct measurement of the Energy Spectra of Individual Auger Cascade steps in solids, University of Texas at Arlington.

[12] D.E. Ramaker, Journal of Vacuum Science Technology A Vacuum, Surfaces and films **7**, 1614 (1989).

[13] E. Jensen, R.A. Bartynksi, R.F. Garrett, S.L. Hulbert, E. D. Johnson, and C.-C. Kao, phys. Rev. B 45, 13636(1992).

[14] C.P. Lund, S. M. Thurgate, and A. B. Wedding, Phys. Rev. B 49, 11352 (1994).

[15] D. E. Ramaker, J. S. Murday, N. H. turner, Journal of Electron Spectroscopy and Related Phenomena, **17,** 45-65,(1979).

[16] M. P. Seah, Surface Sci., **17**, 132, (1969).

[17] M. Inokuti, Rev. Mod. Phys., **43**, 297, (1971).

[18] S. F. Mukherjee, K. Shastry, A. H. Weiss Physical Review B 84, 155109 (2011).

[19] Y. Lin and D.C. Joy, Surf Interface Anal. 2005; 37:895-900.

[20] Origin of the low- energy tail in the Al L2, 3VV Auger spectrum studied with Auger-photoelectron coincidence spectroscopy- E.Jensen, R.A. Bartynski, R.F. Garrett, S.L. Hulbert, E. D. Johnson, C.-C. Kao.

[21] Wolfgang S. M. Werner et al., Physical Review B **78**, 233403 (2008).

[22] Andrei G. Kochur, Vitali A. Popov, Radiation Physics and Chemistry 75 (2006) 1525-1528.

BIOGRAPHICAL INFORMATION

Suman Satyal started his undergraduate studies from Truman State University, Kirksville, MO as a computer science student in 2003. He had his associate degree in General Science from Navarro College, Waxahachie, TX in 2007 and Bachelor of Science in Physics from University of Texas at Arlington, TX in 2009. He then continued his career as a master's student at UTA and started working as a research assistant for Prof. Dr. Alexander H. Weiss. He went to work at the Brookhaven National Lab, Upton, NY as a part of his research and studied the Auger Photoelectron Coincidence Spectroscopy in the summer of 2011.

Suman Satyal graduated in December 2011 from UT Arlington with Masters Degree in Physics.